THE BAUSCHINGER EFFECT

being a thesis presented by

Robert Lewis Woolley, M.A.,

to the University of St.Andrews

in application for the degree of

Doctor of Philosophy.

ms 1,452

DECLARATION

I hereby declare that this thesis is entirely based on the results of work carried out by myself in the Department of Natural Philosophy, St.Andrews University. The thesis is my own composition, and it has not been previously presented for a higher degree.

CERTIFICATE

I hereby certify that Robert Lewis Woolley has spent nine terms in research work on the Bauschinger effect, that he has fulfilled the conditions of Ordinance 16 (St.Andrews), and that he is qualified to submit this thesis in application for the degree of Doctor of Philosophy.

Research Supervisor.

STATEMENT OF CAREER

I matriculated in the University of Cambridge in the Michaelmas term 1940, and was admitted to the degree of Bachelor of Arts in June 1943 and to the degree of Master of Arts in June 1947.

I was appointed a lecturer in the Department of Natural Philosophy, St.Andrews University, in the Candlemas term 1946. In the Candlemas term 1948 I matriculated as a research student in the University of St.Andrews and commenced the research which is now described in this thesis.

CONTENTS

Page

I

GENERAL INTRODUCTION

I(a) AUTHOR'S PREFACE

The author's interest in the Bauschinger effect was first stimulated by Dr. E. Orowan, with whom he worked in Cambridge for a few months in 1945. In 1946 the author was appointed to a lectureship in Natural Philosophy in St. Andrews University, and began some X-ray studies on biological material under Professor J.T. Randall. This was discontinued when Professor Randall left St. Andrews. In 1947 the author wrote a short paper on the Bauschinger effect (Woolley 1948), and in 1948 resumed experimental work on this subject.

In 1948 and 1949 measurements of the Bauschinger effect in copper were made in the Mechanical Engineering Department, University College, Dundee, but the apparatus there used was not sufficiently sensitive and the testing machines were of too large a capacity for really satisfactory results. A small testing machine was therefore constructed in St. Andrews, with which the systematic study of section II (below) was carried out. The later experiments described in the other sections below were also all carried out in St. Andrews.

It gives the author great pleasure to record his gratitude to Professor J.F. Allen and the staff of the department for helpful criticism and discussion.

I(b) SCOPE OF THE PRESENT STUDIES

If a work-hardenable metal is deformed plastically by a tensile stress $+\sigma_0$ and unloaded, its mechanical properties become anisotropic; in particular, though its tensile yield stress is now $+\sigma_0$, it will deform plastically if compression stresses numerically smaller than σ_0 are applied. This is known as the Bauschinger effect (Bauschinger 1886).

When this research was commenced, very few experiments had previously been carried out to elucidate the effect as a function of the several possible variables and there was practically no satisfactory theory, except perhaps that of Masing (1923), which in any case could be severely criticised on purely theoretical grounds. It was clear that various classes of metals would probably show different types of effect. In particular the metals with face-centred and body-centred cubic lattices which deform by slip only, should show a very different effect from that exhibited by the metals of hexagonal lattice, where twinning plays an important part in the deformation. Single crystals might well show a different effect from polycrystals. In nominally pure metals the effect might well depend on grain size, elastic anisotropy, amount of previous work-hardening, temperature, purity, magnetic properties, degree of preferred orientation of a polycrystal, and orientation of a single crystal. In alloys the situation might be even more complex, especially if more than one phase were present.

For the purposes of this present research it was decided to examine the effect thoroughly and systematically in polycrystalline metals deforming entirely by slip, and to carry out exploratory experiments on other metals and in other conditions, including in particular, polycrystalline hexagonal metals and single crystals. Studies of macroscopic mechanical properties alone are not usually very conclusive in establishing the mechanism of the physical processes occurring, and it seemed very desirable to obtain additional information by examining the accompanying changes of other physical properties. Some experiments on these lines are discussed in sections III and V (below). The exploratory experiments of

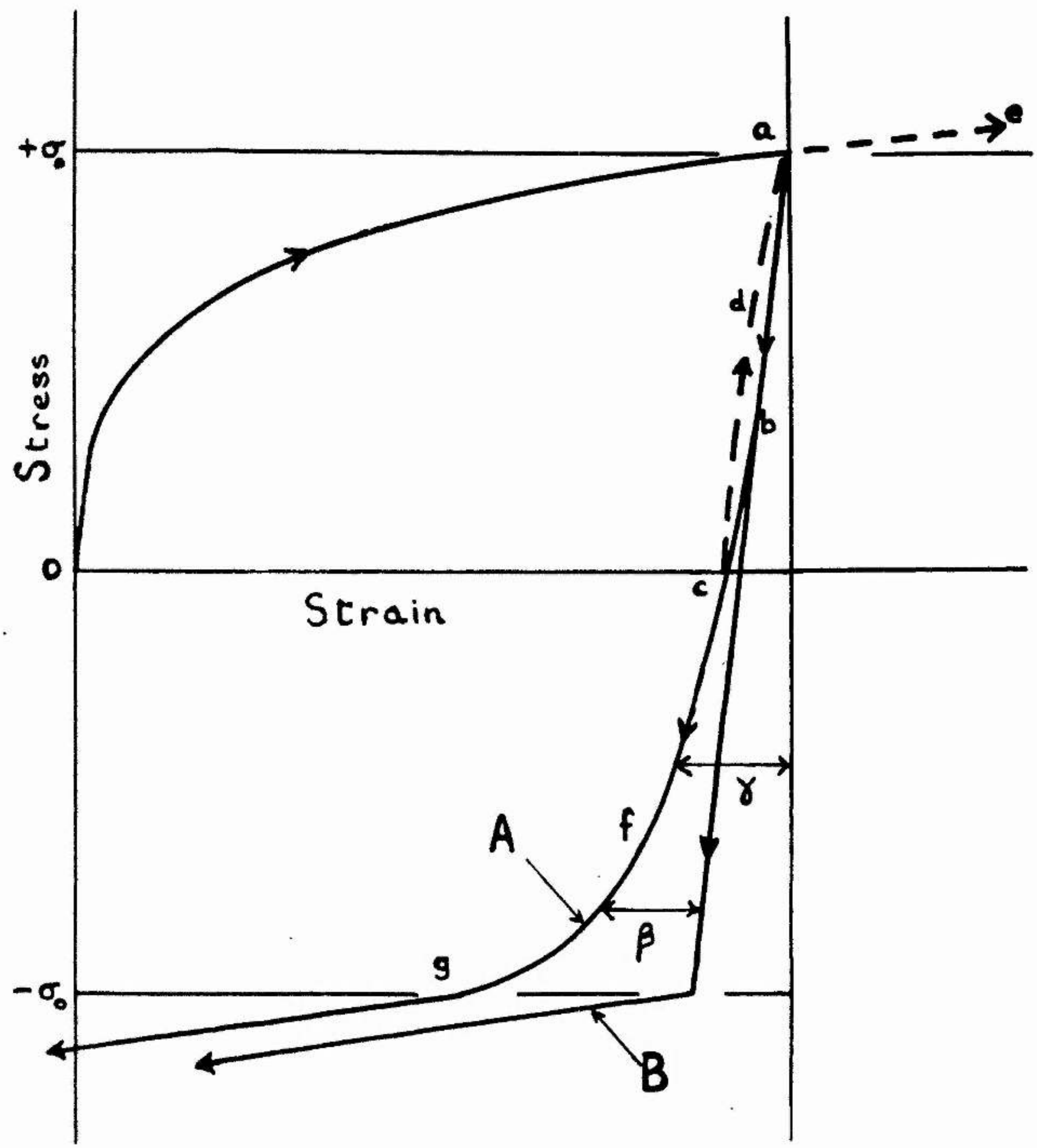

Figure 101

A - material showing Bauschinger effect
B - material showing no Bauschinger effect

sections III, V, VI and VII, were deliberately restricted usually to one metal under well-defined conditions, in view of limitations of time. It is hoped to extend these experiments in the near future.

I(c) DEFINITION OF THE BAUSCHINGER EFFECT

Figure 101, curve A, is a stress-strain curve typical of metals such as copper and aluminium which deform by slip only. The specimen starts at O, fully annealed. It is then stressed in a given direction by a stress $+\sigma_0$. The accompanying plastic strain is represented by Oa, and is called the prior strain. At a the specimen is unloaded and the line abc is traversed. If the stress is applied again, the line cda is followed, enclosing a narrow hysteresis loop. When the stress exceeds $+\sigma_0$ the curve turns sharply and follows ae , which is a prolongation of Oa. If at c , however, the specimen is loaded in the reverse direction, the curve cfg is followed. The rate of deformation increases steadily, and at the point g where the stress is $-\sigma_0$, it is closely equal to the rate of work-hardening observed at $+\sigma_0$ just before the point a. Beyond g the stress-strain curve is essentially the same as the forward curve ae.

The Bauschinger effect is often defined by saying that after plastic extension the tensile elastic limit is raised and the compressive elastic limit is lowered. The tensile elastic limit is usually tacitly identified with the yield point a , ignoring the plastic deformation between c and a. The compressive elastic limit is very poorly defined also, as there is a continuous curvature of the whole line abcfg . A definition in terms of elastic limits is therefore not adequate. The only really satisfactory procedure is to compare in detail the forward and reverse stress-strain curves after finite prior strain.

The external stress is merely the resultant of the stresses in the grains of the aggregate. As these are in general unequal, it follows that when the external stress is zero there are residual non-zero stresses in the actual grains. Thus the point c ($\sigma = 0$) has no great significance, and the plastic deformation along ac must be closely related to the deformation occurring along cg. It is therefore more rational to define the Bauschinger effect as the existence of the finite plastic strain β between $+\sigma_0$ and $-\sigma_0$. Curve B of figure 101 shows a hypothetical material with zero Bauschinger effect. In practice of course it is the strain γ which is measured directly, and β is deduced from this by extrapolating the initial part of the unloading curve.

In metals such as magnesium, which deform by twinning and slip, substantial plastic flow occurs at negative stresses numerically smaller than σ_o and a reasonable compressive yield point exists. This is discussed at greater length in section VI.

II.

THE BAUSCHINGER EFFECT IN POLYCRYSTALLINE FACE-CENTRED AND BODY-CENTRED CUBIC METALS

II(a) INTRODUCTION

One of the factors which has made the Bauschinger effect unattractive for experimental study is the difficulty of measuring the strain. It is obviously desirable to use a homogeneous stress, which necessitates using a specimen suitable for tension and compression. The difficulty of making accurate strain measurements in the compression test is well known; in the Bauschinger effect the strains are only a small multiple of the elastic strain. Some previous workers used headed specimens with a length/diameter ratio of about two. Under these circumstances there is considerable inhomogeneity of strain for deformations exceeding a few per cent. The advantages of the tension-compression specimen are therefore limited. In the present work the torsion test has been used. The test-piece is a tube with a wall-thickness/diameter ratio of nine. This gives an inhomogeneous strain-distribution but as shown below this is not very serious. The torsion test has the advantage that

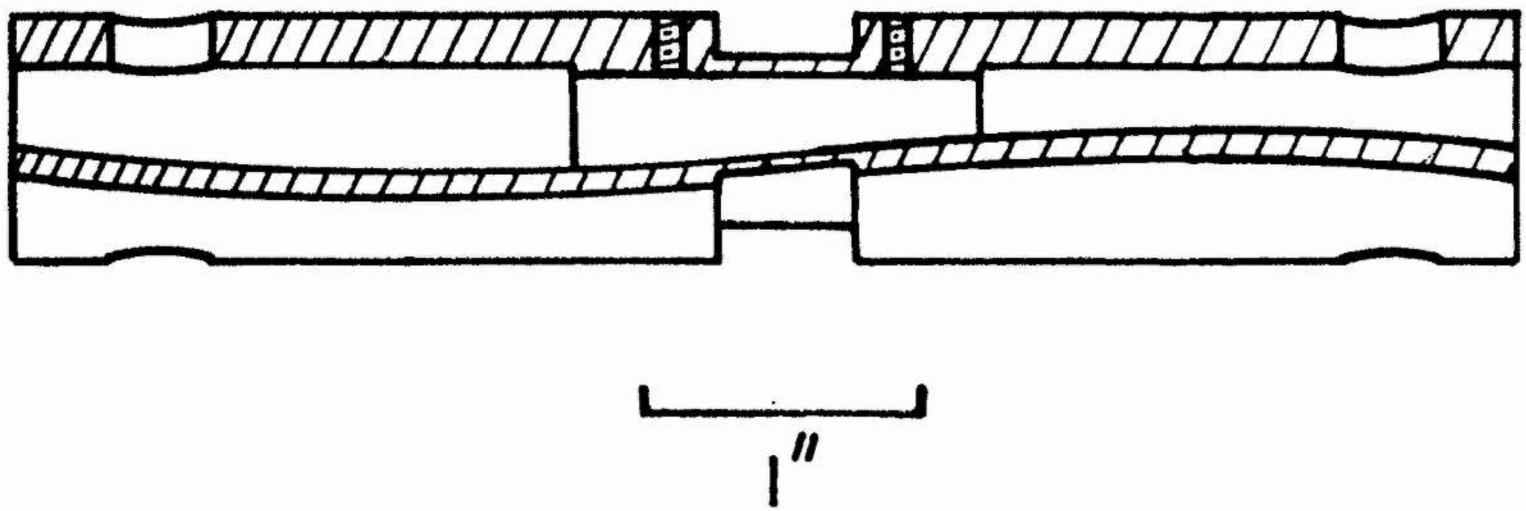

Figure 201. Standard torsion specimen.

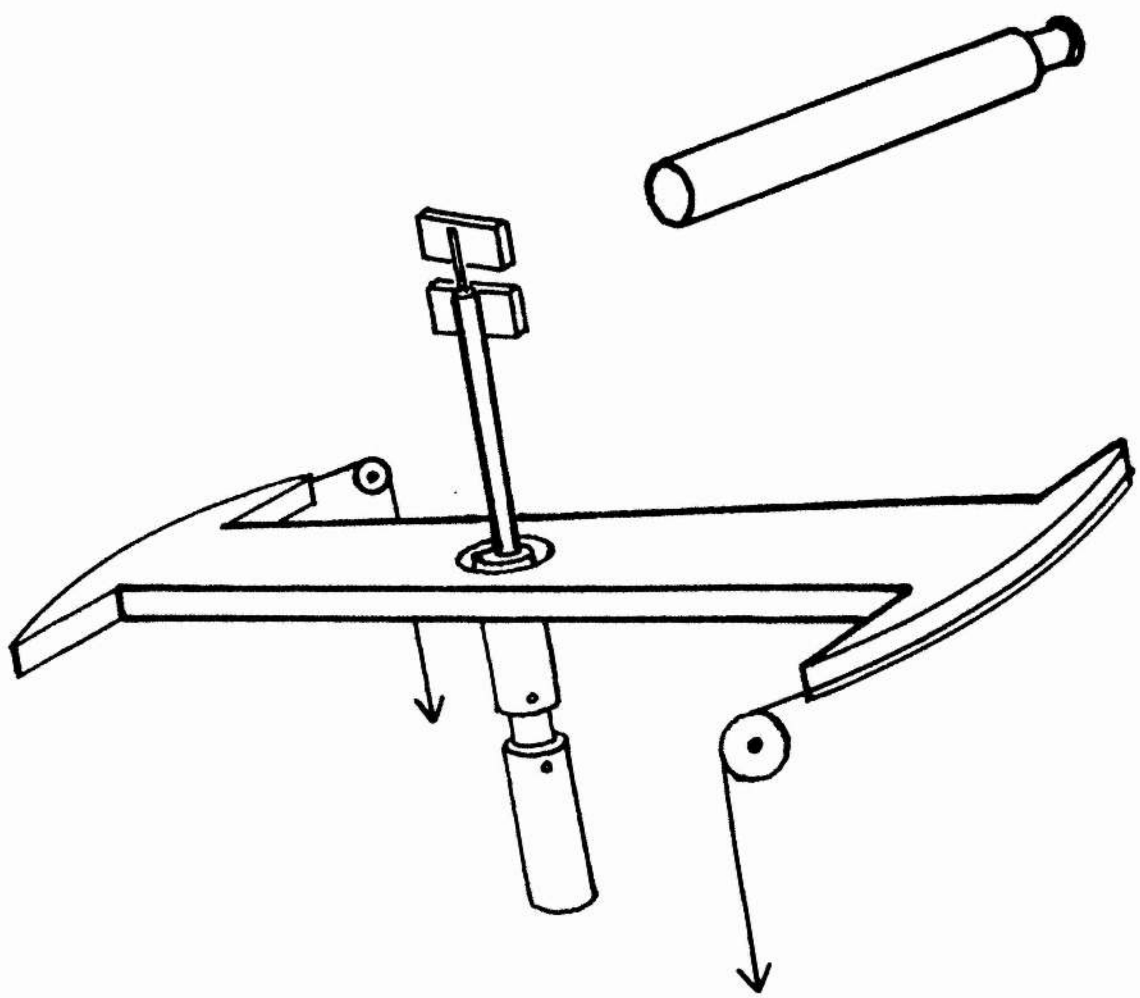

Figure 202

Torsion-testing machine

the shape of the specimen remains unaltered, and the shear strain is easily measured optically.

II(b) APPARATUS

(i) Description

The dimensions of the standard test-piece are shown in figure 201. The wall-thickness for softer metals (Cu, Al, Pb) was usually 1/16", but was sometimes 1/32" for the harder metals (Fe, Ni) to suit the limited capacity of the testing machine.

The tests were carried out in the simple machine shown schematically in figure 202 and in the photograph of figure 203. The test-piece is vertical. Its lower end is fixed, and its upper end is twisted about the vertical axis by a horizontal lever loaded by weights attached by flexible steel strip passing over pulleys. The capacity is approximately 1000 cm-kg. It is estimated that the error due to friction is less than 1% of σ_o . It is possible to carry out tests at elevated or reduced temperatures by immersing the specimen in a suitable bath.

The shear strain is measured with a telescope and scale by observing the rotation of a pair of mirrors attached to either end of the test length. The mirrors

Figure 203

Torsion-testing machine

are fixed to the upper ends of a pair of coaxial nickel silver tubes, separated by a ball race. The lower ends of these tubes each carry a pair of points on one side. These points are pressed into the inner wall of the test piece by two 4 B.A. set screws passing through the wall of the end portion of the specimen. In some experiments the gauge length was 1/2" and the points were opposite the ends of the reduced centre section of the specimen. In other experiments the gauge length was 3/4" and the points were opposite the 4 B.A. screws; in this latter case an end correction is applied. The results using the two different gauge lengths were consistent. In no case was any evidence of backlash obtained. The angle between the mirrors can be read to an accuracy of 10^{-4} radian, which corresponds to a shear strain of 0.005%. The dimensions of the specimens can be measured to an accuracy of about 1%.

(ii) Correction for finite wall thickness.

To a first approximation the observed torque-twist diagram (τ, φ) with a suitable change of scale is identical with the stress strain diagram of the metal. Owing to the finite wall thickness a small correction is needed. The exact calculation of this is difficult. But an upper limit can be found as below.

Consider a tube of length l, internal radius a and external radius b. Let dT be the torque on an elementary tube of radius r and thickness dr. Suppose that initially during the forward deformation the shear stress is uniform over the cross-section and is σ_0 . Let the specimen be unloaded from this point and let the ensuing true stress-strain curve of the metal be $\sigma(\theta)$ where θ is the shear strain. Let c be a mean radius, as yet unspecified, between a and b. Expanding as a Taylor series and neglecting powers higher than the second, we then have

$$T = \int_a^b 2\pi r^2 \left[\sigma_c + (r-c)\frac{d\sigma}{dr} + \frac{1}{2}(r-c)^2\frac{d^2\sigma}{dr^2}\right] dr$$

$$\therefore \quad \frac{T}{2\pi} = \Delta_3\sigma_c + (\Delta_4 - c\Delta_3)\frac{d\sigma}{dr} + \frac{1}{2}\left(\Delta_5 - 2c\Delta_4 + c^2\Delta_3\right)\frac{d^2\sigma}{dr^2}$$

where $\Delta_n \equiv (b^n - a^n)/n$

But $\theta l = \varphi r$

$$\therefore \quad \frac{d\sigma}{dr} = \frac{\varphi}{l}\cdot\frac{d\sigma}{d\theta} \qquad \text{and} \qquad \frac{d^2\sigma}{dr^2} = \frac{\varphi^2}{l^2}\cdot\frac{d^2\sigma}{d\theta^2}$$

It is convenient to take $c = \Delta_4/\Delta_3 = 0.284''$ if $a = 0.250''$ and $b = 0.312''$. (This gives the correct scale for the strain. If some other value is chosen for c then there is a further correction term involving $\varphi dT/d\varphi$ which automatically compensates for the difference). The approximate solution is then $T = 2\pi\Delta_3\sigma_c$, which is used to express the correction term as a function of T, giving

$$\frac{T}{2\pi} = \Delta_3\sigma_c + \frac{A}{2\pi}\varphi^2\frac{d^2T}{d\varphi^2}$$

$$\text{or } 2\pi\Delta_3\sigma_c = T - A\varphi^2 d^2T/d\varphi^2$$

$$\text{where } A = (\Delta_5 - 2c\Delta_4 + c^2\Delta_3)/2c^2\Delta_3$$

$$= (b-a)^2/24a^2 - (b-a)^3/24a^3 \;\ldots\ldots$$

This gives the true stress at radius c, the corresponding true strain being given by $\theta = \varphi c/l$. If initially during the forward deformation the material is work-hardening, the stress at the outer wall will exceed the stress at the inner wall. In this case it can be shown that the correction term is reduced, and lies between A and A/2.

The correction term is very small. For b/a = 5/4, A has the value 0.002. The correction is negligible unless there is a sharp bend in the stress-strain curve. Figure 204, curve A, is a typical stress-strain curve

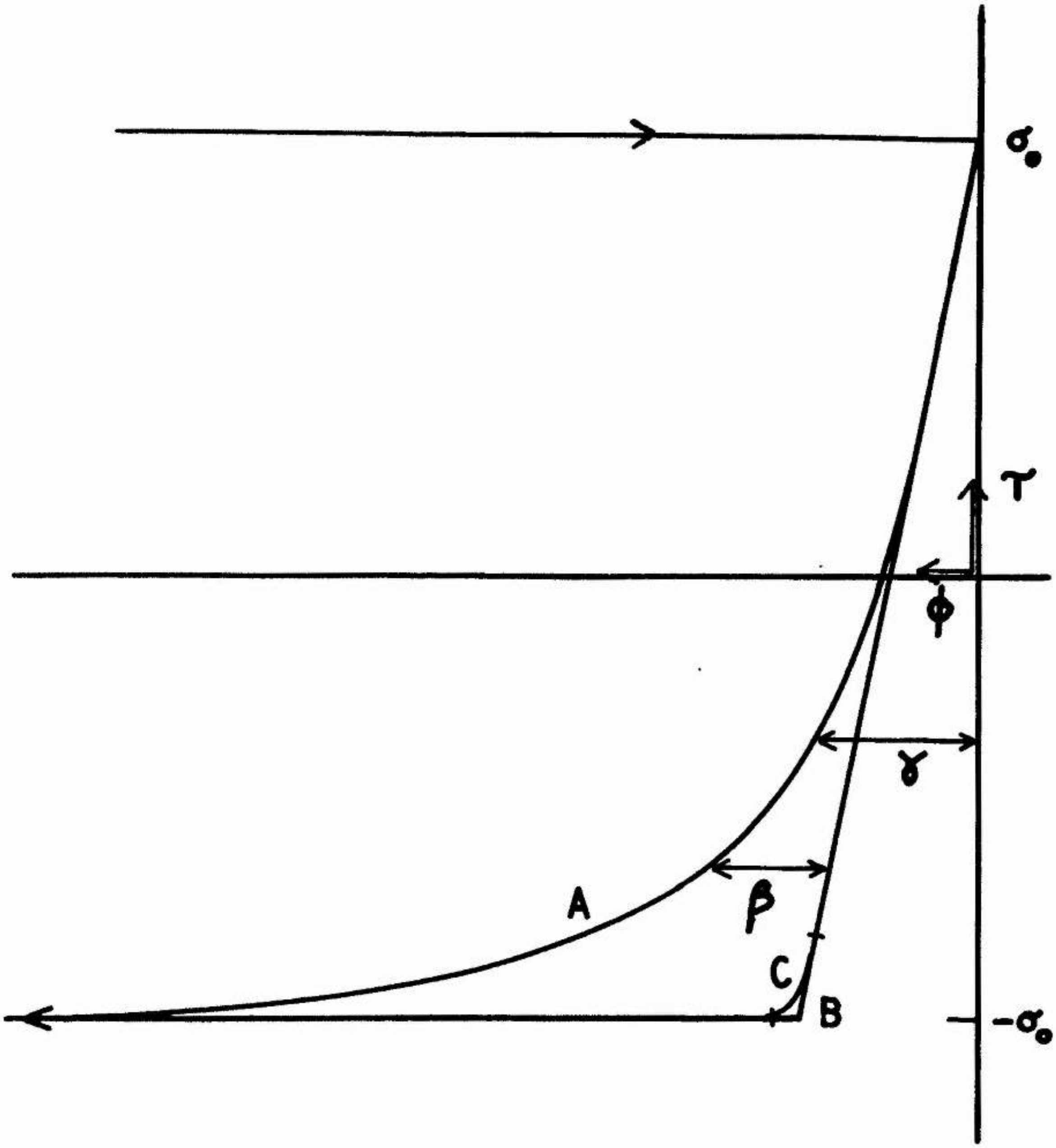

Figure 204

A - typical stress-strain curve
B,C - effect of finite wall thickness

determined experimentally. The correction is too small to be shown. It is of interest to see what would be the effect of finite wall thickness with a specimen possessing zero Bauschinger effect, i.e. whose true stress-strain curve is linear between $+\sigma_0$ and $-\sigma_0$. The extreme case, for a material showing no work-hardening, is easily calculated. Figure 20A, curve B, shows the $\tau:\varphi$ curve for zero wall thickness, and curve C the curve for $b/a = 5/4$.

II(c) <u>RESULTS</u>

(i) Copper. Dependence of Bauschinger effect on amount of previous cold work.

The specimens were machined out of 1" diameter drawn HC copper rod, and were annealed for one hour at 970°C in air at a pressure of 0.1 mm Hg to remove as far as possible all internal stresses and effects due to previous mechanical treatment. After cooling in the furnace they were electrolytically polished and etched. The mean grain size was 147 grains/mm^2, each grain containing an average of three twin elements. Since twin boundaries obstruct slip on at least six out of the twelve possible slip-systems, the effective grain size is taken as the number of twin elements

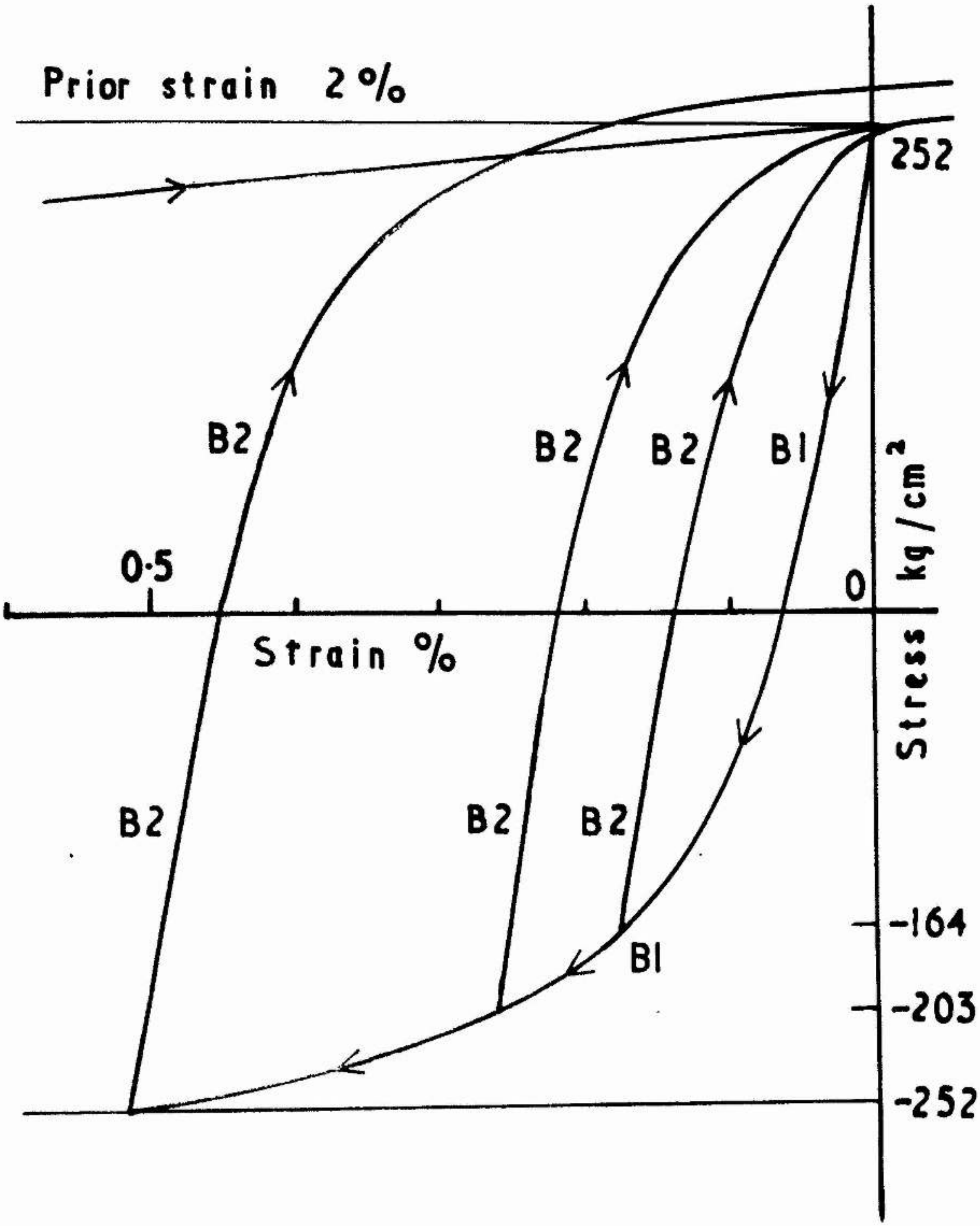

Figure 205

Bauschinger effect after 2% strain

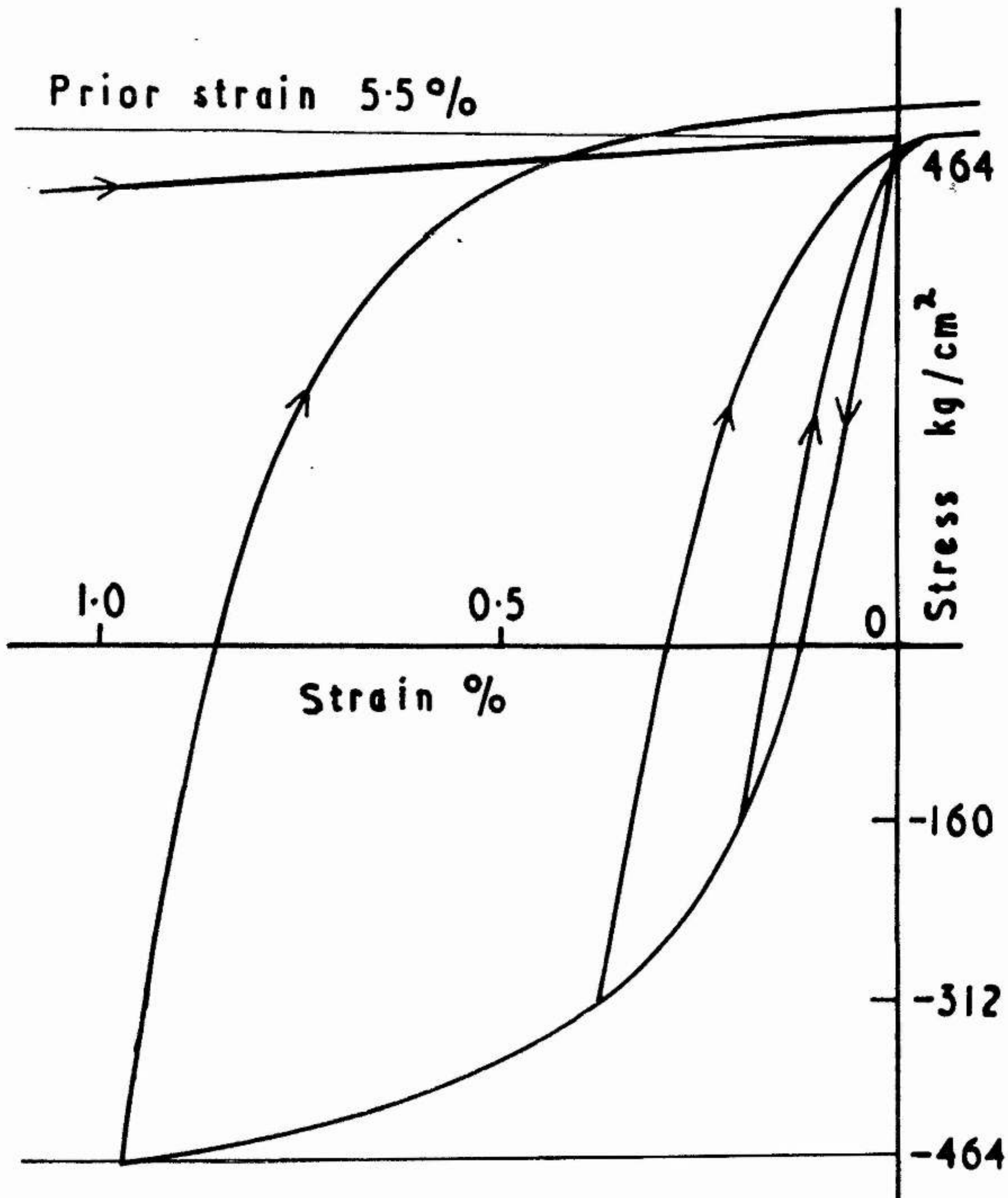

Figure 206

Bauschinger effect after 5.5% strain

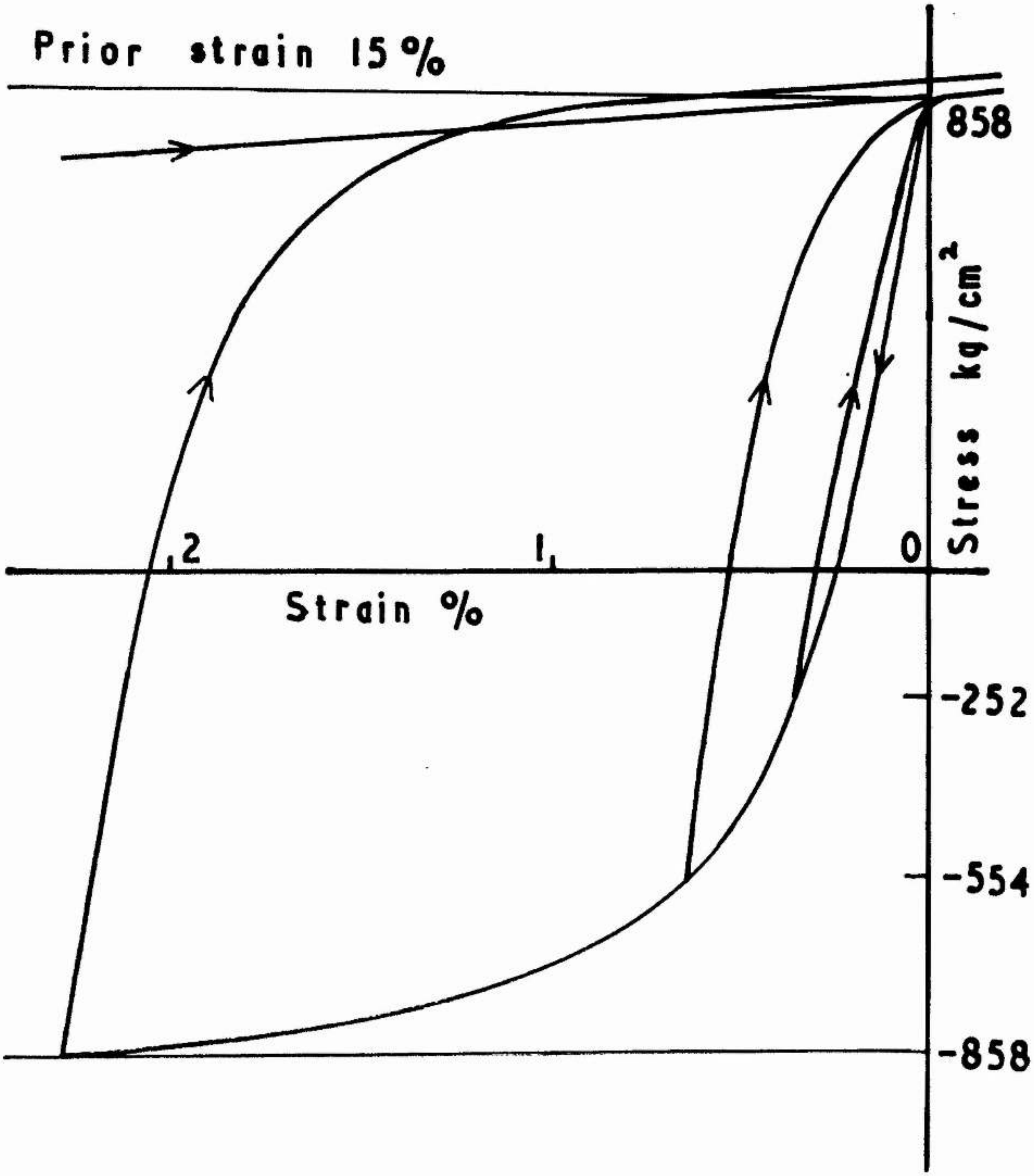

Figure 207

Bauschinger effect after 15% strain

per mm^2, in this case 440 twins/mm^2.

Three specimens were tested by applying a forward shear stress of 252 kg/cm^2 producing a strain of 2% , followed by reverse stresses of 164, 203 and 252 kg/cm^2 respectively, followed by a forward stress exceeding 252 kg/cm^2. The resulting stress-strain curves are shown in figure 205. In figures 206 and 207 are shown the results of six other specimens tested at stress levels of 464 and 858 kg/cm^2, the stress level being defined as the forward stress immediately before unloading begins, and denoted by σ_o .

Creep effects are considerable during the forward deformation. The stress was usually changed in steps of about $\sigma_o/10$, and the strain observed after one or two minutes, when the creep rate had greatly diminished. The observations near $+\sigma_o$ on the unloading curve are a little unreliable as slight creep occurs here. However, along most of the unloading curve, and along the reverse stress curve between zero and about $-3\sigma_o/4$, no creep effects were discernable. Usually a small creep was observed when the stress reached $-3\sigma_o/4$, and this became quite noticeable by $-\sigma_o$.

The curve running from $+\sigma_o$ to $-\sigma_o$ is denoted by B1 (cf figure ~~4~~ 205). There is a considerable resemblance between the B1 curves at the three stress levels. This

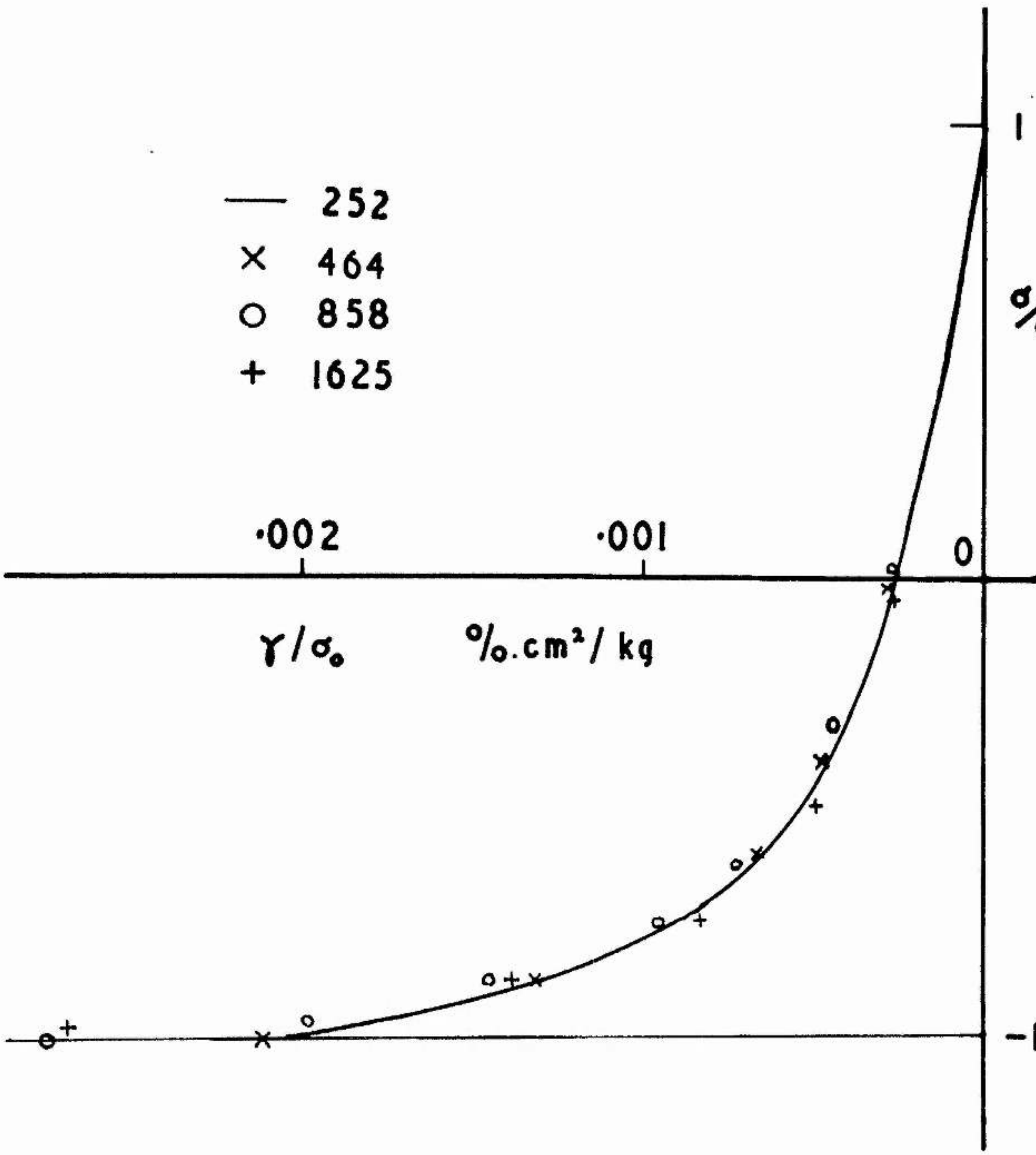

Figure 208

Copper. B1 curves of figures 205-7
replotted with reduced scale

is illustrated in figure 208, which shows the B1 curves of figures 205-7 replotted with the scale of both stress and strain divided by 252, 464 and 858 respectively. The B1 curves now nearly coincide, except near $-\sigma_0$. This strain-difference observed near $-\sigma_0$ corresponds to a relatively small stress-difference. It may be partly due to the larger creep rate associated with the higher stress levels. It is seen that to a good approximation the Bauschinger strain from $+\sigma_0$ to at least $-0{\cdot}9\sigma_0$ can be written

$$\beta = \sigma_0 f(\sigma/\sigma_0) \qquad \text{or} \qquad d\beta/d\sigma = f'(\sigma/\sigma_0)$$

The function f thus provides a measure of the Bauschinger effect independent of σ_0.

In the experiments described below it was found that the results for other metals and other conditions were of the same general character as those shown in figures 205-7, and by suitable adjustment of the scale could also be made to coincide with the curve of figure 208 to a first approximation. To obtain a single parameter which would be an experimental measure of the effect in any given test, it was decided to take the strain γ at the stress $\sigma = -0{\cdot}75\sigma_0$ divided by the strain γ at $\sigma = 0$. This ratio is denoted by ρ. The value $-0.75\sigma_0$ was chosen as this is the largest negative stress at which creep effects can be neglected. For a material with no Bauschinger effect $\rho = 1.75$. In figures 4, 5 and 6, ρ has the values 3.47, 3.43 and 3.43 respectively. The accuracy of ρ in any one test is usually ± 2 or 3%.

In the above tests the prior strain was limited to about 20%, because at larger deformations the specimens showed signs of buckling. To overcome this a greased 1/2" diameter rod was inserted in one specimen in place of the mirror assembly, and the specimen was given a preliminary twist of about 120° corresponding to a shear strain of 115% ; this effectively prevented buckling. The rod was then withdrawn, the mirror assembly was inserted, and a further strain of 6½% was given, the stress level now being 1625 kg/cm^2. The B1 curve springing from this point is shown in figure 208, with the appropriate reduced scale. The effect is relatively slightly smaller than at lower stresses ; this difference may not be significant, as the specimen was constrained by the 1/2" rod during its preliminary deformation.

In these tests, and in those described below, the prior strain usually exceeded 1%. With prior strain less than 1% the Bauschinger strain β is less than that given in figure 208. β of course must tend to zero when the prior plastic strain tends to zero. Thus the region between 0% and about 1% prior plastic strain (the material being initially thoroughly annealed) represents a transition region in which the Bauschinger strain increases from zero to its normal value as given in figure 208, this normal value being characteristic up to a prior strain of at least 120%.

In figures 205-7 it will be seen that the B2 curves to a first approximation are symmetrical to the part of the B1 curve already traversed. The B2 curve springing from $-\sigma_0$, however, does not usually close on the B1 curve at $+\sigma_0$. The strain amplitude of the B2 curve between $-\sigma_0$ and $+\sigma_0$ is approximately 2/3 the amplitude of the B1 curve between $+\sigma_0$ and $-\sigma_0$. The difference between these two curves measured in terms of stress is relatively much smaller, owing to the small value of $d\sigma/d\theta$ and is only two or three times the uncertainty in the stress measurements. A similar difference was however observed in experiments with aluminium and nickel and it does appear to be significant.

Cycles of stress taken between the limits $+\sigma_0$ and $-\sigma_0$ give further curves which may be denoted by B3, B4, etc. One copper specimen and one aluminium specimen were tested, with similar results. Figure 209

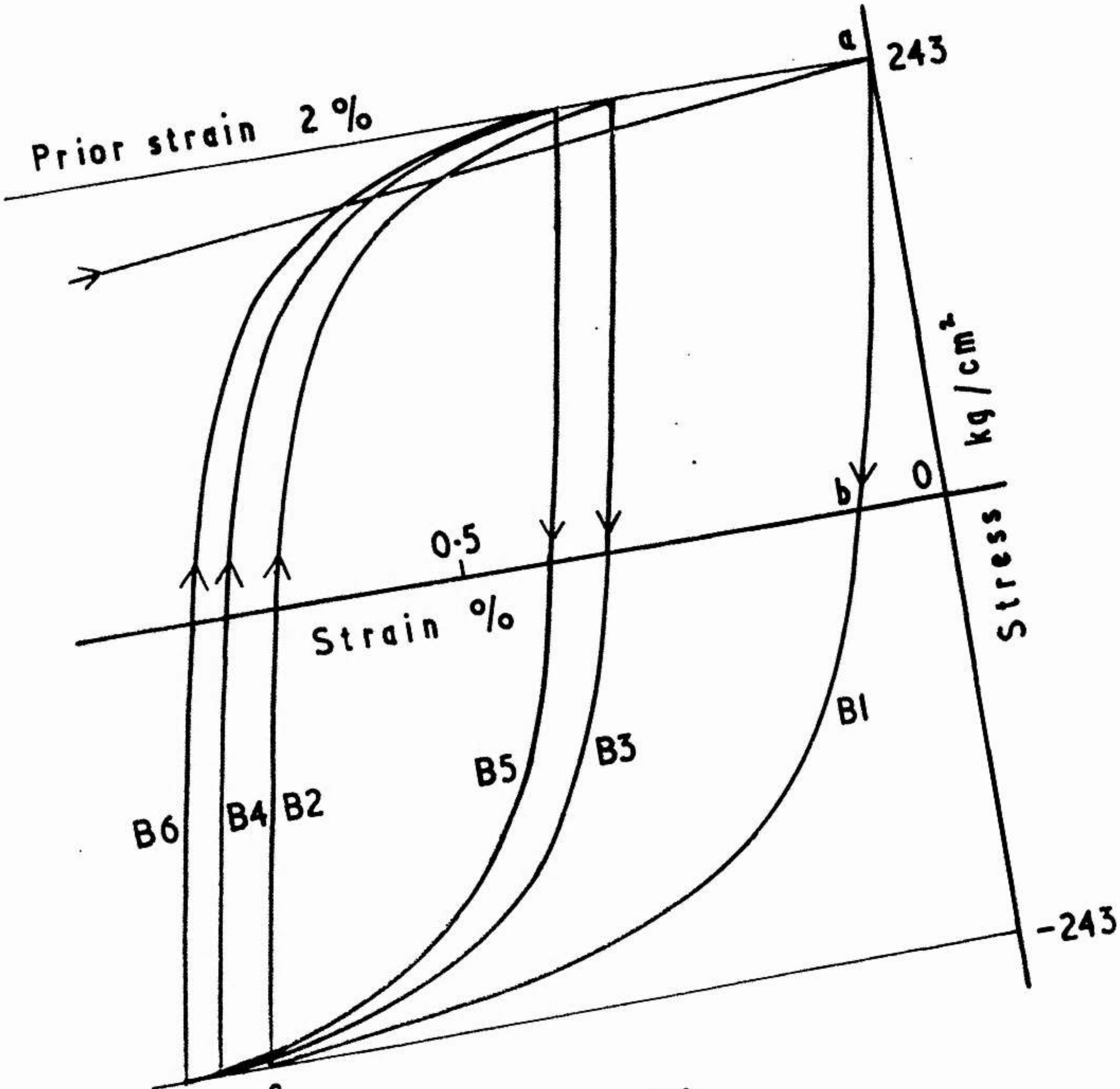

Figure 209

Aluminium
Stress cycles after 2% strain

shows the results for aluminium. The curves B2, B3, B4, etc. are to a first approximation equal. The strain-amplitude of B3, however, slightly exceeds that of B2, and B5 exceeds B4; but this may not be significant, as the corresponding stress-difference is of the same order of magnitude as the accuracy of measurement. It is worth noting that in the test shown in figure 209 the stress-level was sufficiently low to give no creep effects; the difference between the strain-amplitudes of B1 and B2 cannot therefore be attributed to creep.

(ii) Copper. Effect of previous reversal of direction of deformation.

In (i) the deformation preceding the B1 curve was entirely in one direction, but it was noted that the B2 curve springing from $-\sigma_0$ was very similar to the B1 curve springing from $+\sigma_0$. This suggested that if a specimen were stressed to $+\sigma_0$, unloaded, stressed to $-\sigma_1$, unloaded, and then stressed to $+\sigma_1$ $(\sigma_1 > \sigma_0)$, the B1 curve springing from $-\sigma_1$ would probably be identical with the B1 curve obtained from a specimen stressed to $-\sigma_1$ by unidirectional loading. This was tested on two specimens, Cu 20 with σ_0 and σ_1 equal to 252 and 462 kg/cm^2, and Cu 21 with

Table 201

Copper. Effect of grain size.

Specimen Cu	11 – 22	11	12	13	14	17	16	15	19	18
Grains/mm^2	147	2	2	2	28	28	28	78	78	78
Twins/mm^2	440	105	105	105	170	170	170	310	310	310
σ_0 kg/cm^2	252 – 858	252	464	850	252	464	858	252	464	850
Prior strain, %	2 – 15	$3\frac{1}{2}$	9	21	3	6	$17\frac{1}{2}$	$2\frac{1}{2}$	6	16
ρ_0	3.40 – 3.65	3.77	3.77	3.61	3.68	3.37	3.45	3.56	3.42	3.63
$-\sigma_1$ kg/cm^2	–	495	655	–	433	720	–	433	729	–
Total prior strain, %	–	$9\frac{1}{2}$	15	–	7	14	–	6	13	–
ρ_1	–	3.63	3.39	–	3.45	3.52	–	3.33	3.43	
Mean ρ	3.49		3.57			3.49			3.47	

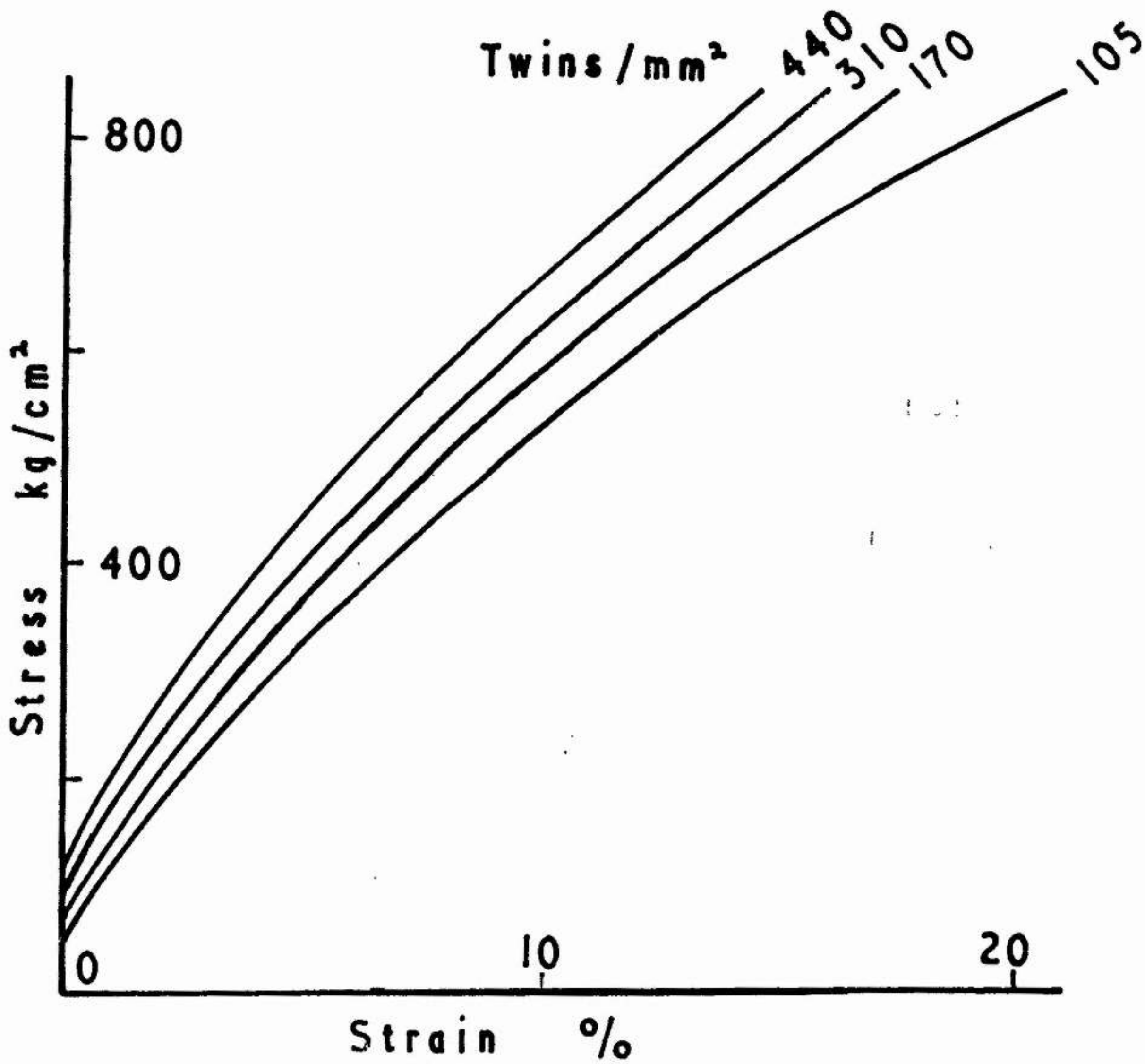

Figure 210

Copper. Forward stress-strain curves, showing effect of grain size values 464 and 728 kg/cm^2. The resulting reduced B1 curves at stress levels σ_0 and σ_1 all fitted figure 208 quite well. These observations, together with a more extensive set given below in (iii), show that the "memory" of a stress-reversal during deformation may be erased by a further strain of a few per cent.

(iii) Copper. Effect of grain size.

The specimens used in (i) were annealed again for one hour at 970°C. This produced three different grain sizes. These specimens were then tested as in Table 201, σ_0 and σ_1 having the same significance as in (ii) above. The first column gives the results from (i). The remaining columns give the results for the recrystallised specimens.

The values of ρ in Table 201 agree to within 5%. The variations appear random and there is no significant variation with grain size. The range of grain size used was somewhat limited, but it was quite sufficient to affect the prior forward stress-strain curves, shown in figure 210. In addition it was later observed with aluminium that specimens with a grain diameter as large as 2 mm and negligible twinning gave the normal

Table 202

Metal	Nominal purity	Heat treatment
Aluminium	99.9%	1 hour at 580°C
Super purity Al	99.99%	1 hour at 580°C
Nickel	99%	1 hour at 1260°C
Lead	99.98%	8 hours at 100°C
Iron	Armco ingot	8 hours at 680°C
Copper	99.9%	1 hour at 980°C

Table 203

The Bauschinger effect at 12°C.

Metal	Cu	Al	S-P Al
Number of tests	36	20	14
σ_0 kg/cm^2	73 - 1625	110 - 616	36 - 251
Prior strain, %	$\frac{1}{2}$ - 115	1 - 21	$\frac{1}{2}$ - 135
ρ	3.35 - 3.65	2.85 - 3.15	3.70 - 4.30

Metal	Ni	Pb	Fe
Number of tests	5	7	6
σ_0 kg/cm^2	425 - 1230	24 - 73	790 - 1820
Prior strain, %	$1\frac{1}{2}$ - 16	1 - 23	1 - 24
ρ	3.40 - 3.70	3.15 - 3.50	3.00 - 3.50

Bauschinger effect.

Table 201 also shows clearly that there is no systematic difference between the values of ρ and ρ_1, as mentioned in (ii) above.

(iv) Other metals.

Stress-strain curves were taken of the metals listed in Table 202. Table 203 gives the summarised results, including the results for copper. With nickel, for example, five B1 curves were measured, at stress levels varying from 425 to 1230 kg/cm^2, corresponding to prior deformations of 1½% to 16%, and the observed values of ρ were between 3.4 and 3.7.

The various values of ρ obtained for any one metal appear to be randomly distributed and not correlated with the stress level, except that ρ is somewhat low when the prior strain is 1% or less, as mentioned in (i) above. The variation is only a little larger than the estimated experimental error. Comparing the various metals, it is seen that the values of ρ are substantially the same, with the exception of S.P.Al which is high, and Al which is slightly low.

The fact that ρ is approximately the same for various metals is equivalent to saying that metals give

Table 204

The Bauschinger effect at -182°C.

Metal	Cu	Al	S-P Al
Number of tests	5	6	3
σ_0 kg/cm^2	152 - 970	334 - 970	304 - 456
Prior strain, %	1 - 16	2 - 30	20 - 34
ρ	2.9 - 3.5	2.6 - 2.9	3.5 - 3.7

Metal	Ni	Pb	Fe
Number of tests	3	4	3
σ_0 kg/cm^2	729 - 1700	48 - 170	2960 - 3680
Prior strain, %	1 - 12	1 - 16½	1 - 9
ρ	3.1 - 3.9	3.2 - 3.3	2.3 - 2.45

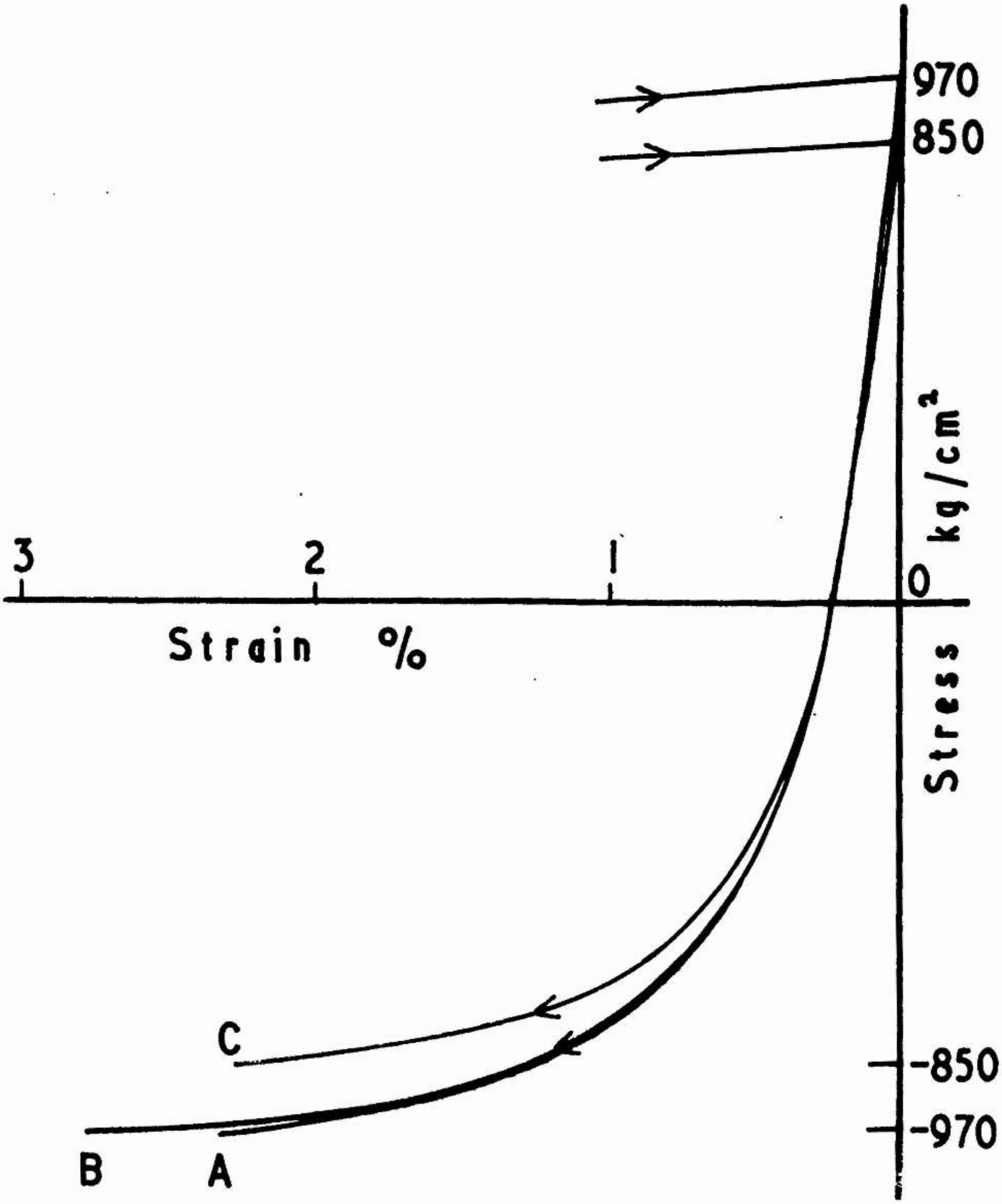

Figure 211

Copper. B1 curves showing effect of temperature.

A at -182°C. B,C at 12°C.

the same Bauschinger strain β when tested at stress levels giving the same elastic strain σ_0/G, where G is the modulus of elasticity. Metals work-hardened by stresses proportional to their respective elastic moduli may thus be regarded as being in corresponding states and thus presumably have similar internal distribution of lattice defects, trapped dislocations, etc.

(v) Effect of temperature of deformation.

Table 204 gives the summarised results of tests carried out at -182°C. It was found that temperature has only a relatively small influence on the Bauschinger effect. The principal difference is that for a given stress level the strain amplitude γ at $-\sigma_0$ is somewhat smaller at -182°C than at room temperature. Figure 211 shows typical results for copper, effective grain size 440 twins/mm^2.

It is reasonable to assume that one effect of temperature is to cause local stress-fluctuations. If these are of mean amplitude S_1 when the temperature is T_1 and the external stress is S, the peak local stress is $S + S_1$. The plastic flow at T_1 produced by the external stress S should therefore be the same as the flow produced at T_2 by an external stress $S + S_1 - S_2$. The thermal component of the stress can be estimated by observing the dependence of the yield point on temperature. Thus if an annealed specimen is deformed at −182°C by an external stress 970 kg/cm^2, unloaded, and warmed to room temperature, the yield point in the original direction of loading is found to be 850 kg/cm^2. Figure 211 curve C shows the B1 curve obtained for a room temperature copper specimen at a stress level of 850 kg/cm^2. Its amplitude γ at −850 kg/cm^2 is approximately equal to the amplitude of the curve A at −970 kg/cm^2. Similar results were obtained in a limited number of experiments with the other face-centred cubic metals. The diminution of the Bauschinger strain at low temperatures is thus attributed to the reduction of the thermal component of the peak local stress.

Iron is slightly exceptional. At −182°C the prior deformation is accompanied by sharp clicks presumed due to twinning, and the creep component of the extension is jerky. During unloading and reverse loading to $-\sigma_D$ twinning noises are absent, but they recommence when the stress passes $-\sigma_o$. The Bauschinger strain is somewhat reduced in amplitude, but its general character is similar to that of the metals which deform by slip only. It differs considerably from the B1 curve for hexagonal metals, which are discussed in section VI.

(vi) Summary.

The results of section II(c), (i) to (v), above may be summarised as follows. In the cubic metals the strain associated with the Bauschinger effect is approximately proportional to the stress level, and the stress-strain curve representing the effect has a characteristic shape. The B1 stress-strain curves for a wide range of metals can all be shown on one graph with suitably reduced axes. The effect is largely independent of grain size, and the small dependence on temperature is explicable in terms of a thermal component of stress.

II(d) COMPARISON WITH PUBLISHED RESULTS OF OTHER WORKERS.

The most interesting work is that of Masing and Mauksch (1926) who carried out a range of tension-compression tests on brass (Cu 58, Pb 2), the prior strain varying from 0.7% to 17.5%. Unfortunately, very little information is given about the portion of the B1 curves between $+\sigma_0$ and 0. From what is given it appears that the B1 curves are very similar to those obtained in the present work on pure metals, the strain being a little smaller, ρ having values between 2.5 and 2.65. Masing and Mauksch' experiments were designed to test Masing's theory (Masing 1923, 1926) of the Bauschinger effect, which predicts that the B1 curve should be the same as the preceding stress-strain curve from zero to $+\sigma_0$, but with doubled scale and reversed sign. Good agreement between the observed and predicted curves was not obtained; the agreement is even less satisfactory when it is seen that these authors made their computed curve coincide with the beginning of the compression curve, neglecting the plastic deformation that occurred during unloading. Masing's theory can hardly be expected to explain the Bauschinger strain after a prior deformation exceeding 1%, for, as shown in section II(c), the effect in this region is quite unrelated to the prior stress-strain curve. For deformations of order 0.1% Masing's theory probably agrees with experiment ; but in this region the Bauschinger effect in any case tends to zero, and is extremely difficult to measure accurately.

Later, Rahlfs and Masing (1950) examined the Bauschinger effect in torsion, using 1 mm diameter wires of various metals with prior surface strains exceeding 3.5%. The considerable inhomogeneity of strain causes the observed torque-twist curve to deviate a little from the true stress-strain curve, but even so it is interesting to notice that the published curves are very similar to the general curve described by the present author. Values of ρ calculated from Rahlfs and Masing's curves lie between 2.9 and 4.0. Rahlfs and Masing compared their results with Masing's theory and again found that the agreement is not good.

Experimental work on the Bauschinger effect has also been described by Polakowski (1951) and Wilson (1952), who are chiefly interested in hardness as a function of strain, and also by Kunze and Sachs (1930) whose experiments were entirely confined to the transition region below 1% prior strain. These results are therefore not easily compared with those described in section II(c) above.

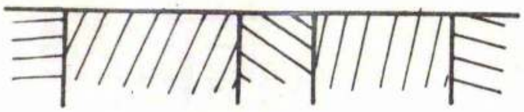

Before deformation

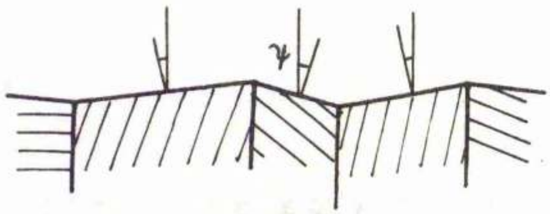

After deformation

Figure 301

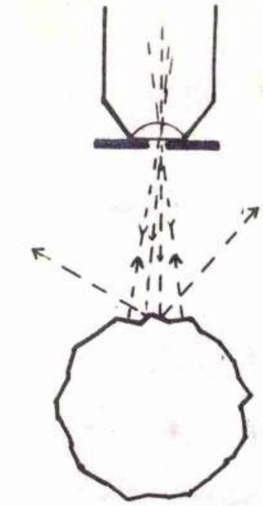

Figure 302

Specimen axis

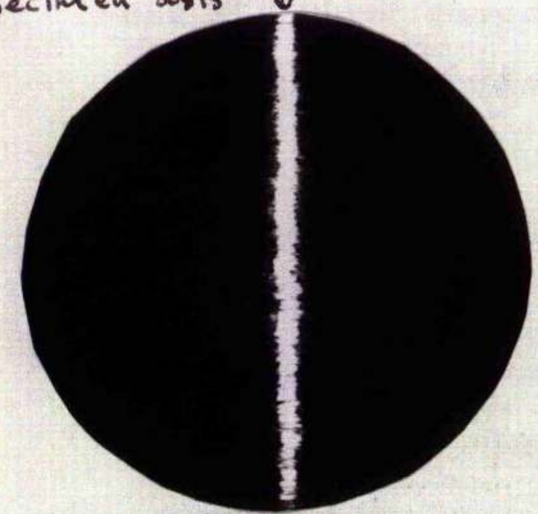

Figure 303
Undeformed

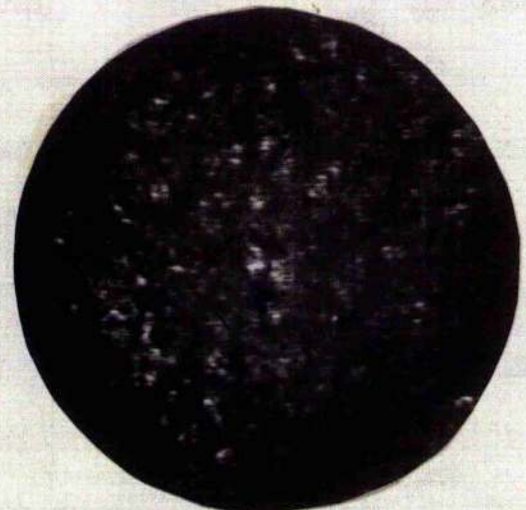

Figure 304
Resultant strain 12%

Figure 305
Resultant strain 6%

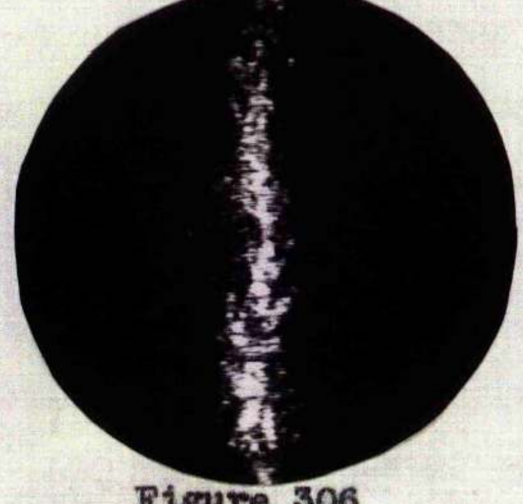

Figure 306
Resultant strain zero

III.

SURFACE STUDIES

III(a) RUMPLING

If the surface of a specimen is initially flat, it becomes somewhat rumpled after plastic deformation, because the individual grains do not have exactly the same shear as the aggregate (cf. figure 301). It was noticed that this rumpling was greatly reduced in specimens which had been subjected to forward and reverse strains of about equal magnitude, so that the resultant strain was nearly zero. Some measurements were therefore made to examine this quantitatively.

The experimental arrangement is shown in figure 302. A slit is fixed on the front lens of a $1\frac{1}{4}$" microscope objective, parallel to the axis of a standard cylindrical torsion specimen lying on the microscope stage. Only those parts of the field of view whose normal intersects this slit can reflect light back into the objective. Figure 303 shows a typical reflection from an undeformed specimen with a true cylindrical surface. After a shear of 12% the appearance is as in figure 304. A further shear of 6% in the reverse direction brings the resultant strain back to 6% and gives figure 305. A further reverse shear of 6% brings the resultant strain to zero and gives figure 306. If the individual grains all had the same strain as the aggregate, then their deformation would be in the plane of the surface of the specimen and all these microphotographs would be similar to figure 303.

Consideration of the geometry of the arrangement shows that bright spots on the edge of the field of view correspond to grains whose normal lies at an angle $\psi = 9°$ to the mean surface. Analysis of observations on two specimens of aluminium and one of copper gives the following results for strains below 20%.

i. During a forward strain θ, surface rotations ψ occur, proportional to θ, the ratio ψ_{max}/θ being about 0.7.

ii. During subsequent reverse strain the surface rotations diminish in the same proportion, reaching zero when the resultant strain reaches zero.

No observations were made at strains greater than 20%.

The results above correspond to rotations about an axis in the plane of the surface and parallel to the axis of the specimen. By turning the slit through 90° and tilting the specimen through a measured angle it was found that the same results apply to rotations about the transverse axis in the surface. If the rotations about the two axes are uncorrelated, then the total maximum rotation is

$$\psi_{max} / \theta = \sqrt{(0.7^2 + 0.7^2)} = 1$$

We conclude that in a deformed aggregate the strain in the individual grains on the free surface is by no means equal to the mean strain of the aggregate, rotations ψ of the grains being observed, having magnitude from zero up to the mean strain θ. This result must also to some extent apply to grains below the surface, and ought to be taken into account in assessing the validity of Taylor's (1938) theory of the strain of an aggregate. Further, the fact that the change of shape of the grains is mechanically reversible would be explained most simply if we assume that during both forward and reverse deformation the same slip systems are active in any given grain.

It is unfortunate that observations of this type are not sufficiently sensitive to give any information on the mode of deformation during the Bauschinger strain from $+\sigma_0$ to $-\sigma_0$.

III(b) SLIP LINES

Since slip is the mechanism of plastic deformation in the metals with cubic lattice, the explanation of the Bauschinger effect essentially involves finding out where, and how much, slip occurs during the Bauschinger strain. Unfortunately, slip is only easily studied by examination of the free surface of a polished specimen. It is not clear at present whether or not the free surface is entirely typical of the interior of a plastically deformed metal, especially in view of the influence of the mode of polishing (Brown and Honeycombe 1951). Even if the surface behaviour is typical of the interior during ordinary plastic deformation, it may not be so during the Bauschinger strain. Despite these limitations it is of interest to know how the surface behaves during the Bauschinger strain.
A short experiment was therefore carried out to see whether or not slip lines are produced during the Bauschinger strain.

Slip lines are not easily observed at plastic strains much less than 1%. It is essential therefore to work at a high stress level, to give a Bauschinger strain larger than this. Three torsion tests were

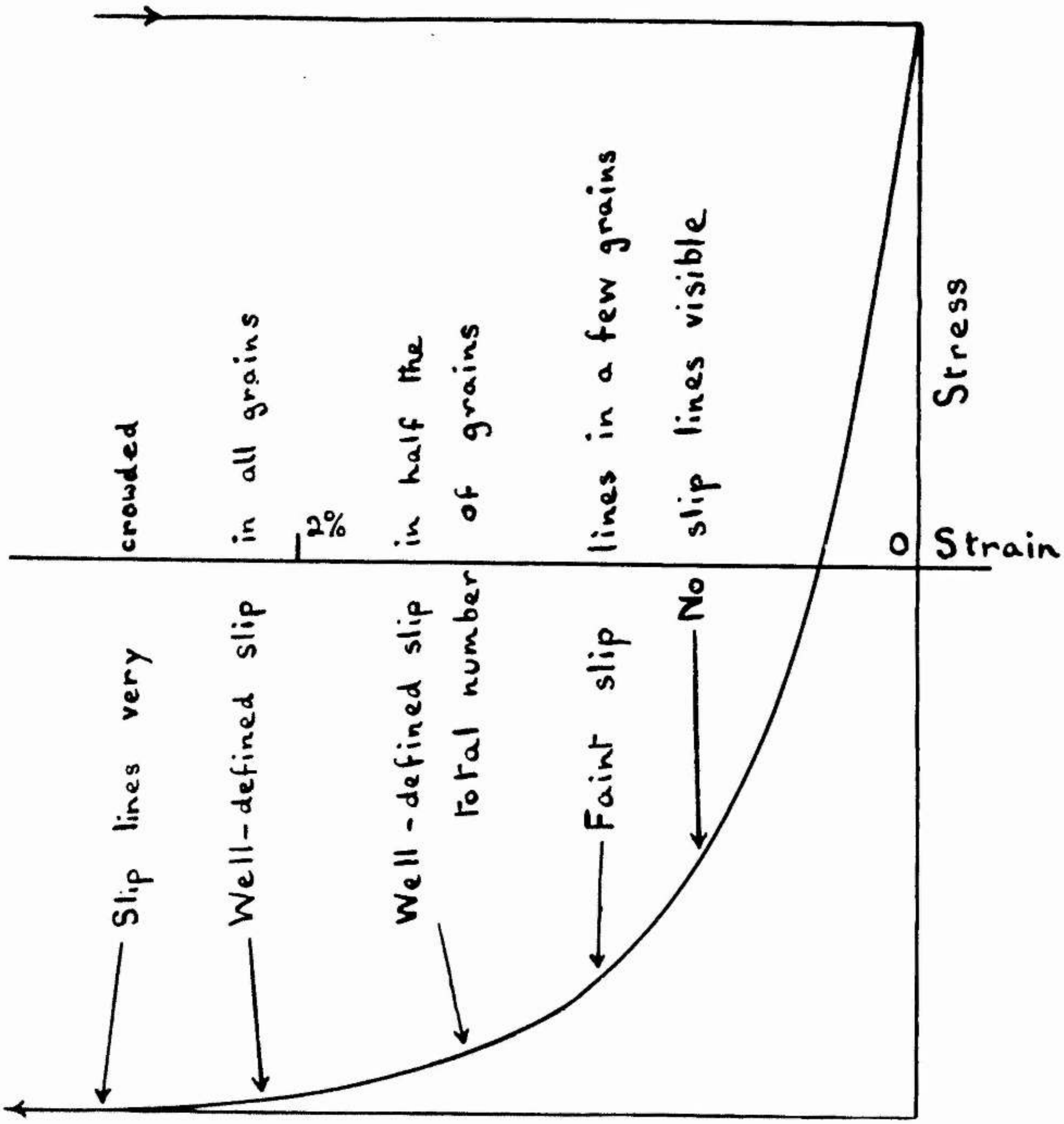

Figure 307

Slip lines observed during
Bauschinger strain

therefore carried out at stress levels of 940, 1030 and 1100 kg/cm^2, with copper having about 100 twin elements per sq.mm. The corresponding prior strains were 30%, 45% and 70% and the Bauschinger strain about 2% in each case. The prior strain was given partly as a forward deformation and partly reverse, so that surface rumpling was minimised. After unloading from the prior strain, the specimen was electrolytically polished in 50% orthophosphoric acid solution. The specimen was then loaded in reverse. At three points during the Bauschinger strain (i.e. while the stress was between 0 and $-\sigma_o$) the specimen was unloaded and examined microscopically at magnifications of 100X and 400X.

The qualitative observations were the same in all three cases, and are shown in figure 307. When the reverse plastic strain β is less than 1% few slip lines are seen, but as the strain increases to 2% the slip lines become more prominent, more closely spaced and visible in more grains. The general appearance of the slip lines is much the same as during the first stages of unidirectional deformation. We may therefore say that in the surface grains most of the Bauschinger strain takes place by the formation of the customary slip lines.

IV.

THE THEORY OF THE BAUSCHINGER EFFECT

IV(a) INTRODUCTION

Few theories of the Bauschinger effect have been put forward in the past, and none of these account for the results of section II, where it was shown that (i) the Bauschinger strain is proportional to the stress level, and (ii) the general B1 curve has a characteristic shape. Masing's treatment (1923) was based on textural stresses, and is discussed in section IV(b), where it is shown that these can contribute only a small part of the observed effect. The effect must therefore be attributed to a process occurring in the individual grains and probably in single crystals also. Such an effect may be explained in terms of dislocation theory as a rearrangement of dislocations already present or as the generation of new ones.

In discussing the relation between Bauschinger strain and stress level it is convenient to call the Bauschinger strain at $-\sigma_0$, divided by the yield strain σ_0/G , the <u>Bauschinger ratio</u>. This has an experimental value of about 8. In sections IV(c) to IV(f) some possible mechanisms are discussed, and it is concluded that the Bauschinger ratio has the magnitude which would be expected if the effect were due to a rearrangement of dislocations during stress reversal. The actual shape of the Bauschinger curve depends on the effective frictional resistance experienced by a dislocation, due to dynamic damping effects and to geometrical effects caused by increasing density of defects in the lattice, and is not further discussed here.

It is not reckoned that the generation of new dislocations contributes largely to the observed effect, as in general a Frank-Read source will generate equally well with positive or negative stresses and so produce no Bauschinger effect. This is further discussed in section IV(f).

Section IV(g) discusses a possible small contribution from grain-boundary slip, and IV(h) discusses the effects of vacancy-generation mechanisms.

The theory of Brandenberger (1947) is not discussed as it is based on very unusual ideas about elasticity and plastic deformation, and appears to have little relevance to physical reality. The theory of Nabarro (1950), which in some respects is related to Masing's treatment, refers to the length of the initial elastic

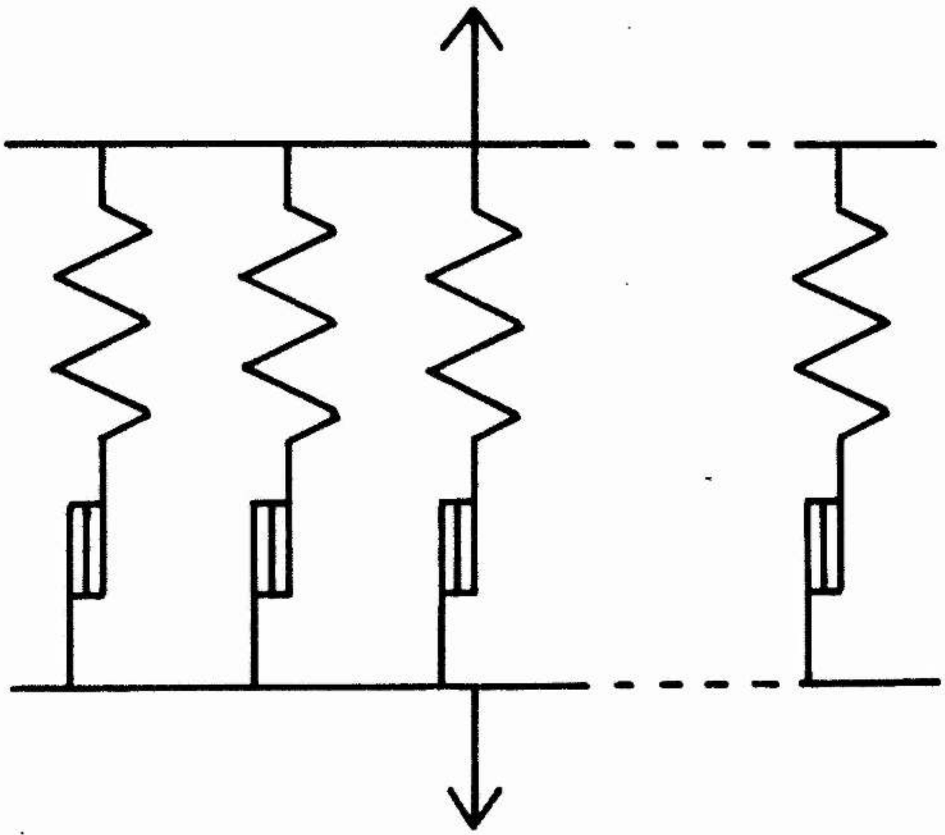

Figure 401

Grains in parallel

Figure 406

Grains in series

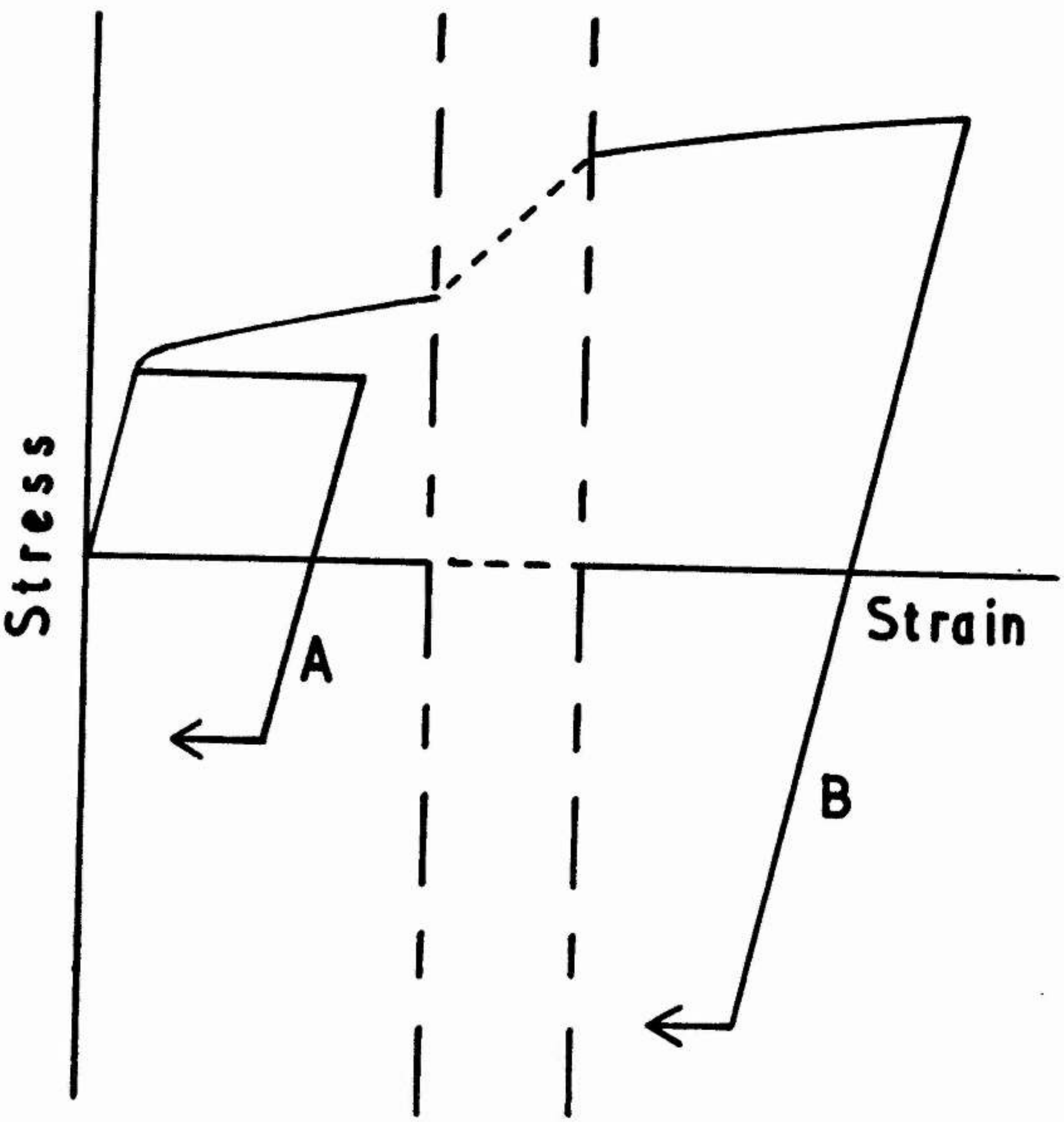

Figure 402

Stress-strain curve of a single grain, A - showing no work-hardening and no Bauschinger effect, B - showing work-hardening but no Bauschinger effect.

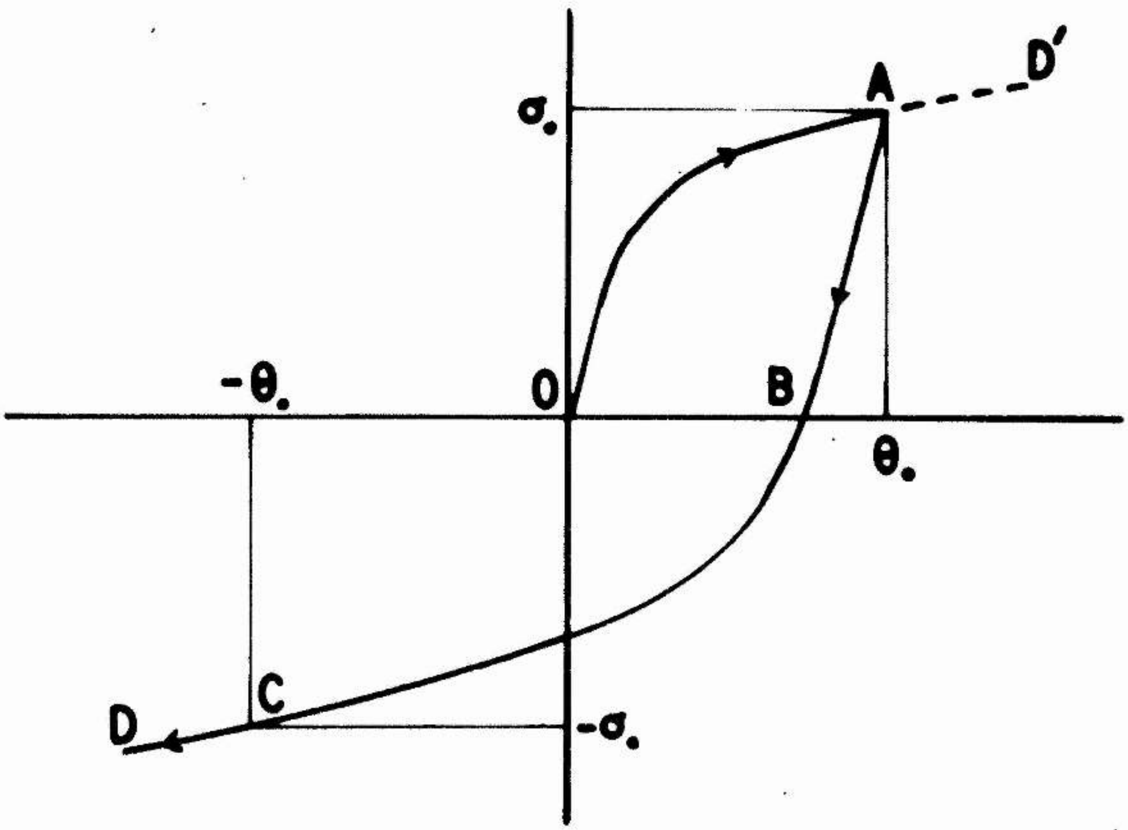

Figure 403

The B1 curve predicted by Masing's theory.

portion of the B1 curve, and is not further discussed here.

IV(b) TEXTURAL STRESSES

Masing (1923) considered essentially the model shown in figure 401. Each grain is represented by a spring in series with a friction element. The grains are regarded as ideally plastic, showning no hardening and no Bauschinger effect in the region examined, as in figure 402, curve A. Experimentally it was reckoned that this was achieved by a plastic strain to produce hardening, followed by a low-temperature anneal to remove textural stresses, the following strain being kept small, usually less than 1%. This model gives a B1 curve ABC (figure 403) geometrically similar to OA but with the scale of both axes doubled. The continuation CD is identical with AD'. This model is used by Masing to account both for the beginning of work-hardening and also for the Bauschinger effect. As Masing himself envisaged, it obviously cannot be used to account for work-hardening beyond a plastic strain of say 1%, as in this model the finite slope $d\sigma/d\theta$ of the work-hardening curve is attributed to grains which have not yet reached their yield point and therefore have an elastic strain equal to the overall plastic strain. For finite plastic strain (> 1%) there cannot be any direct relation of this type between the Bauschinger strain and the prior strain.

Greenough (1949) in discussing residual lattice strains, regarded the grains as work-hardening, and calculated the stresses which would be expected on the basis of the theories of Cox and Sopwith (1937) and of Taylor (1938). His experimental results agree better with Taylor's theory. We have used a similar method to calculate the exact size and shape of the Bauschinger curve which is given by this model, as below.

Figure 401 is again taken to represent the grains of an aggregate extended plastically. During this prior strain the grains have work-hardened. They are regarded as showing no Bauschinger effect and negligible further work-hardening during a subsequent small compression, as in figure 402, curve B. Let the (work-hardened) tensile yield stress of a given grain be denoted by $\xi\sigma_0$ where $0 < \xi < \infty$. Let the total volume of the grains whose yield stress is in the range $\xi\sigma_0$ to $(\xi + d\xi)\sigma_0$ be a fraction $g(\xi)$ of the volume of the specimen. $g(\xi)$ satisfies the equations

$$\int_0^\infty g(\xi)\,d\xi = \int_0^\infty \xi . g(\xi)\,d\xi = 1$$

In practice $g(\xi)$ is non-zero only when ξ lies between limits ξ_{min} and ξ_{max}. Since each grain is regarded as showing no Bauschinger effect, its compressive yield stress is equal to its tensile yield stress. The aggregate, however, shows a Bauschinger strain, owing to the range of yield strains present. Taking the origin of stress and strain at the point A, figure 403, plastic deformation begins at an applied stress $\sigma_0(1-2\xi_{min})$ and a strain $2\xi_{min}\sigma_0/G$; the specimen is entirely plastic when the applied stress reaches $-\sigma_0$ and the strain is $2\xi_{max}\sigma_0/G$. The shape of the B1 curve between these points is calculable in terms of $g(\xi)$, being given by

$$d^2\sigma/d\theta^2 = G^2 g(\xi)/2\sigma_0 \quad - - - \quad (1)$$

where $$\xi = G\theta/2\sigma_0$$

The theories of Cox and Sopwith, and Taylor, respectively, may be used to calculate $g(\xi)$. The former treat the grains as single crystals, laterally unconstrained. The relation between tensile stress, σ $(=\xi\sigma_0)$, and extension, ε $(= l/l_0 - 1)$ for a work-hardening single crystal, may be derived from the equations 26/3, 43/1 and 43/4 cited by Schmid and Boas (1950), in the form

$$\sigma = f(\varepsilon)/(\sin\chi_0 \cos\lambda_0)^{1+n}$$

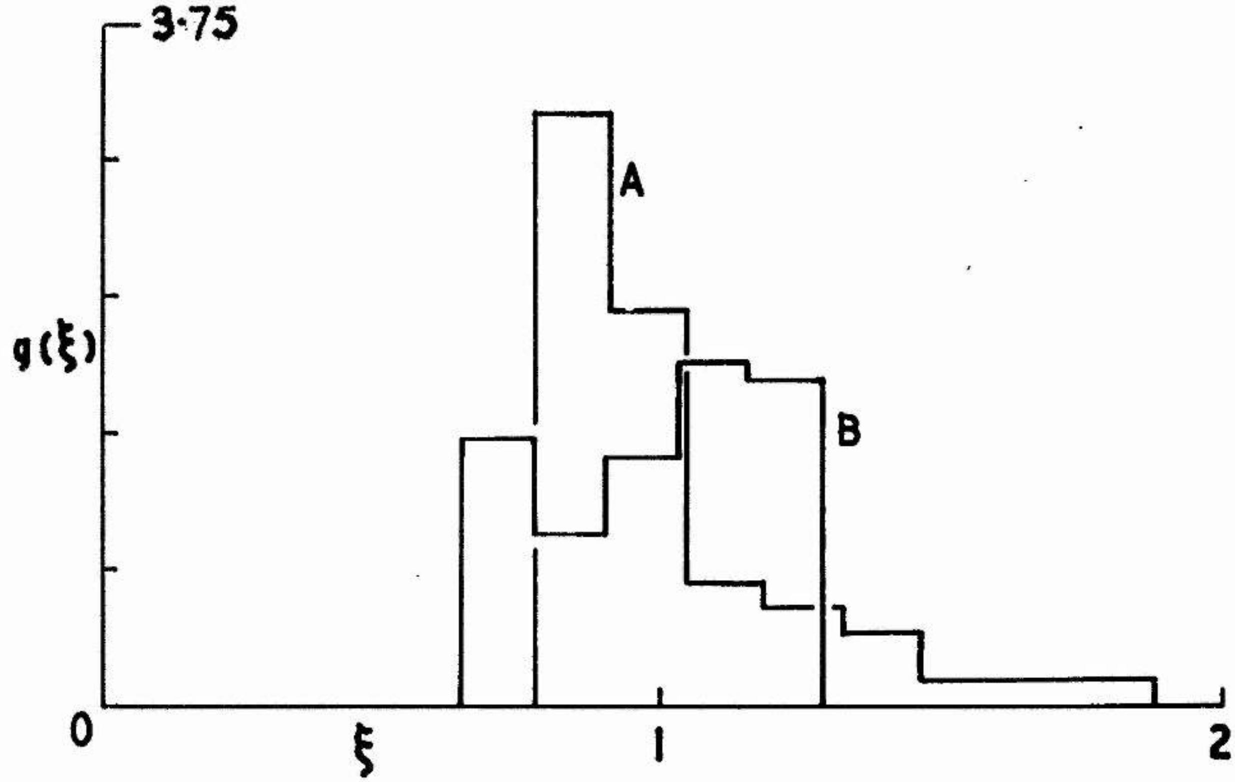

Figure 404

Relative abundance, g, of grains of different strength, $\xi\sigma_0$.

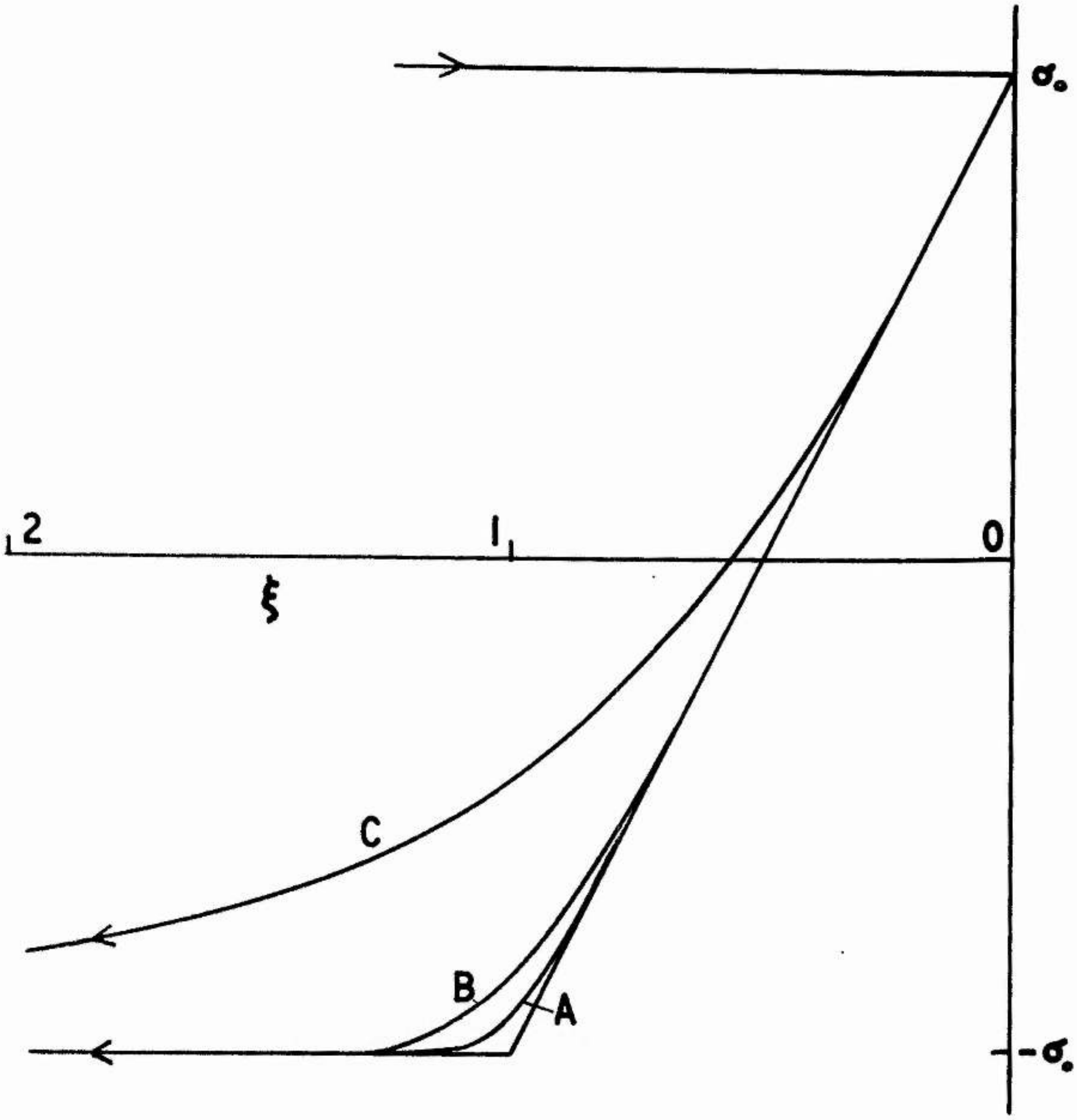

Figure 405

A - Bl curve calculated for grains laterally unconstrained.
B - Bl curve calculated for grains with same strain as aggregate.
C - Observed Bl curve.

where χ_0 and λ_0 specify the initial orientation of the tensile axis, and where $n = \frac{1}{2}$ for a parabolic law of work-hardening. Values of $(\sin \chi_0 \cos \lambda_0)^{-3/2}$ are plotted on a stereographic projection at 5° intervals and the mean value M_1 obtained. The ratio $(\sin \chi_0 \cos \lambda_0)^{-3/2}/M_1$ is then the value of ξ for the orientation $\chi_0 \lambda_0$. $g(\xi)$ is simply the relative frequency of the various values of ξ. The frequency distribution is shown in figure 404, curve A. It is given as a histogram owing to the limited number of points computed on the stereogram. From this and equation 1 the B1 curve can be calculated; this curve is shown in figure 405, curve A.

The B1 curve may be deduced in a similar way on the basis of Taylor's theory. Greenough writes $\sigma . \varepsilon = \tau_c \Sigma s$ where τ_c is the resolved shear stress, Σs the arithmetical sum of the five shears producing a strain in the grain equal to the overall strain in the specimen, σ the tensile stress and ε the extension. For a parabolically work-hardening material $\tau_c \propto \sqrt{\Sigma s}$, so that $\sigma \propto (\Sigma s)^{3/2}$. Taylor (1938, figure 13) gives values of Σs computed at 5° intervals over a stereographic projection. These are converted to $(\Sigma s)^{3/2}$ and the mean value M_2 calculated. The ratio $(\Sigma s)^{3/2}/M_2$ is the value of ξ for any given orientation. Figure 404, curve B, shows the relative frequency of various values of ξ, and figure 405, curve B, the stress-strain curve calculated from this with equation 1.

These models neglect the continuity of stress between adjacent grains. If we consider the model of figure 406 where stress continuity is preserved at the expense of uniform strain, it is easy to see that here there will be no Bauschinger effect, the B1 curve being linear and elastic between $+\sigma_0$ and $-\sigma_0$, whether the elements be ideal as in figure 402, curve A, or work-hardening as in figure 402, curve B. The real state lies between these two extremes, though probably nearer the case of uniform strain than of uniform stress. Thus curves A and B of figure 405 represent upper limits to the Bauschinger strain.

In comparing the predicted B1 curves with the experimental results, it must be noted that the former refer to tension-compression, while the latter refer to shear. This difference is not likely to affect the order of magnitude of the quantities involved. Figure 405, curve C, shows the observed Bauschinger strain, which is decidedly larger than that calculated. Thus we conclude that textural stresses alone are inadequate to explain the Bauschinger effect.

A further contribution to the Bauschinger strain arises in the following way. Consider a grain in an aggregate, initially fully annealed. Apply an increasing stress to the aggregate. When the stress is sufficiently high, plastic deformation first occurs in the grain by slip on the slip system with highest resolved shear stress. In general, this slip on one system alters the shape of the grain, this being opposed by the surrounding medium. Thus the plastic deformation is very limited until the stress rises to such a value that, together with the local restoring forces in the surrounding medium, it is sufficient to produce slip on two other slip-planes. The grain can now deform plastically without change of shape (other than a strain equal to the overall strain of the specimen). During a stress reversal a similar process occurs, but with doubled scale. The small plastic deformation which occurs while the stress is changed from the point where slip begins on only one plane to the point where slip begins on three planes, contributes to the Bauschinger effect. It has not proved possible, as yet, to make a satisfactory numerical estimate of this contribution. It is small if there are two or three slip planes making angles with the external stress not greatly different from 45°. This is usually satisfied in the case of the metals with cubic lattice.

IV(c) THE REARRANGEMENT OF DISLOCATIONS

According to Taylor (1934), work-hardening is attributed to the stress-system set up by dislocations distributed throughout the lattice. At some points this stress-system aids the motion of dislocations on a given slip system, and at other points opposes it. For substantial plastic flow to occur, an external stress must be applied which is larger than the mean opposed internal stress. Thus σ_0 is approximately equal to the mean absolute internal stress due to the system of dislocations. If the stress is reversed, we argue that the dislocations responsible for the internal stress-system will themselves move to new equilibrium positions, thus giving a Bauschinger strain, as below.

Let there be N edge dislocations per cc, each of length 1 cm.. Then these are separated by a mean distance $r = 1/\sqrt{N}$ and the yield stress is of order $\sigma_0 = Gb/2\pi r = Gb\sqrt{N}/2\pi$, where b is the Burgers vector. If a stress $-\sigma_0$ is now applied, the dislocations should take up new equilibrium positions and in doing so each will move a distance presumably of the same order as their mean distance apart. Thus the Bauschinger strain $\beta(-\sigma_0)$ is given by

$$\beta(-\sigma_0) = Nrb = b\sqrt{N}$$

Thus β/yield strain $= \beta G/\sigma_0 = 2\pi$.
Experimentally this ratio is about 8. This agreement is fortuitously good, as substantial approximations are made in this theory. It does show, however, that this mechanism is capable of contributing to the observed effect.

Mott (1952) has put forward an improved theory of work-hardening in terms of groups of n primary dislocations on slip planes a distance x apart which are terminated by barriers a distance 2L apart. If these dislocations are allowed to move a distance $R = \sqrt{Lx}$ during the Bauschinger strain, then the same expression $\beta(-\sigma_0) = 2\pi\,\sigma_0/G$ is obtained. R is the mean separation of the primary groups of piled-up dislocations, so this motion corresponds to a substantial rearrangement of the primary stress-field. Mott also considers small groups of n' secondary dislocations at a distance r from the primary groups, which relieve local strain

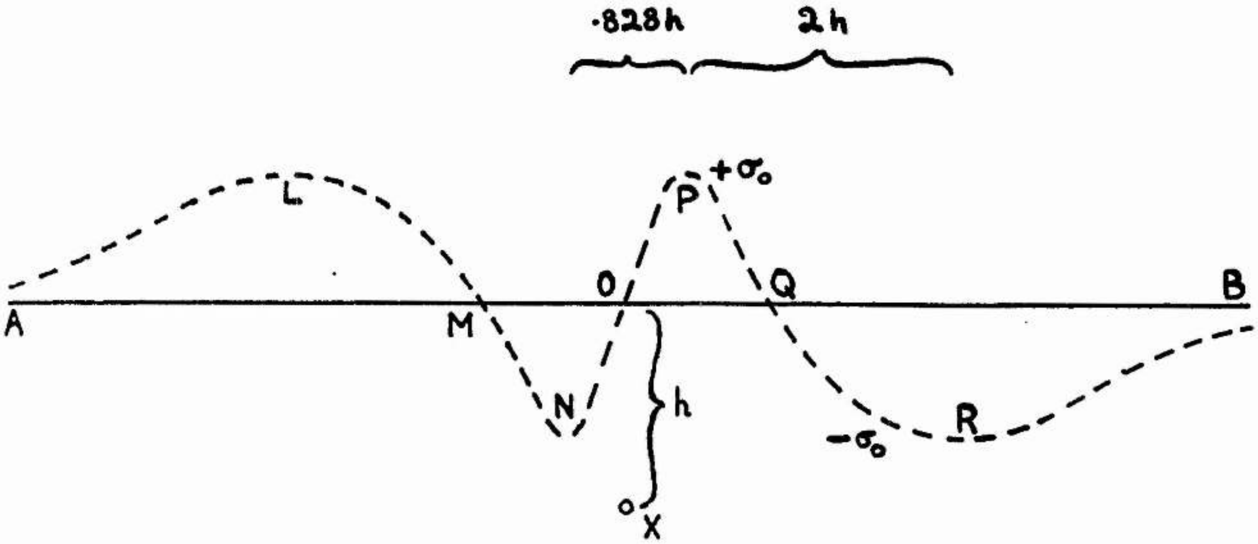

Figure 407
The horizontal component of the force between two dislocations (after Cottrell)

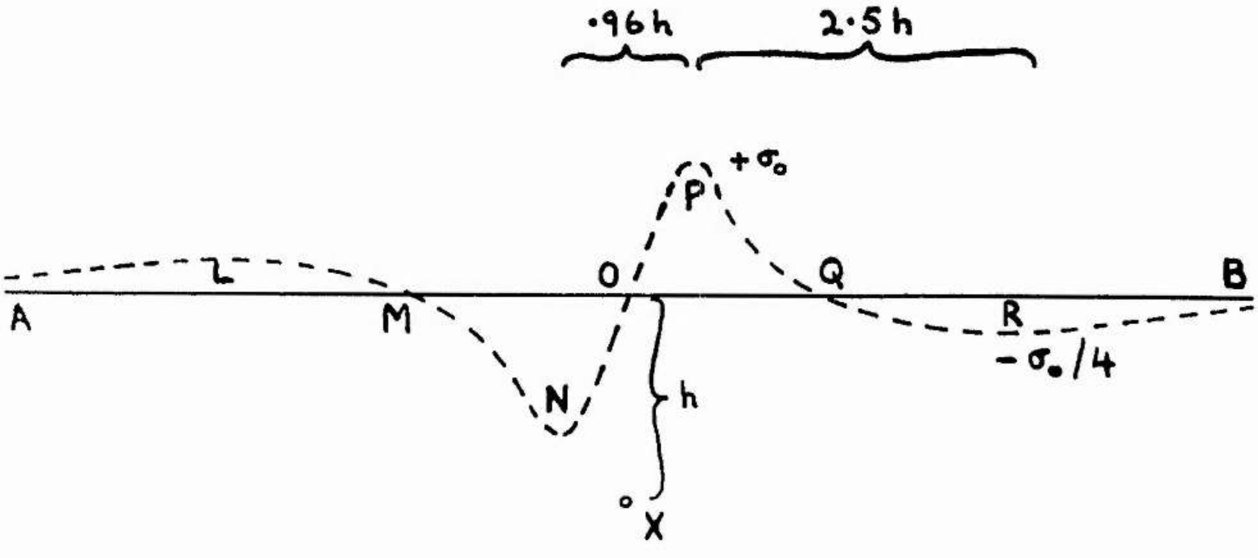

Figure 408
The horizontal component of the force between two dislocations (after Koehler)

by moving from sources a distance l apart ($\sim 10^{-4}$ cm) through a distance l . If these are able to move back when the applied stress is reversed, their contribution to the Bauschinger strain is

$$\beta(-\sigma_0) = \left\{(n'/l^2)lb\right\}_{mean}$$

Mott gives $n' = nl/2\pi r$

so $\beta(-\sigma_0) = nb/2\pi R = \sigma_0/G$

Thus the secondary dislocations can contribute to the Bauschinger strain, though rather less than do the primary dislocations.

IV(d) DISLOCATION-PAIRS

If a positive edge dislocation be fixed at X (figure 407) and a negative dislocation Y be free to move in the slip plane AB, a distance h from X, the force on Y parallel to AB is given by the sinusoidal dotted curve (Cottrell 1949). M and Q are positions of stable equilibrium in the absence of applied stress, while the regions AL, NOP and RB are unstable. We may use this model to calculate a Bauschinger effect, as follows.

On application of a suitably directed shear stress $+\sigma_0$, a dislocation initially at M or Q moves to L or P respectively; if a stress $-\sigma_0$ is applied, the dislocation moves to N or R. The stress required for this is $\sigma_0 = Gb/8\pi(1-\nu)h$ where G is the shear modulus, b is the Burgers vector, and ν is Poisson's ratio. Smaller stresses produce a smaller strain. Larger stresses disrupt the pair and carry Y off to infinity; σ_0 is thus the yield stress. When the stress is reversed from $+\sigma_0$ to $-\sigma_0$, Y moves a distance 2h along AB. If we had taken X and Y to be dislocations of the same sign, then NOP is the stable region, and the motion of Y when the stress is reversed is 0.828 h.

Let there be N cm of dislocation per cc. The mean separation of these is then $1/\sqrt{N}$. We arrange these dislocations in pairs by associating each with its nearest neighbour. There are thus N/2 pairs of dislocations, each 1 cm long. For want of any definite estimate we assume that half of these pairs are dislocations of like sign, and half of unlike sign. (In regions where the lattice is bent we should take them to be mostly of like sign). The mean separation of the two dislocations in any pair cannot exceed $1/\sqrt{N}$ and we take this to be the value of h. The plastic strain on reversal of stress from $+\sigma_o$ to $-\sigma_o$ is then $N/4.\ 2h.\ b$ due to the unlike pairs, and $N/4.\ 0.828h.\ b$ due to like pairs. This we identify with the Bauschinger strain

$$\beta(-\sigma_o) = \frac{2.828}{4}\,Nhb = 0.707b\sqrt{N}$$

The yield strain is

$$\theta_o = \sigma_o/G = b/8\pi(1-\nu)h = b\,N/8\pi(1-\nu)$$

The Bauschinger ratio is then

$$\beta(-\sigma_o)/\theta_o = .707 \times 8h(1-\nu) = 11.5$$

This is a little larger than the experimentally observed value of about 8. We have assumed that h takes its maximum value, $1/\sqrt{N}$. If we assume that all values of h between 0 and $1/\sqrt{N}$ are equally likely, then the Bauschinger ratio is reduced to 3.9. Thus this mechanism is capable of making a substantial contribution.

According to Koehler (1941) the stress exerted by one dislocation on another is as shown in figure 408. A like dislocation is stable on PON and contributes the same strain as in Cottrell's picture. An unlike dislocation which is at P when the stress is $+\sigma_o$ moves past R when the stress is reversed to $-\sigma_o$. If we suppose that this dislocation only goes as far as the next dislocation-pair, then it moves a distance a little larger than $1/\sqrt{N}$. Thus the Bauschinger strain is a little larger than that deduced on the basis of Cottrell's function, but is of the same order of magnitude.

Both these estimates of the Bauschinger ratio are in a sense special cases of the general case of rearrangement of dislocations treated in section IV(c).

IV(e) THE EXHAUSTION THEORY

It has been pointed out (Woolley, 1948) that the exhaustion theory as applied to creep (Mott, 1948) is capable of giving a Bauschinger effect, provided the reasonable assumption is made that the stress required to activate a dislocation might in some cases be direction-sensitive. Exhaustion alone is however not adequate to explain the effect, for it is clear that if a specimen is strained by a stress $+\sigma_0$ and then by $-\sigma_0$, all dislocations with activation-stress in this range should be exhausted, i.e. no longer available for plastic deformation in this stress range. Consequently the B2 curve should be linear and elastic between $-\sigma_0$ and $+\sigma_0$, which is contrary to what is observed. This conclusion holds whether the dislocations are regarded as originating at the grain boundaries as in the author's treatment, or at Frank-Read sources, as is now more generally supposed.

Some conclusions can be drawn from the shape of the B2 curves. In figure 209 at the point A there are no dislocations in the specimen capable of being activated or moved by a stress between 0 and $+\sigma_0$. At c, after the strain B1, the number of dislocations capable of being activated and moved by a stress between 0 and $+\sigma_0$ is such that their motion produces the strain B2, which is about 2/3 of B1. Thus at c either (i) the dislocations which moved during B1 have activated a slightly smaller number of other dislocations, and the B1 dislocations take no further part in the deformation, or (ii) about 1/3 of the dislocations which moved during B1 have become trapped and the remaining 2/3 simply move back when the stress is raised to $+\sigma_0$ again. The latter seems the more reasonable explanation. The same argument leads to the conclusion that no further substantial loss of dislocations by trapping occurs, the dislocations responsible for B2 also producing B3, B4 etc. Furthermore, in figures 205-7 it is seen that the B2 curves springing from between 0 and say $-3\sigma_0/4$

have the same amplitude as the preceding part of the B1 curve. We infer that in this case there is no loss of active dislocations. The loss of active dislocations which causes the strain amplitude of B2 to be less than that of B1 therefore takes place when the stress is near $-\sigma_0$. This is a reasonable conclusion, as the larger the stress the more easily some dislocations may be pushed into regions of distorted lattice from which they may not easily escape.

The B1 and succeeding B curves to a first approximation form closed hysteresis loops of twofold rotation symmetry. This implies that the external stress is needed not to activate the dislocations but to move them through a resisting lattice. For, suppose that the stress is required merely to activate dislocations, and that the lattice offers no resistance to a dislocation once it is activated and removed a small distance from its original anchorage. During the B1 strain a certain number of dislocations would be activated and would move at once a certain distance, this giving the B1 strain. Some of these are trapped as described in the above paragraph. Unloading would be fairly elastic, but as soon as the stress becomes positive the remaining dislocations would

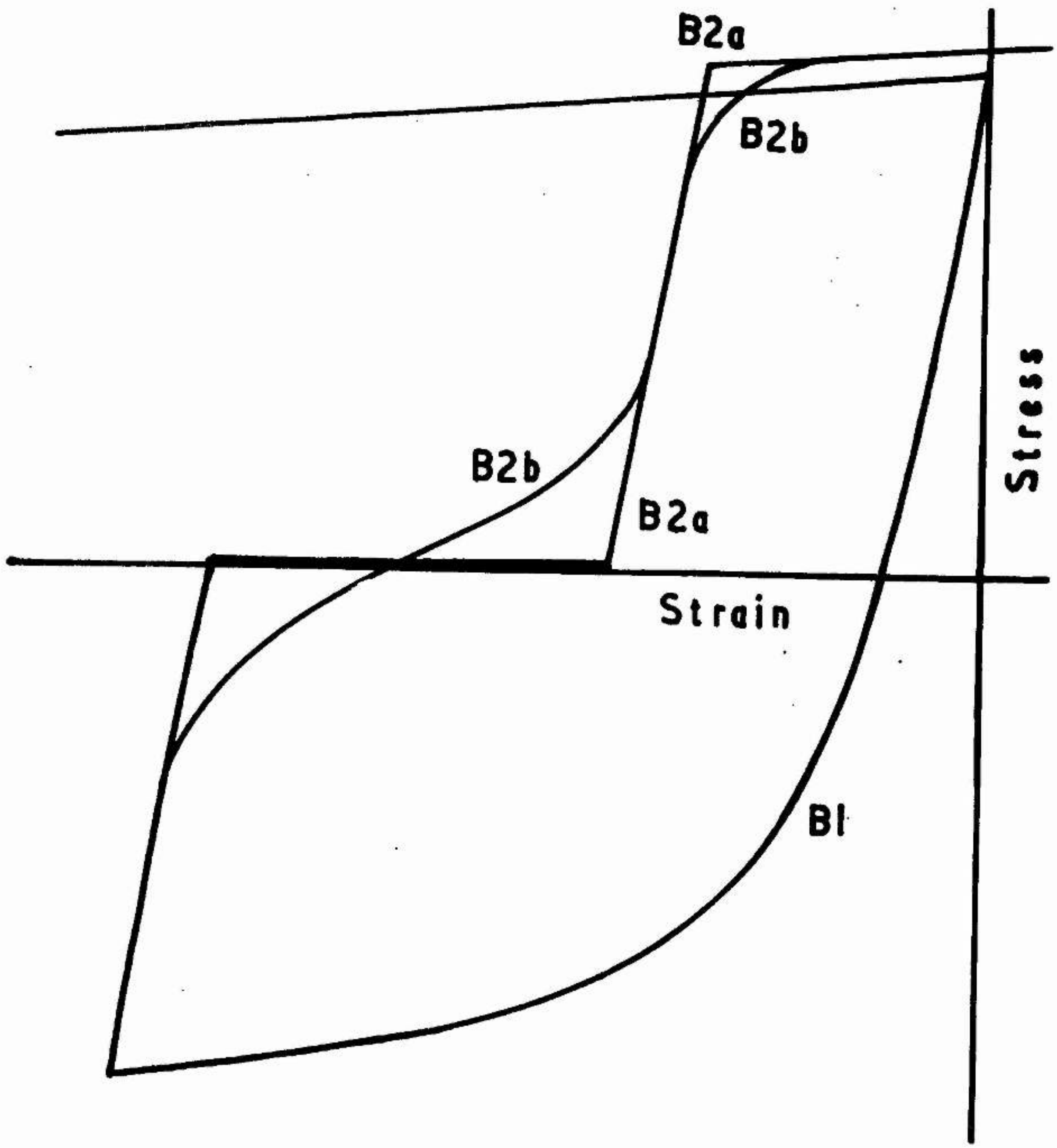

Figure 409

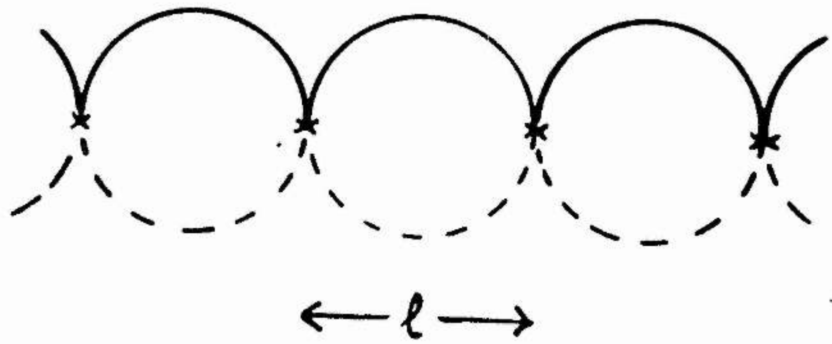

Figure 410

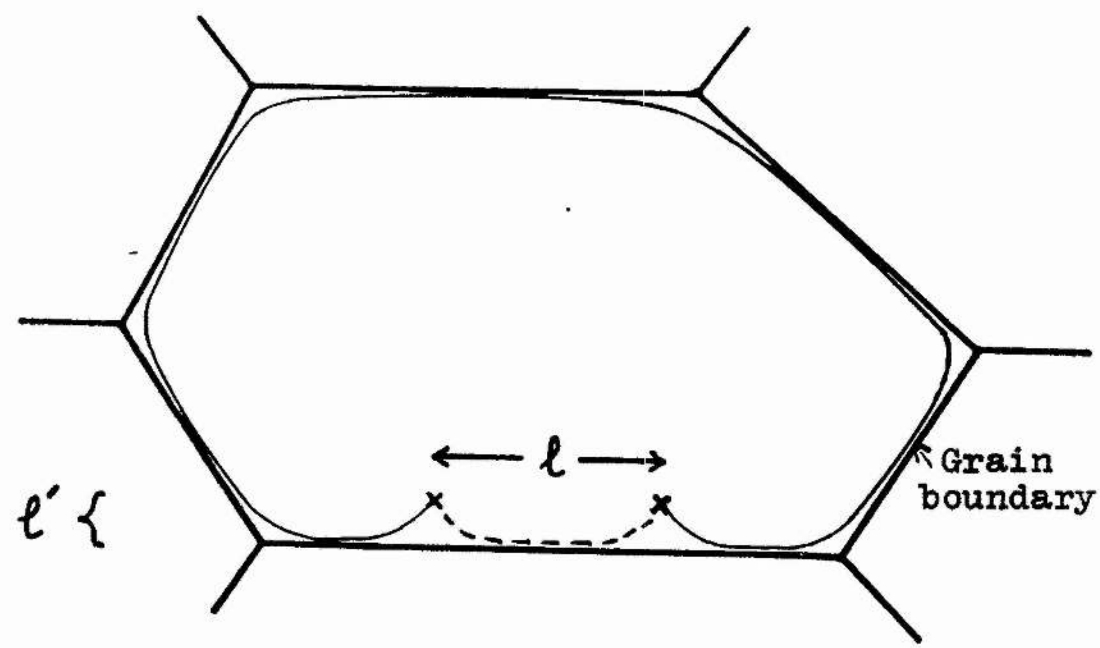

Figure 411

Contributions from Frank-Read sources.

immediately move back to their original positions, giving a B2 curve as in figure 409, curve B2a. Actually, textural stresses would probably cause the curve to be more like B2b. But neither of these curves is symmetrical to B1 or resembles the experimental B2 curve.

IV(f) FRANK-READ SOURCES

We reckon that there are at least two ways in which these can contribute to the Bauschinger effect.

In the first of these we consider a crystal containing a network of sources each of length ℓ. The yield stress is Gb/ℓ. When this stress is applied all the sources become semi-circles, as in figure 410 (full lines). If the stress is reversed the sources become semi-circles in the opposite direction (figure 410, broken lines). The strain associated with this motion is at most

$$\frac{1}{\ell^2} \cdot \pi \left(\frac{\ell}{2}\right)^2 \cdot b = \frac{\pi b}{4 \ell}$$

The yield strain is $\theta_0 = b/\ell$, so the Bauschinger ratio is $\pi/4$. This is decidedly smaller than the observed ratio of about 8.

A second way in which Frank-Read sources can contribute to the Bauschinger effect is seen when we consider a source inside a grain, as in figure 411. Let the length of the source be ℓ and its distance from the boundary be ℓ'. If $\ell' < \ell$ then one dislocation is generated when the external shear stress σ is suitably directed and $Gb/\ell' > \sigma > Gb/\ell$. This dislocation crosses the whole grain until it is held up by the small gap ℓ', as shown in figure 411, full line. If the stress had been oppositely directed, the dislocation would have moved to the position represented by the dotted line. If the grain diameter is L, then we calculate the Bauschinger ratio as follows.

Number of sources in volume ℓ^3	$= 1$
Surface area of one grain	$= 6L^2$
Number of sources within a distance of the grain boundary, per grain	$= 6L^2\ell \cdot \frac{1}{\ell^3} = 6\frac{L^2}{\ell^2}$
Number of ditto per cc	$= 6\frac{L^2}{\ell^2} \cdot \frac{1}{L^3} = \frac{6}{L^2\ell}$
Area each dislocation moves	$= L^2$
Bauschinger strain	$= \frac{6}{L^2\ell} \cdot L^2 b = \frac{6Lb}{\ell^2}$
Yield strain	$= b/\ell$
Bauschinger ratio	$= 6L/\ell$

This result indicates an effect which is proportional to grain size, and therefore disagrees with the results of section II. In any case it is likely that this mechanism would only apply in the early stages of deformation, when the grains are relatively perfect.

IV(g) GRAIN-BOUNDARY SLIP

In a stressed polycrystalline aggregate the applied stress produces a set of shear stresses across the grain-boundaries. Ke (1947) has put forward experimental evidence that at elevated temperatures the grain boundaries slip over each other until these shear stresses are relaxed, in accordance with the theory of Zener (1941). Such slip takes place below the conventional elastic limit, and is not observed at room temperature where the effective viscosity of the grain boundaries is far too high. It produces an extra strain equal to 50% of the true elastic strain.

During plastic deformation, however, many dislocations arrive at the grain boundaries, and it seems possible that these would activate local slip in the neighbourhood of the grain boundaries and relax all or part of the shear stress system responsible for the Ke-Zener effect.

Grain-boundary slip alone cannot explain the Bauschinger effect, as at low temperatures such slip can only occur as a concomitant of plastic deformation produced by some other mechanism. Besides this, the maximum strain it can contribute is only 50% of the yield strain, while the observed Bauschinger strain is about 8 times the yield strain.

IV(h) THE GENERATION OF VACANCIES AND INTERSTITIAL ATOMS

We reckon that the generation of defects by the intersection of screw dislocations may make a small contribution to the Bauschinger effect, as follows.

Seitz (1952) has pointed out that during plastic deformation if a screw dislocation A crosses the axis of another screw dislocation B, a jog is formed in each dislocation and a line of vacancies or interstitial atoms is left behind, joining the two dislocations. An extra force is required to move A, because energy must be supplied to increase the length of the line of defects. Correspondingly, if the direction of strain is reversed, a reduced force should be required to move A back toward B, because energy is obtained by shortening the line of defects. This gives a Bauschinger effect. The effect is very limited however, for two reasons.

Seitz points out that these lines of vacancies or interstitial atoms are unstable at room temperature, and the defects diffuse together to form sheets, which cause less disturbance to the lattice. Also, Mott (1952) points out that the motion of a set of dislocations A_1 A_2 A_3 ... on the same slip plane crossing B generates a sheet of vacancies or interstitials direct, even at low temperatures. No Bauschinger effect is to be expected if the lines of defects are removed by the formation of sheets.

We conclude that vacancy mechanisms do not contribute appreciably to the Bauschinger effect, but we note that some vacancies or interstitial atoms, not lying in a sheet, are generated when the leading screw dislocation of a slip avalanche cuts another screw.

Edge dislocations crossing a screw do not produce lines of vacancies or interstitial atoms. Pure edge dislocations are rare, however, the average dislocation consisting presumably of equal screw and edge elements, so the remarks about screw dislocations, above, are essentially applicable to all dislocations.

IV(j) DISCUSSION

In section IV we have put forward various mechanisms which may contribute to the Bauschinger effect. The contribution of textural stresses has been estimated and shown to be inadequate to explain the observed effect in polycrystalline metals of cubic lattice. Various mechanisms based on the rearrangement of dislocations are found to predict an effect about the size of that actually observed. It is possible that several of these mechanisms are simultaneously active in the Bauschinger effect. Some of these mechanisms could operate in single crystals (see section VII). No discussion of the detailed shape of the Bauschinger curve is offered.

The theory of work-hardening itself not yet being in a satisfactory state, it is difficult to suggest which mechanisms are chiefly responsible for the Bauschinger effect. It would be a very desirable thing if crucial experiments could be devised to distinguish between the contributions of the mechanisms proposed.

V.

THERMOELECTRIC POWER AND THE BAUSCHINGER EFFECT

V(a) INTRODUCTION

Comparatively little experimental or theoretical work has been carried out on the thermoelectric properties of plastically deformed metals. Crussard (1948) gives references to earlier work, and points out that it is important that the plastic deformation should be macroscopically homogeneous, processes such as drawing and rolling being unsatisfactory owing to the high surface strain. He determines the thermoelectric power of various metals after plastic extension, and also gives one result for the plastic torsion of a solid rod. He discusses the origin of the plastic component of the thermoelectric power, and attributes it tentatively to dislocations.

Crussard's observation that elastic shear produces no change of thermoelectric power suggested to the present author a semi-quantitative theory of the contribution of cold work to the thermoelectric power. This theory is outlined in sections V(b) and V(c). It also seemed worth while investigating experimentally the change of thermoelectric power when the direction of plastic strain is reversed.

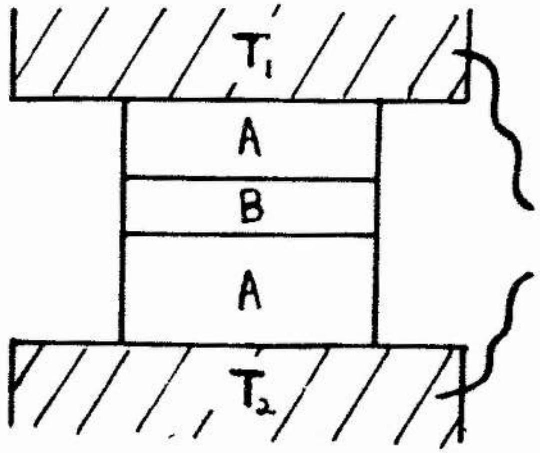

Figure 501
Grains in series

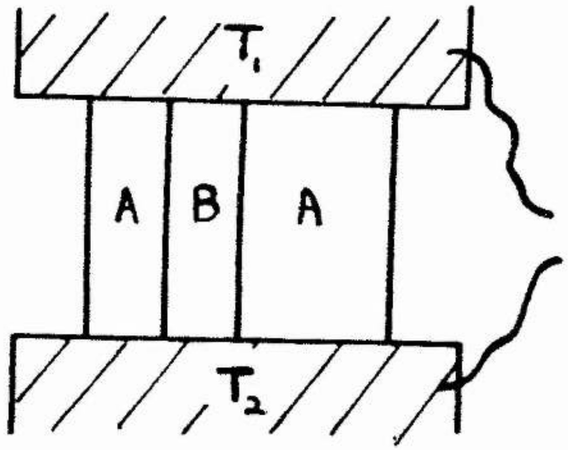

Figure 502
Grains in parallel

T_1 and T_2 are at different temperature

Experiments with copper are described in sections V(d) and V(e), and are discussed in V(f), where it is concluded that the results support the suggestion of section IV that the Bauschinger strain is due to a rearrangement of dislocations already present in a work-hardened metal.

V(b) THE THERMOELECTRIC POWER OF AN AGGREGATE

Consider a set of grains in series, as in figure 501, or in parallel, as in figure 502. If the thermal and electrical conductivities of the grains A and B are equal but their thermoelectric powers are E_A and E_B respectively, then the thermoelectric power of the aggregate is

$$(1-v)E_A + vE_B$$

where v is the fraction of the total volume occupied by B. Masing (1926) gave an elementary derivation of this result for the case in which the grains B are distributed anywhere in the material A. The present author, not being at the time aware of Masing's treatment, deduced a different proof of this result. This proof is given below as it is mathematically more elegant than Masing's proof, though adding little of interest from a purely physical

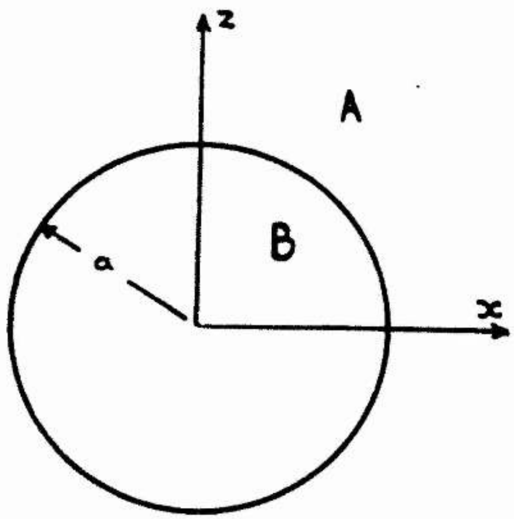

Figure 503
Sphere B embedded in A

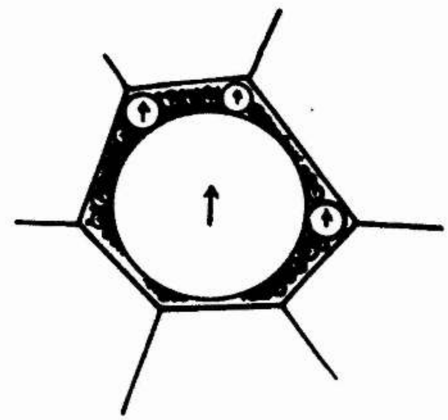

Figure 504
Grain dissected into spheres, each equivalent to a dipole.

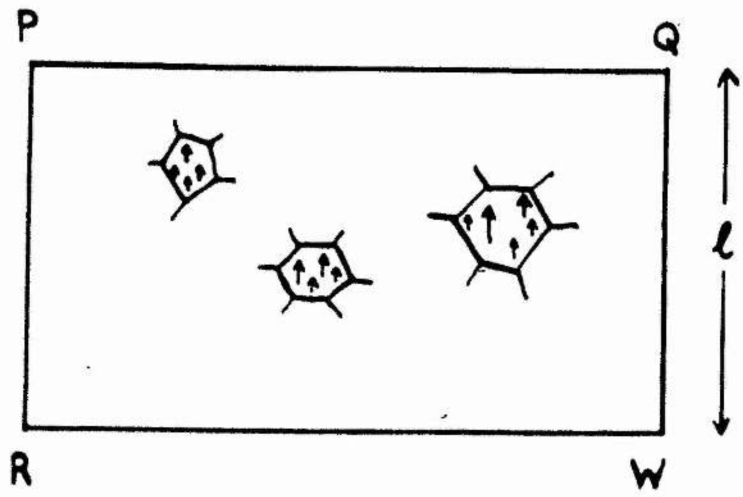

Figure 505
Grains of B replaced by dipoles

viewpoint.

Consider first a sphere of metal B of radius a, embedded in metal A, as in figure 503. Both metals have the same thermal conductivity and electrical resistivity. The heat flow is parallel to the z axis and the isothermals parallel to the xy plane. To calculate the change of effective thermoelectric power produced by the introduction of the sphere B it suffices to take the Thomson e.m.f. per unit temperature difference in A as zero, and the Thomson e.m.f. of B relative to A as s. The current-density $\underline{j}_A$ in A is then given in terms of the potential V_A and the electrical resistivity ρ by

$$\rho \underline{j}_A = -\mathrm{grad}\ V_A \qquad (1)$$

If we consider an element of length $d\underline{r}$ in B, then we have

$$\underline{d}V_B = -\rho j_x dx,\ -\rho j_y dy,\ (-\rho j_z + F)dz$$

or

$$\rho \underline{j}_B = -\mathrm{grad}\ V_B + F\underline{i}_z \qquad (2)$$

where Fdz is the increment of Thomson e.m.f. per unit length in the z direction ($F = s dT/dz$), and $\underline{i}_z$ is unit vector in the z direction. Since there is no accumulation of charge, we have

$$\mathrm{div}\ \underline{j}_A = 0 = \mathrm{div}\ \underline{j}_B \qquad (3)$$

At the surface separating the two media we have a Peltier e.m.f. p, which can be taken as zero at $z = 0$ and increases linearly with z. Thus $p = kz$ where $k = dp/dT \cdot dT/dz$, and so

$$V_A - V_B = kz = ka.\cos\theta \quad \text{on} \quad r = a \qquad (4)$$

Since there is no accumulation of charge on the surface of separation, the radial component of j is continuous, i.e.,

$$\frac{\partial V_B}{\partial r} - F\cos\theta = \frac{\partial V_A}{\partial r} \quad \text{on} \quad r = a \qquad (5)$$

The general solution of equations 1, 2 and 3 is

$$V_A = \Sigma \frac{An}{r^{n+1}} \cdot P_n (\cos\theta)$$

and $$V_B = \Sigma B_n r^n P_n (\cos\theta)$$

Equations 4 and 5 determine the values of A and B leading to

$$V_A = \frac{F+k}{3} \cdot \frac{a^3 z}{r^3} \qquad (6)$$

$$V_B = \frac{F-2k}{3} z \qquad (7)$$

Equation 6 shows that the sphere is equivalent to a dipole placed at O, of strength

$$\mu = \frac{1}{3}(F + K)a^3 = \frac{F + K}{4\pi}\ \frac{4}{3}\pi a^3 \qquad (8)$$

Because of the linearity of equations 1 to 8, the principle of superposition applies. The grains of the aggregate can therefore be dissected into a set of spheres, and each replaced by its equivalent dipole, as in figure 504. To evaluate the mean potential across a surface such as PQ, in figure 505, we consider first the contribution from any one dipole, which we take as origin. If dS be an element of area on PQ then

$$\int_{PQ} V\,dS = \int_0^\infty \frac{\mu z}{r^3}\cdot 2\pi x\,dx = 2\pi\mu \qquad (9)$$

Similarly, $\int_{RW} V\,dS = -2\pi\mu$

If the area PQ is S and the distance PR is l, then the mean potential between PQ and RW is

$$V_{PR} = 4\pi(\Sigma\mu)/S$$

where $\Sigma\mu$ is the total dipole moment in the volume PQRW. But from equation 8,

$$\Sigma\mu/S = \frac{F + K}{4\pi}\left(\Sigma\frac{4}{3}\pi a^3\right)/S = \frac{F + K}{4\pi}\,l\,\sigma$$

where v is the fraction of the total volume occupied by B.

Thus $V = (F + k)\ell v$ (10)

But $F = s\,dT/dz$ and $k = dp/dT . dT/dz$, so

$$V_{PR} = (s + dp/dT)\Delta T . v$$

But $s + dp/dT$ is the thermoelectric power of B relative to A, and equals $E_B - E_A$.

Thus the thermoelectric power of an aggregate of $1 - v$ parts by volume of A and v parts of B is

$$E = E_A + V/\Delta T = E_A + (E_B - E_A)v$$

$$= E_A (1 - v) + E_B v$$

which is the required result.

This can obviously be extended to include the case of an aggregate of v_A parts by volume of A, v_B of B, v_C of C, and so on. The observed thermoelectric power will then be

$$E = E_A v_A + E_B v_B + E_C v_C + \ldots\ldots$$

V(c) A THEORY OF THE THERMOELECTRIC POWER OF A COLD-WORKED METAL

The ideal theory of the change of thermoelectric power due to plastic deformation would involve a detailed knowledge of the actual distribution of lattice defects in the metal and a quantum theoretical treatment of their contribution to the thermoelectric power. Neither of these requirements can at present be met.

An approach to the problem may be made from Crussard's experimental observation that tensile stresses in the elastic range produce a proportional change of thermoelectric power, while shear stresses, being resoluble into equal tensile and compressive components, produce no effect. Thus in a uniformly elastically stressed medium the change of thermo-electric power is proportional to the change of density, $\Delta E = \alpha \Delta \rho$. If the distribution of elastic stress is non-uniform, then there are corresponding local variations of density and thermoelectric power. If the accompanying changes of electrical and thermal conductivity are small we may apply the results of section V(b). The thermoelectric power due to the stresses is then given by

$$\Delta E = \int \alpha . \Delta \rho . \, dV = \alpha \overline{\Delta \rho}$$

where $\overline{\Delta \rho}$ is the mean change of density produced by the elastic deformation, averaged over the whole volume.

The defects present in large numbers in a plastically deformed lattice are dislocations, vacancies and interstitial atoms. Each of these defects has a <u>core</u>, usually about one atom across, in which there are large strains and Hooke's law is not obeyed, and a surrounding <u>stress field</u>, in which the strains are smaller and Hooke's law is obeyed. The contribution of the stress field to the thermoelectric power can be calculated by estimating the mean change of density. The contribution made by the core of a defect is not so easy to estimate, but it is likely that it is of the same sign as the contribution from the stress field, and probably smaller, because the core of the defect is small.

(i) Edge dislocations

. Calculations of the stress field of an edge dislocation by Nabarro (1947) and Koehler (1941) show that the increase of density at any given point above the slip plane is matched by an equal decrease at the corresponding point below the slip plane. Thus in first-order theory, edge dislocations contribute nothing to the thermoelectric power.

(ii) Screw dislocations

The stress field of a screw dislocation is entirely shear, to first order, so these also contribute nothing to the thermoelectric power.

(iii) Interstitial atoms

The stress field of an interstitial atom is such that the density is everywhere increased, and there is therefore a first-order contribution to the thermoelectric power. If there are N_i interstitial atoms per cc, the mean increase of density is mN_i and the thermoelectric power increases by $\alpha m N_i$, where m is the mass of one atom.

(iv) Vacancies

Though a vacancy and an interstitial atom neutralise each other if they diffuse together, they are separately not complementary in their effect on the lattice. A vacancy produces a smaller effect than an interstitial atom, because adjacent atoms do not have to move to make room for a vacancy. The obvious extreme analogy is that it creates very little disorder if one brick is removed from a brick wall, but considerable disorder is produced by the insertion of an extra brick. In this connection it is important to note that the density-change which appears in the thermoelectric equation is the density-change produced by local elastic strains, and does not include any change of macroscopic density due to the formation of voids. Thus it corresponds more to the lattice strain measured by X-ray diffraction, rather than to a density change measured by taking the ratio of the total mass to the total volume.

It appears then that an interstitial atom produces a larger thermoelectric power than does a vacancy or one atom-length of dislocation. The observed thermoelectric power depends on the relative numbers of these three classes of defect.

From Crussard's results it is seen that the sign of the plastic component of the thermoelectric power is opposite to that produced by elastic tension. This therefore corresponds to an increase of true density and thus may be attributed to interstitial atoms. We may estimate their number by calculating α from Crussard's results. A tensile stress of 1 kg/mm^2 gives an elastic contribution to the thermoelectric power of -7×10^{-10} volt/deg. The change of density is

$$\Delta\rho = -\rho(1-2\nu)\sigma/Y = -2.2 \times 10^{-4} \text{ gm/cc}$$

where Y is Young's modulus and ν is Poisson's ratio. Thus

$$\alpha = \Delta E/\Delta\rho = 3.2 \times 10^{-6} \text{ volts/deg per gm/cc.}$$

The mass of a copper atom is 11×10^{-23} gm.

At a plastic strain of 10% the thermoelectric power is about 2.5×10^{-9} volt/deg. This gives

$$N_i = \Delta E/dm = 7 \times 10^{18} \text{ per cc.}$$

This shows reasonable agreement with Seitz' (1952, p 46) rough estimate of 1.6×10^{18} vacancies or interstitials per cc.

However, the fact that an interstitial atom is surrounded by a stronger stress field than is a vacancy, is itself an argument that fewer interstitial atoms than vacancies will be formed. The theory outlined above can be criticised from this viewpoint, and further theoretical and experimental information is desirable.

V(d) APPARATUS

The change of thermoelectric power after cold working is not large, and in the present experiments interest centres on the change of thermoelectric power during the relatively small Bauschinger strain. The usual method of measuring the change of thermoelectric power on cold working is to measure the e.m.f. set up in a thermocouple consisting of

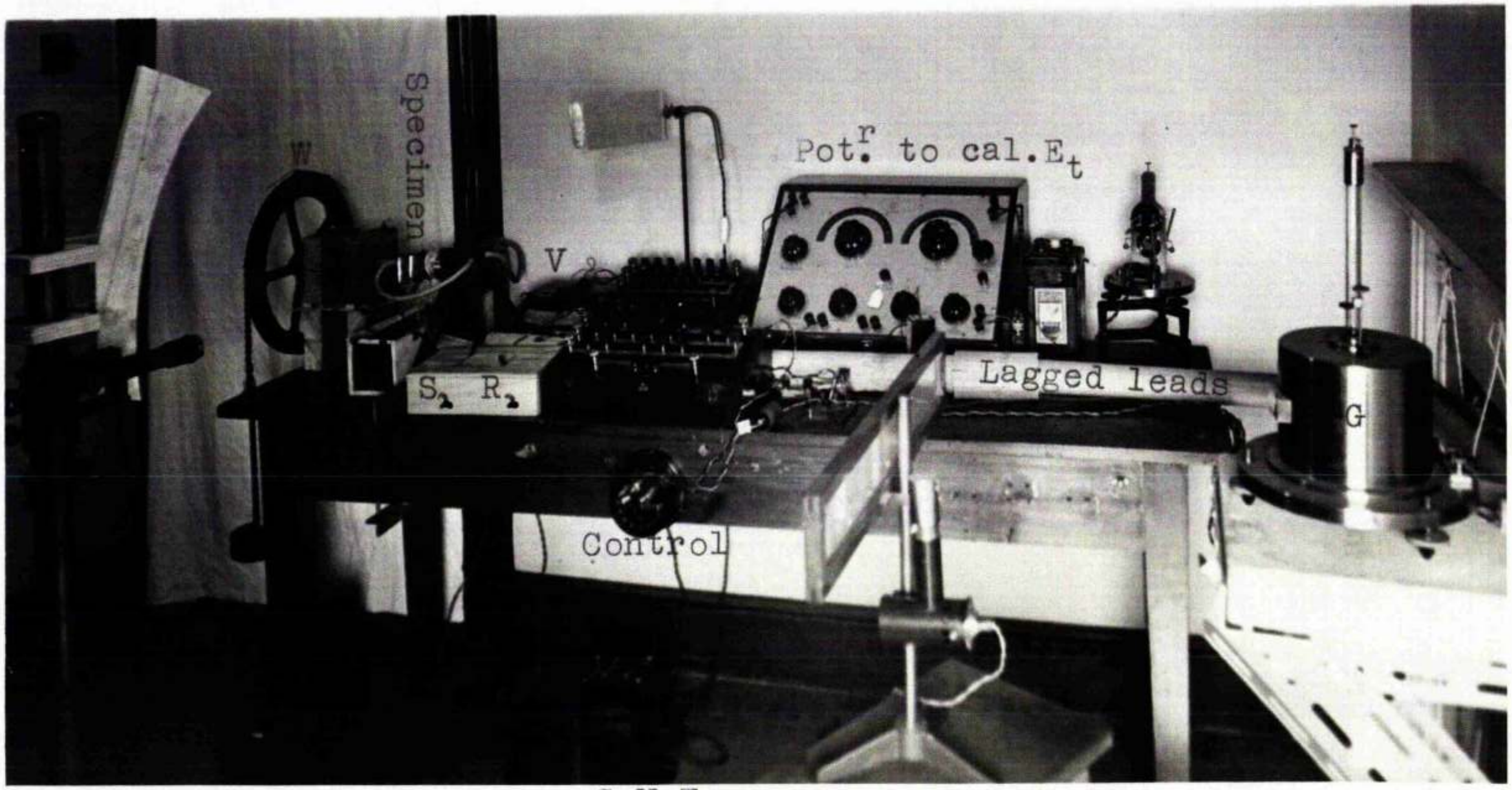

Figure 506. General view of apparatus for measuring thermoelectric power

65

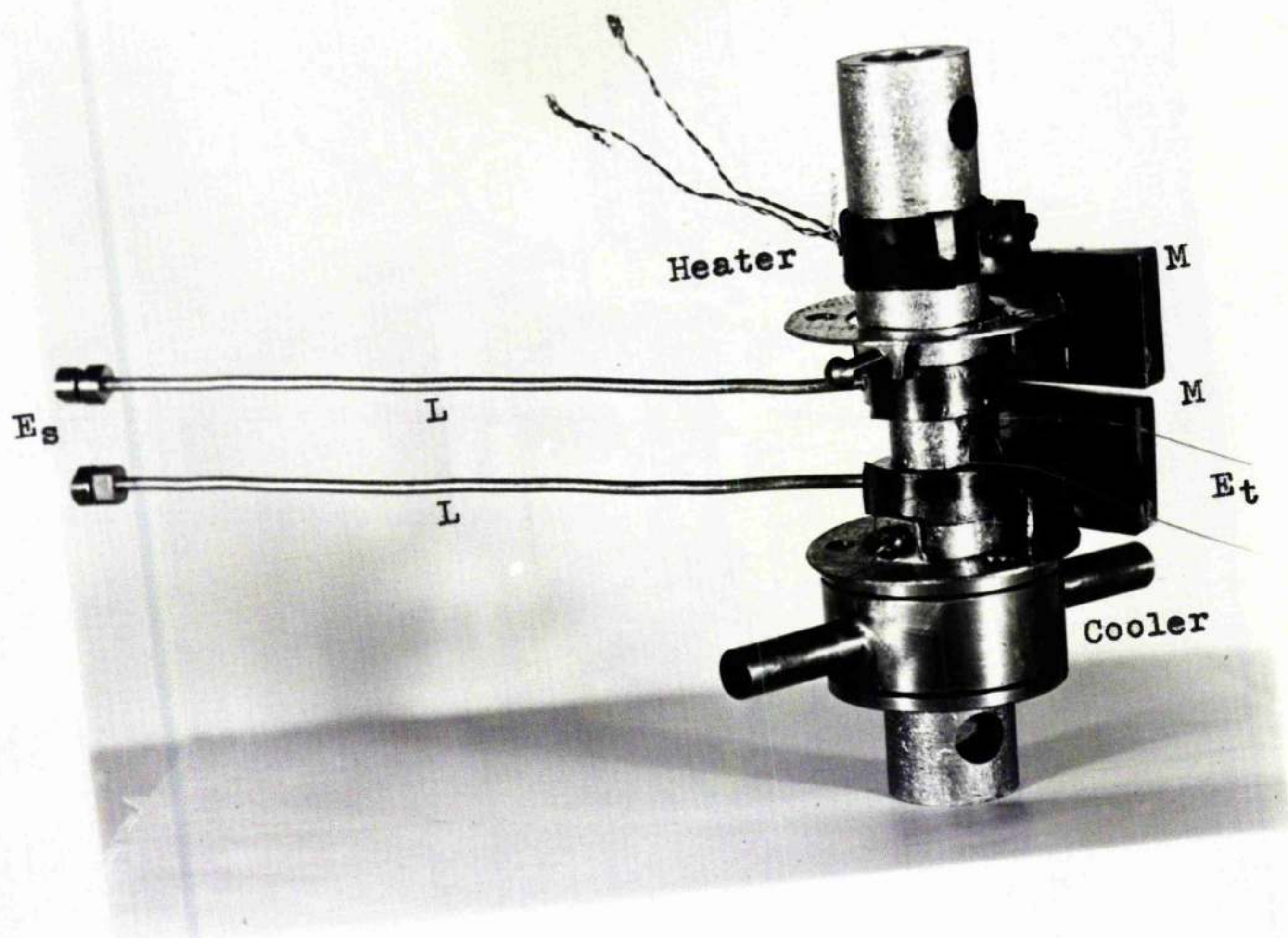

Figure 507
Specimen assembly for
thermoelectric power measurements

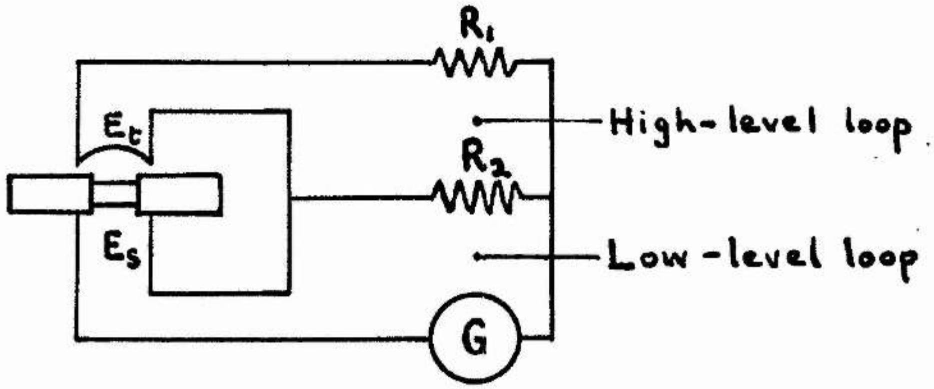

Basic circuit

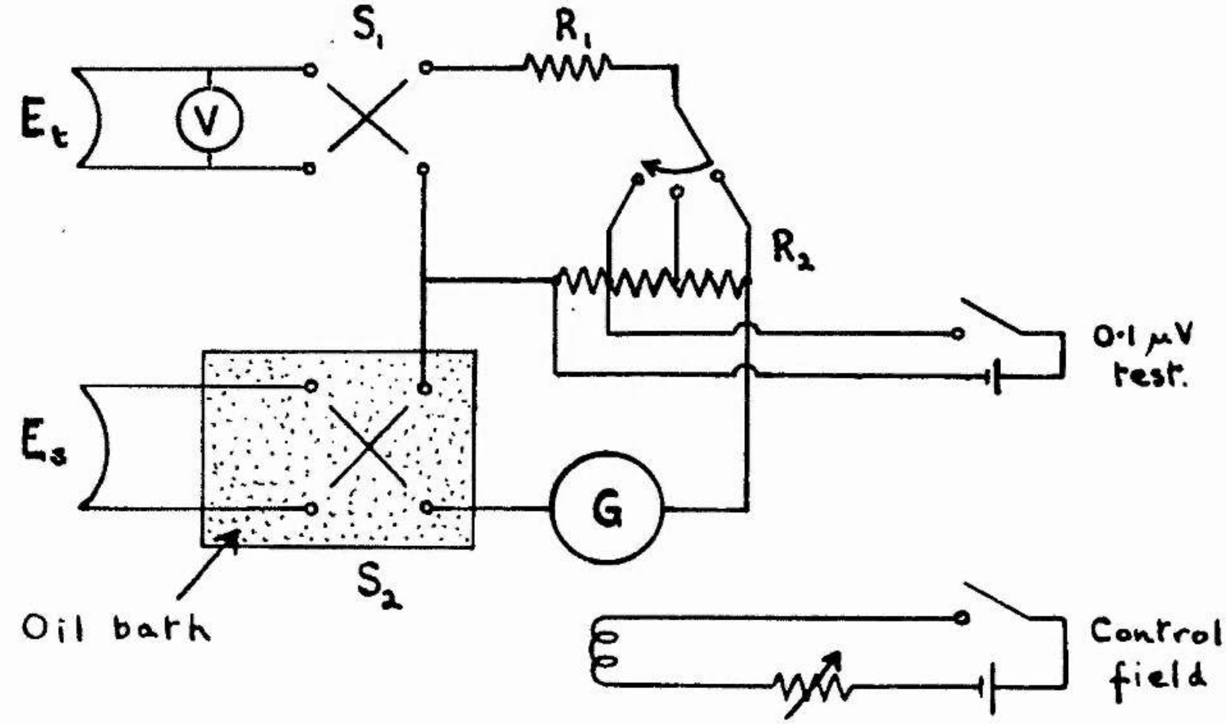

Actual circuit

Figure 508

the cold-worked metal and a standard metal, and at the same time to measure the temperature difference with an independent circuit. This method did not appear to offer sufficient accuracy, and so a null method was employed, in which the thermal e.m.f. of the specimen was compared with the e.m.f. of a standard thermocouple working between the same temperatures.

Views of the apparatus are shown in figures 506 and 507, and the circuit in figure 508. Thick copper leads L are attached to the ends of a standard specimen of 1/16" wall thickness, forming the <u>specimen couple</u> whose thermoelectric power is denoted by E_s. One end of the specimen is heated electrically, and the other end cooled in a current of tap-water. A copper-constantan couple, the <u>temperature couple</u>, E_t, is in thermal contact with the specimen, although electrically insulated from it. When the galvanometer G reads zero, then

$E_s = R_2 E_t/(R_1 + R_2)$.

For high accuracy it is important to avoid the effect of stray thermal e.m.f. This can be achieved in accordance with the following principles.

(i) As far as possible the whole circuit, apart from the thermocouples, must be kept at one temperature. The room was therefore provided with thermostatically controlled electric heaters, which maintained the temperature uniform and constant to $\pm \frac{1}{2}$ C°.

(ii) The low-level loop (figure 508) comprising G, R_2, the specimen couple and the associated wiring, was constructed entirely of copper, with copper terminals at junctions, solder and other metals being completely excluded. Residual stray e.m.f. in this loop is due to the copper in various parts of this circuit being of different purity and hardness; this stray e.m.f. may amount to more than the change of e.m.f. to be measured. The high-level loop is less critical, and a manganin box is used for R_1.

(iii) Since stray e.m.f. cannot be avoided it is essential to keep it constant. This was achieved by substantial lagging and thermal shielding of all important leads and components, to give an estimated thermal time constant of at least 30 minutes.

(iv) Switching is to be avoided in the low-level circuit, as this introduces variable stray e.m.f. For this reason the setting of R_2 is chosen beforehand, and balance obtained on R_1.

(v) Ideally the effect of stray e.m.f. could be eliminated completely by finding a value for R_1 for which the galvanometer deflection is unchanged when the temperature difference is altered. This method is not of use in the present experiments, for two reasons. Firstly it takes about 10 minutes for the specimen to settle down after a change of heat input, so it is unduly slow. Secondly, the second-degree dependence of thermal e.m.f. on temperature ($e = at + bt^2$) is different for the two couples and so the value of R_1 for balance is slightly dependent on the temperature difference, unless E_s or the temperature difference is very small.

(vi) The procedure finally adopted was to find a value of R_1 which was unchanged on simultaneous reversal of S_1 and S_2. This eliminates stray e.m.f. in R_1, R_2, G and the associated wiring. S_2 is made of annealed copper and is connected direct to the specimen couple, these leads and S_2 being immersed in a continuously-stirred oil-bath, so no stray e.m.f. is anticipated here. S_1 is also made of annealed copper, and should introduce negligible stray e.m.f. in the high level loop. No compensation is provided for stray e.m.f. in the leads from the temperature couple to S_1, and in the millivoltmeter V ; estimates of the magnitude of stray e.m.f. here show that it may be neglected.

The galvanometer G is a Paschen galvanometer with 3-ohm coils connected in series-parallel. An extra auxiliary coil system was fitted to provide an additional control field, to reduce the sensitivity without altering the positions of the control magnets or switching in extra resistance into the low level loop. This is very convenient when finding a rough balance. The sensitivity was usually 500 mm/μV. An external voltage of 0.1 μV was available to check the sensitivity if desired.

The temperature difference of about 20 C° across the specimen was obtained by heating one end electrically and cooling the other with a stream of tap-water. The heat input was derived from the A.C. mains and was maintained nominally constant with a constant-voltage transformer. Slow variations of up to ± ½ degree were however observed. These

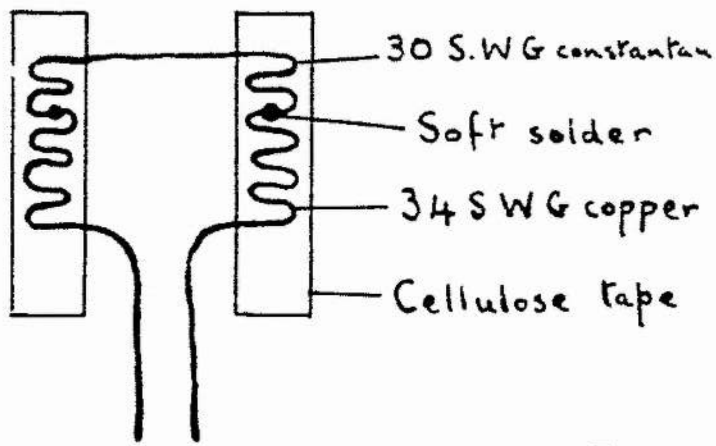

Fig.509. Temperature couple

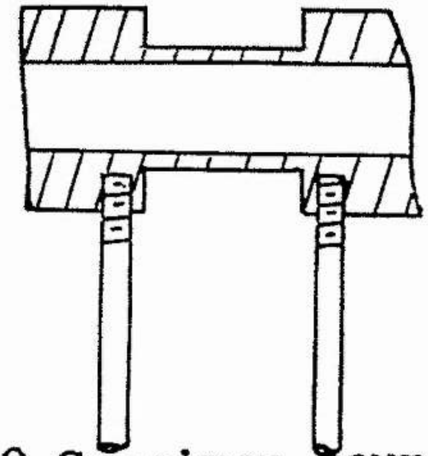

Fig.510 Specimen couple

were attributed (i) to variations in the temperature of the cooling water, coupled with the 10 minute thermal inertia of the specimen, and (ii) to poor frequency stability of the A.C. supply, impairing the performance of the constant-voltage transformer. As mentioned above, the balance value of R_1 depends slightly on the temperature difference; a small correction was therefore applied to take account of the variation of temperature.

The temperature couple junctions were soft soldered, bent into the form shown in figure 509, insulated with cellulose tape, pressed in contact with the ends of the specimen by a pair of springy copper hoops, and lagged with felt. Preliminary tests had shown that this could record the temperature difference across the specimen to an accuracy of about 0.1%.

The specimen couple was constructed by tightly screwing two copper rods into threaded blind holes drilled in the walls of the ends of the specimen, as in figure 510. The assembly was annealed for one hour at 980°C during which time the threads at the junctions became firmly sintered together. The lower ends of these rods were also threaded,

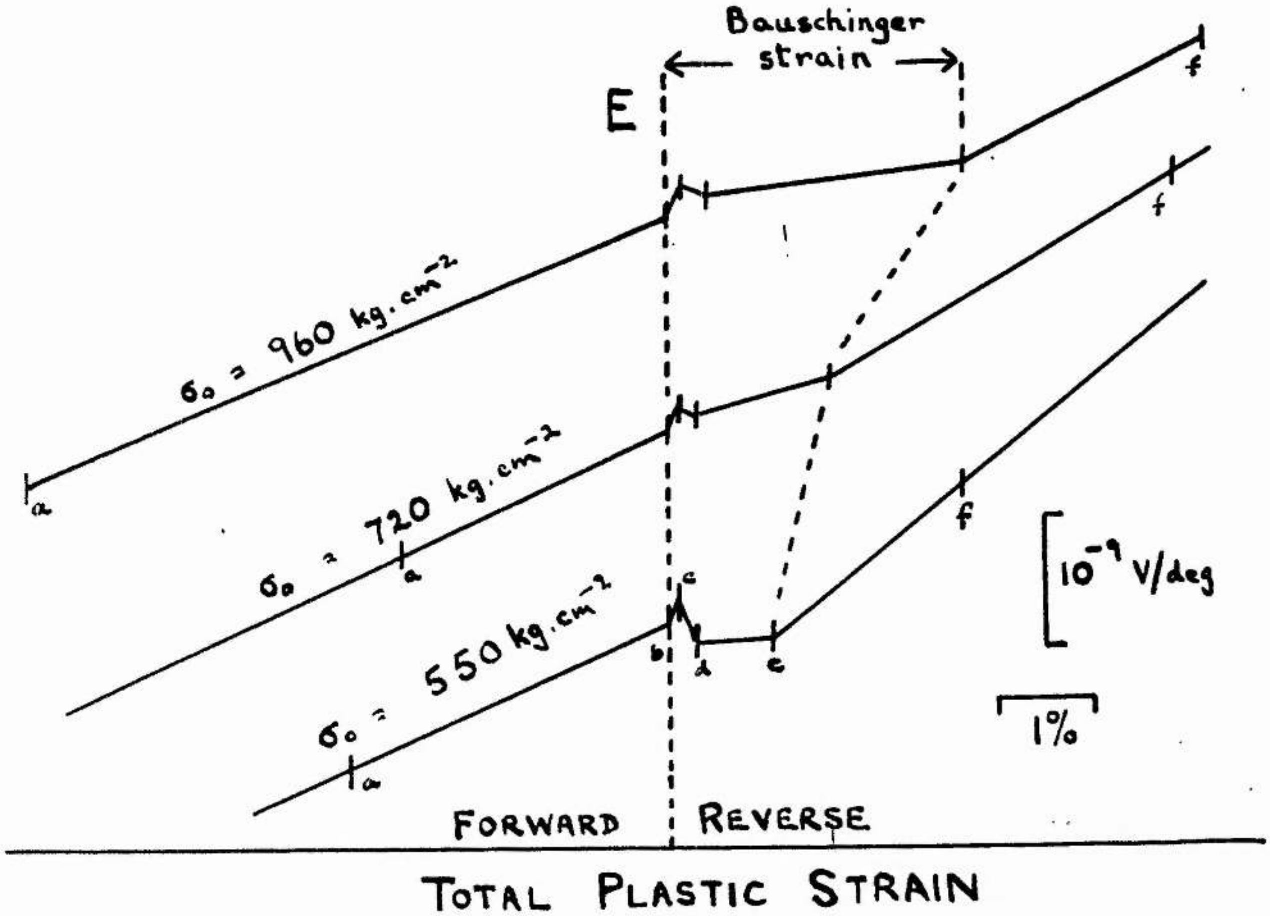

Figure 511
The change of thermoelectric power during the Bauschinger strain is relatively small.

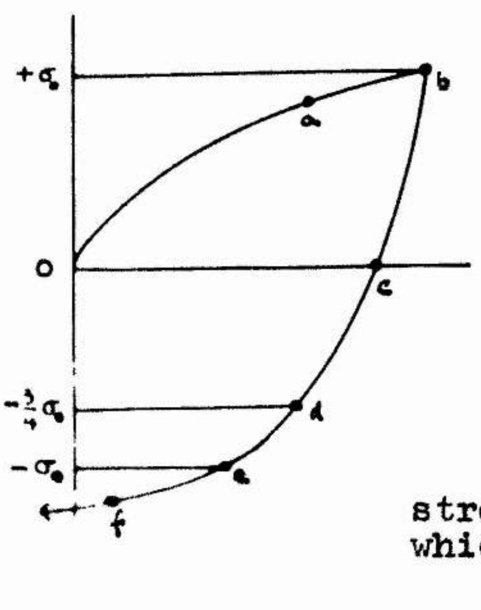

Figure 512
Showing points on stress-strain curve at which E was measured.

and carried copper terminals which were connected to S_2 by a spiral of annealed copper wire. The switch S_2, the two spiral leads, and the lower ends of the two rods were all immersed in an electrically stirred oil-bath.

The specimen was plastically deformed by application of a load to the rim of the wheel, W (figure 506). The shear strain was measured by the telescope and scale T, and by the mirrors M attached to the ends of the specimen.

V(e) RESULTS

(i) It was confirmed that in the elastic range the thermoelectric power is independent of shear stress, within an accuracy of 7×10^{-11} volt/deg, up to a shear stress of 700 kg/cm^2. [The thermoelectric power produced by a tensile stress of 700 kg/cm^2 is 490×10^{-11} volt/deg. (Crussard 1948)].

(ii) Figure 511 shows the typical variation of thermoelectric power during a stress reversal. The horizontal axis shows the total plastic strain. The thermoelectric power was measured at six points on each curve, corresponding to the points marked in figure 512. The vertical line through each point indicates the experimental accuracy.

V(f) DISCUSSION

In figure 511 it is seen that during the Bauschinger strain from $+\sigma_b$ to $-\sigma_b$ there is relatively small change in the thermoelectric power, which rises at the normal rate after $-\sigma_b$ is passed. This is taken to indicate that during the Bauschinger strain there is little change in the number of interstitial atoms. Since these are produced by the intersection with a screw dislocation of leading dislocations of a slip avalanche, we argue that leading dislocations do not cut each other during the Bauschinger strain. In section IV(b) it was suggested that the magnitude of the Bauschinger strain is what would be expected if each dislocation moved a distance equal to the mean separation of the dislocations present, or if groups of dislocations moved a distance equal to the mean separation of the groups. In such a rearrangement no leading dislocations intersect each other, which is what is now suggested by the thermoelectric power measurements.

After the Bauschinger strain is complete and the stress $-\sigma_0$ passed, the rate of generation of interstitial atoms rises to the value it had before $+\sigma_0$ was reached; this implies that leading dislocations are cutting each other as frequently as before.

A somewhat surprising experimental observation in figure 511 is that there is a small rise of thermoelectric power on unloading from $+\sigma_0$ to 0. This effect is real and is invariably observed on unloading after plastic deformation. Its origin is at present unexplained. If at this point a stress less than $+\sigma_0$ is applied, and unloaded, no change of thermal e.m.f. is observed.

In the theory above, and in the theory of electrical resistivity discussed by Seitz (1952), no account is taken of a possible contribution from stacking faults due to collapsed sheets of vacancies, or to sheets produced from interstitial atoms. This contribution is at present being further considered. It is likely to be of the same order of magnitude, but somewhat smaller, than the contribution from interstitial atoms.

The accuracy of the results is not as high as could be desired; it is hoped to repeat these observations with a modified apparatus in the near future.

VI.

THE BAUSCHINGER EFFECT IN POLYCRYSTALLINE MAGNESIUM

VI(a) INTRODUCTION

The primary purpose of this experiment was to obtain some information on the Bauschinger effect in a metal where twinning processes play an essential part in the deformation, for comparison and contrast with the results obtained with face-centred cubic metals and especially with iron. No stress-strain curves of the Bauschinger effect in hexagonal metals have apparently been published. The polar behaviour of twinning, however, makes it extremely likely that a large effect would be observed.

VI(b) EXPERIMENT

Specimens of standard form with 1/16 in. wall thickness were made up out of 99.98% pure magnesium obtained from Messrs. Magnesium Elektron Ltd. These were annealed at 300°C for 8 hours in air, producing complete recrystallisation with a

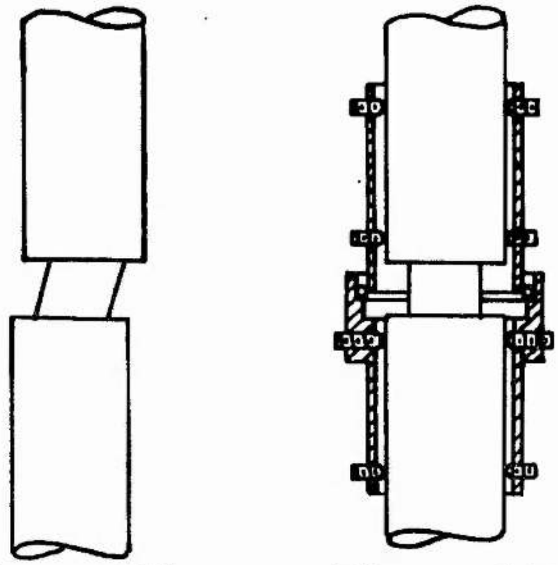

Figure 6.01 Figure 6.02
Ball bearing prevents buckling

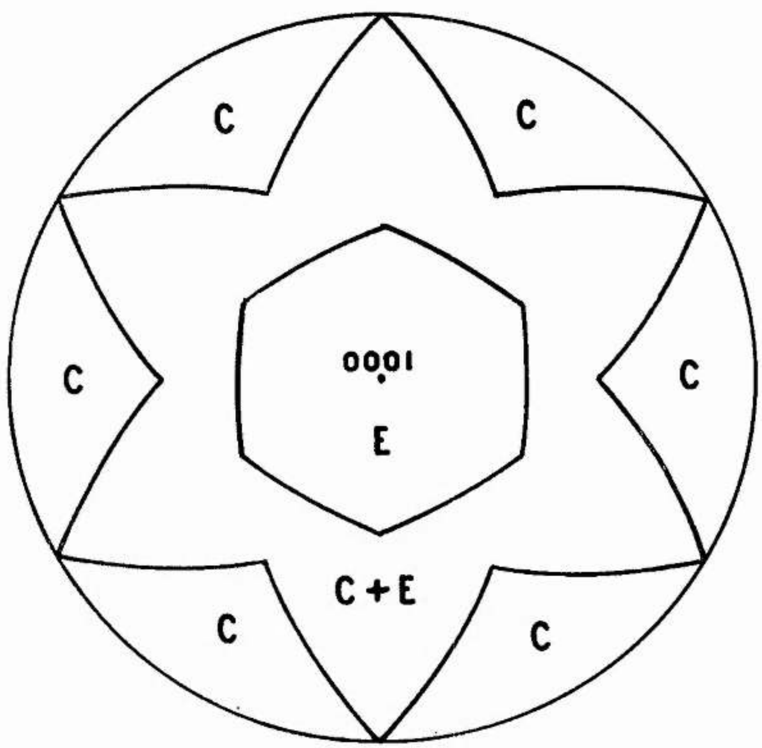

Figure 6.07

Stereographic projection
of magnesium single crystal.

grain size of 220 grains/mm^2. This temperature was chosen as being the highest at which surface oxidation was negligible. Some preliminary experiments with tin had shown that unless the wall thickness of the specimen is very uniform there is a tendency for the specimen to twist about one of its generators rather than about its axis, as shown in figure 601. This form of instability had not occurred in the experiments of Part I. To prevent the possibility of this behaviour the specimens were fitted with a ball bearing, as shown in figure 602.

Stress-strain curves with suitable reversals of stress were then taken; these are shown in figures 603-606. In two of these experiments notes were made of the amount of noise emitted by the specimen when twinning occurs. These are noted in figure 606. Creep effects were very noticeable whenever the strain rate was large, and contributed up to 30% of the observed strain. Readings were generally taken about 2 minutes after a stress increment, when the creep rate was fairly small.

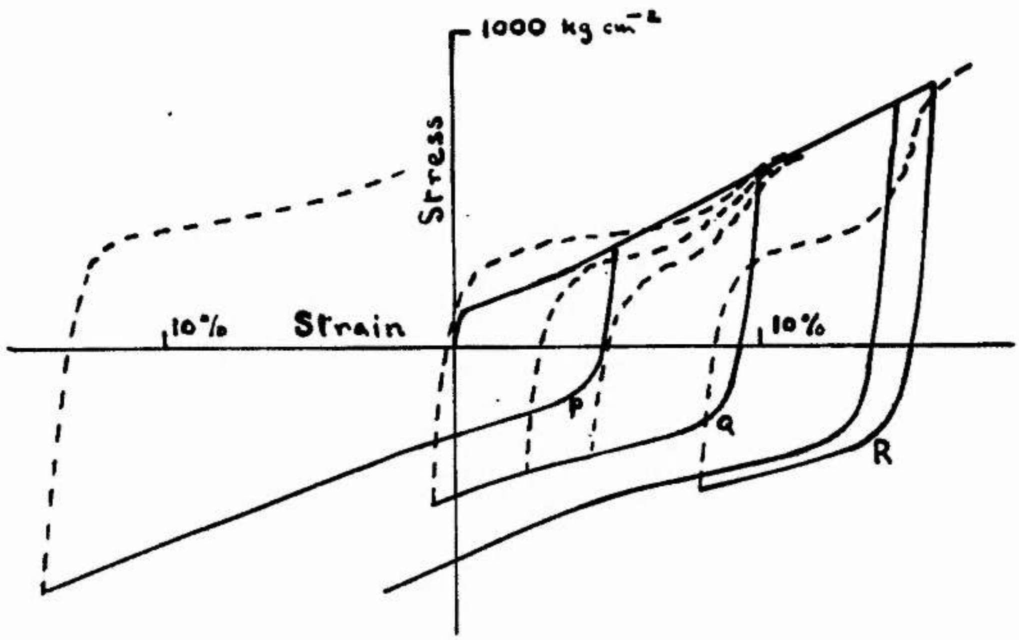

Figure 603. Superposed curves of all specimens tested.

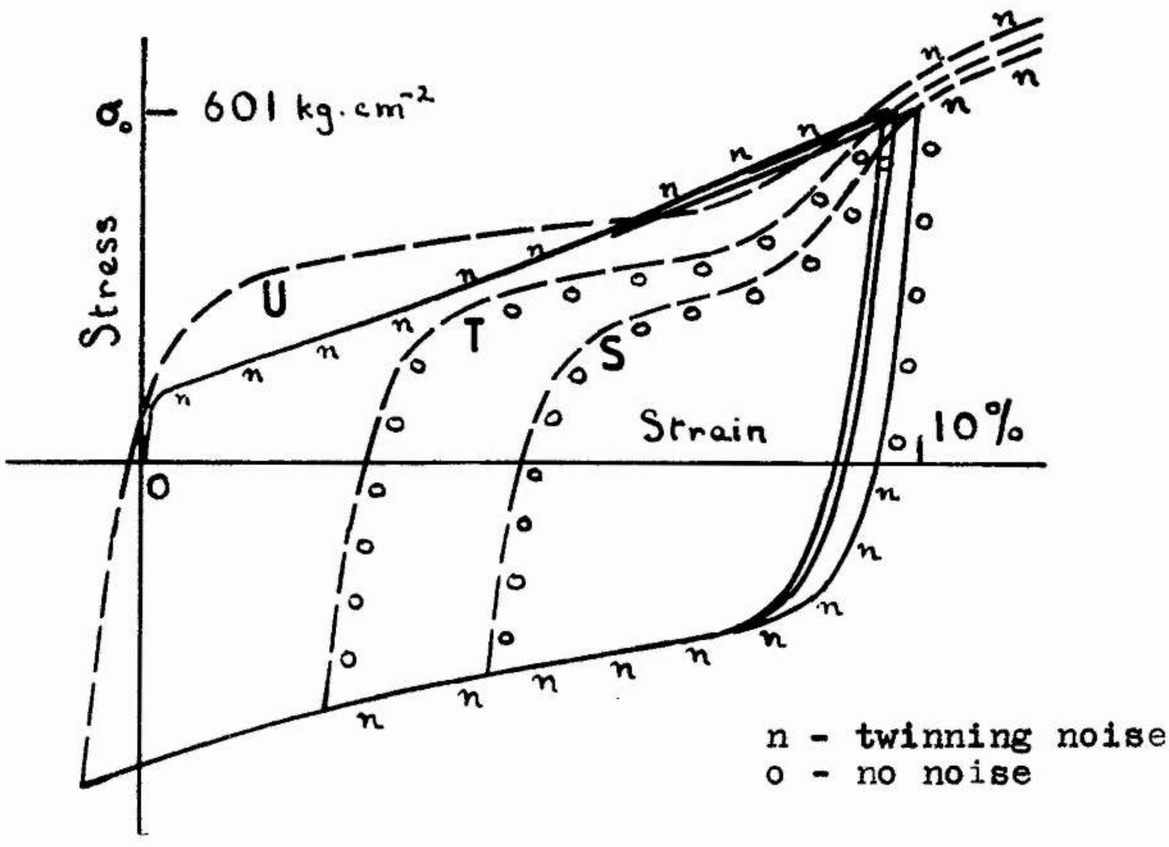

Figure 606. Detail from figure 603.

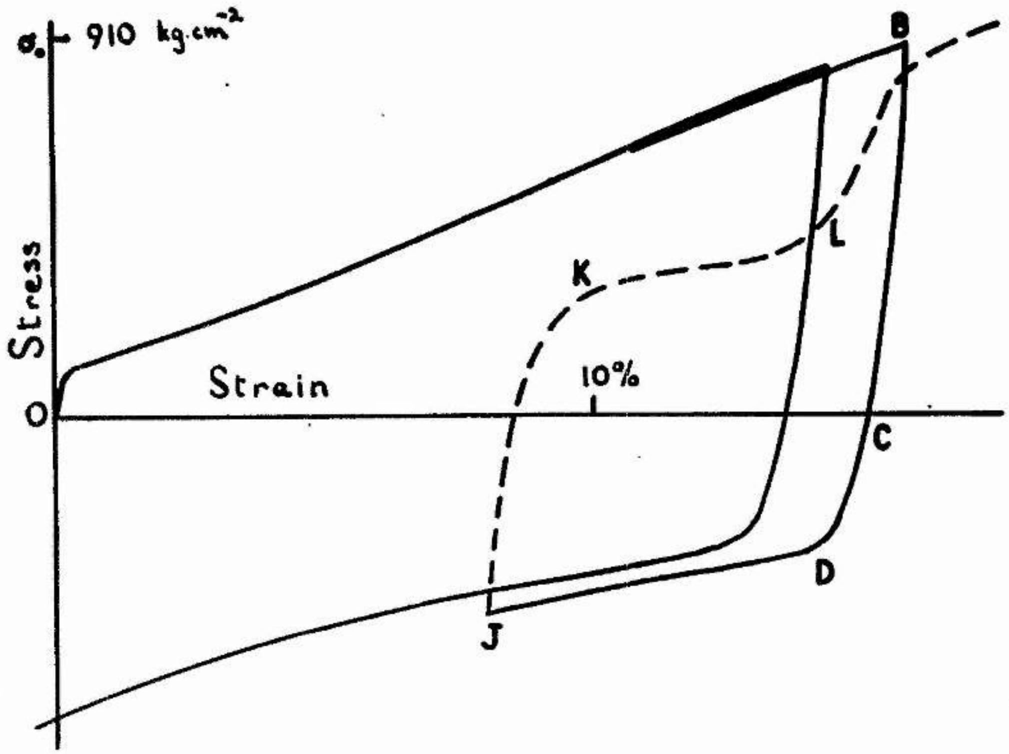

Figure 604. Detail from figure 603.

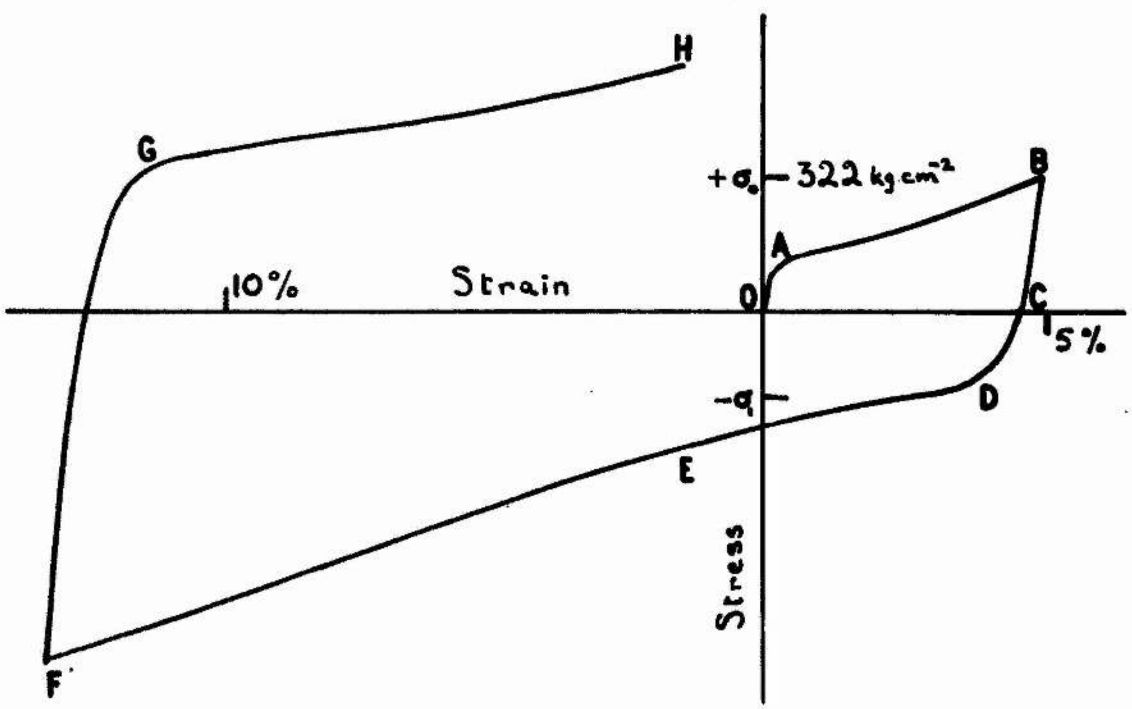

Figure 605. Detail from figure 603.

VI(c) DISCUSSION

The results shown in figures 603-6 are notably different from those given in Section II. Consider for example figure 605. During unloading after a prior deformation to $+\sigma_0$, the curve resembles those of Section II in showing only slight curvature, and substantially no plastic flow. Small negative stresses produce appreciable deformation, which increases very rapidly beyond a stress $-\sigma_1$, where $\sigma_1 < \sigma_0$. The strain rate here exceeds the strain rate just before $+\sigma_0$, but after a certain further deformation in the negative direction it drops off to a value nearly equal to the rate just before $+\sigma_0$. B2 curves obtained by removing the negative stress and applying again a positive stress are quite unlike those of Section II as, provided the negative strain is not too large, they show two steps, (figures 604 and 606), the second of which brings the specimen back very nearly to the point $+\sigma_0$ from which the B1 curve originally sprang.

These results are broadly intelligible in terms of the mechanism of deformation. If a grain in an aggregate is to deform in a specified way, in general five distinct shear systems are required

(Taylor 1938), which means at least three active shear planes. This condition may occasionally be relaxed a little for a grain whose neighbours have a favourable orientation (cf Section III(a)). In hexagonal metals slip takes place only on the basal plane (0001), so that slip alone is inadequate to allow the aggregate to deform without cavitation. On the other hand, twinning can occur on the six $(10\bar{1}2)$ planes, in the six $[10\bar{1}\bar{1}]$ directions. If a rod-shaped single crystal is subjected to tension, it can extend by twinning on any $(10\bar{1}2)$ plane if its axis lies in the area E of the stereographic projection of figure 607; but if it is compressed, no twinning can occur when it is in this orientation. The area C represents orientations in which twinning occurs only during compression, while the area C + E represents orientations where twinning can occur on at least one twin plane in tension and at least one in compression. The areas C, E and C + E of the pole sphere are approximately equal. Thus, in a polycrystalline aggregate with no preferred orientation, about 1/3 of the grains will be unable to deform by twinning if a specified unidirectional stress is applied. If a single crystal is twinned by the application of a stress of suitable direction, it can be untwinned by a stress in the same direction but with opposite sign; the same result presumably applies to a grain in an aggregate.

Twinning gives extra shear planes which enable Taylor's condition to be satisfied. It is a discontinuous process, leading to large local stresses where twin lamellae meet grain boundaries; these stresses must be relieved by local slip (where possible) and by local twinning. The strain energy associated with these stresses is less if the twin lamellae are numerous and narrow, rather than few and broad; this is presumably one reason why even heavy twinning may be invisible under microscopic examination, though visible by X-ray diffraction (Calnan and Tate 1951, Barrett and Haller 1946). Simple twinning is able to give a maximum shear of only 13% in magnesium. Further deformation can take place by slip and secondary twinning within the twin lamellae. In the present work the largest strain was 16%, so it is not reckoned that these secondary processes contribute greatly here.

In view of the complexity of the internal stresses it is not possible to give a full analysis of the present experimental results. These are therefore discussed merely from the point of view of the contribution of twinning and untwinning to the shape of the B1 and B2 curves.

First of all it must be pointed out that asymmetry of the B1 curve will arise if the specimen is initially anisotropic. Extruded magnesium rod can be anisotropic for tension-compression along its axis; Schmidt (1933) found tensile and compressive yield points of 2300 and 1300 kg/cm^2 respectively in an unrecrystallised Elektron AZM alloy. But in the present experiments using torsion of a tube whose axis is the axis of the fibre texture, this objection should not apply.

The positive direction of stress is defined as the direction of stress first applied, producing the prior strain. Positive strain and positive twinning are strain and twinning taking place during application of a positive stress. Positive untwinning is the untwinning of a positive twin, and is produced usually by a negative stress. Positive retwinning is the retwinning of an untwinned positive twin, produced by the re-application of a positive stress.

Along OAB in figure 605 deformation occurs by positive twinning and accompanying slip. This twinning takes place in about 2/3 of the total number of grains, the remaining 1/3 being in unfavourable orientations. Some of these latter may deform by slip, and near their edges there will in any case be local slip and twinning to accommodate twinning in adjacent grains. Along BC the deformation is small and resembles the corresponding curve in the cubic metals; in particular, BC can exceed 2OA without any clearly-defined yield-point on it, showing that Masing's theory is inapplicable here also. No substantial untwinning occurs during unloading. Along CD the plastic component of the deformation increases until at D there is well-marked yield where the strain rate $d\theta/d\sigma$ increases substantially, subsequently settling down to a smaller value beyond E. The part CD probably corresponds to incipient twinning in a limited number of weak grains. At D the stress is large enough to produce twinning in all grains, and general plastic flow. The strain rate along DE should exceed that along AB for the following reasons.

(i) Along AB we have only positive twinning, which occurs in only 2/3 of the grains. But along DE these 2/3 undergo positive untwinning while the remaining 1/3 undergo negative twinning, both of which contribute to the total strain. Other things being equal, the strain rate along AB should be 2/3 of that along DE.

(ii) Along AB the 'hard' grains, forming 1/3 of the total number, will tend to 'lock' their immediate neighbours and hinder their extension. Thus the ratio of strain rates should be less than 2/3 to 1. The ratio is not likely to be less than 1/3 to 1, so we may take as a mean value 1/2 to 1.

The influence of textural stresses has not been calculated. By analogy with section IV(b), however, we may say that these probably cause a 'rounding' of the yield point at D, but do not affect the strain rate along DE.

Untwinning is a limited process and must end when all the twinned material is untwinned. Let the prior strain be $+\theta_o$. Then, assuming that 2/3 of the B1 strain is attributable to untwinning, a further strain of $-3/2 \cdot \theta_o$ will complete the untwinning process. Thus at a resultant strain of $-\theta_o/2$ the strain rate should be due solely to negative twinning in 2/3 of the grains, and should therefore have the same value as along AB. This is shown in figure 605, curve EF. Along EF the material is, to a first approximation, deforming exactly as if it had been subjected only to negative stresses. A B2 curve springing from F therefore shows the same Bauschinger effect as a B1 curve, the strain rate along GH being nearly double that along EF, and falling off toward the value of EF at H, where this particular test terminated. It is noteworthy that the strain-amplitude of GH is only about 10%, while on the argument above it should be more like $1\frac{1}{2}$ x strain-amplitude of OF, i.e. about 19%. This discrepancy is probably due to the fact that OF is slightly larger than the maximum strain obtainable in a single crystal by simple twinning. We are here moreover considering a polycrystal, where many grains will not be favourably oriented. Part of the strain OF must therefore be attributed to secondary slip and twinning, and these apparently limit the strain recoverable in the form of negative untwinning.

A somewhat different B2 curve springs from points along DE (figure 604, cf also figure 606). Here positive retwinning and negative untwinning occur along KL. This cannot exceed the positive untwinning and negative twinning that occurred along DJ, and so must give the same strain as DJ. At L the material is therefore internally in the same state as it was at O, and so the stress-strain curve rises till it passes through B, and then continues in prolongation of AB.

In assessing the observations of twinning noise it is important to note that the material adjacent to the 3/8" diameter pins, which transmit the torque to the ends of the specimen, is stressed nearly as highly as the reduced centre section, and also undergoes some plastic deformation. This must contribute to the noise. Thus it is only the absence of noise that is here significant. The only region in which considerable plastic deformation occurs without twinning noise is along KL (figures 604 and 606) and we may conclude that in this region twinning takes place by the formation of very small twin lamellae and their steady growth, rather than by the sudden twinning of relatively large volumes of metal.

In figure 603 it will be noted that the negative yield stress (P, Q and R) on the B1 curve increases, the greater the prior strain. A similar effect is seen in the B2 curves of figure 606. (S, T and U). According to Masing's interpretation of cold work and the Bauschinger effect, the reverse yield stress should decrease with increasing prior forward deformation. Thus these results are inconsistent with Masing's theory, but would accord with the idea of the hardening of the lattice, due to the accumulation of defects produced by the cold work.

The above explanation is plausible, but it requires confirmation by other methods, such as microscopic observation or X-ray diffraction. More experimental stress-strain curves are desirable, and including other hexagonal metals and tin. These extensions are however outside the scope of the present study, whose prime object was to show the considerable difference between the Bauschinger effect in hexagonal and cubic metals.

VII.

THE BAUSCHINGER EFFECT IN CADMIUM SINGLE CRYSTALS

VII(a) INTRODUCTION

The experimental results of Sachs and Shoji (1927) who found a Bauschinger effect in single crystals of 70/30 alpha brass were at the time regarded as exceptional, and even in 1951 it was remarked by Seitz that "irregularities such as the Bauschinger effect .... are not observed generally in crystals" (Seitz, 1952), though in late 1951 he agreed (private communication) that there appeared to be no experimental evidence to support this statement. It would in fact be surprising if single crystals showed no Bauschinger effect. For with a sensitive extensometer limited plastic flow can be detected at the beginning of the extension of a single crystal, at stresses below the conventional yield point as measured with a less sensitive extensometer (Boas and Schmid 1929). If such behaviour is observed at the beginning of plastic extension, there seems no particular reason why some flow should not occur

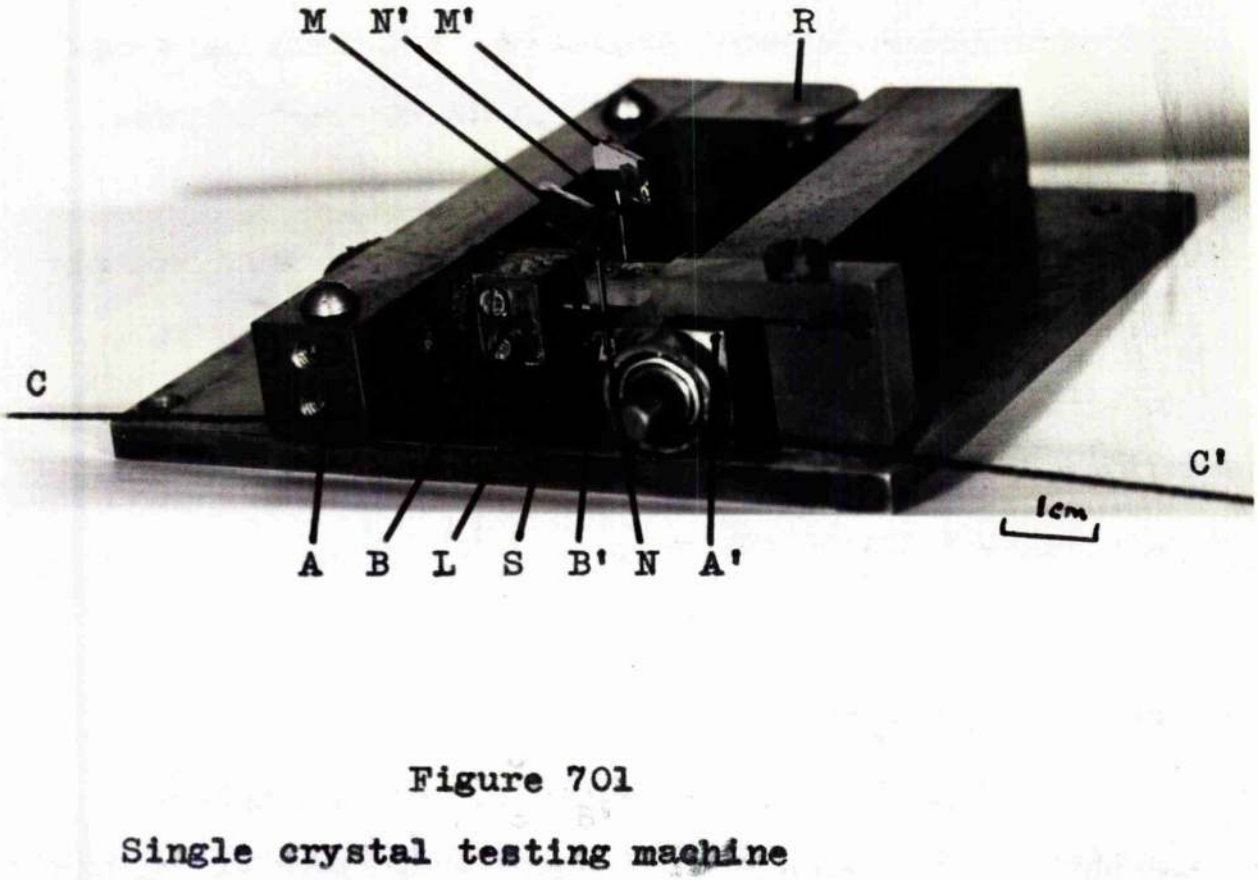

Figure 701

Single crystal testing machine

at a low stress during subsequent plastic compression. It was therefore decided to investigate the Bauschinger effect in single crystals of a pure metal. Cadmium, being the least work-hardening of the hexagonal metals, was felt to be the metal of greatest interest. If a Bauschinger effect could be observed in cadmium then a Bauschinger effect should also be observed in the other hexagonal metals where work-hardening is more apparent, and even more so in the cubic metals where slip on several planes is possible.

During the progress of this work a Bauschinger effect has been reported in single crystals of aluminium (Thompson 1951, private communication) and magnesium (Weinberg 1952), so that the effect does appear to be general.

VII(b) APPARATUS

Figure 701 shows details of the testing machine. The specimen S is soldered into the brass blocks B, B' which are fixed to the steel arms AA'. These are pivoted by a ball race at R, so that when a load is applied to either of the cords CC', the specimen is extended or compressed. The block B carries a pair of leaf springs LL' which press a pair of needles NN' against the sides of the block B'. These needles carry mirrors MM'. Extension of the specimen rotates the mirrors, and the angle of rotation is measured with a telescope and scale. The linear magnification is 6600, i.e. an increase in length of the specimen by 1 μ causes a change in scale reading of 6.6 mm. The strain of the specimen can be measured to .002%.

The pressure of the leaf springs LL' is sufficient to exert a small restoring force on the machine and thus to influence the accuracy of stress measurement. These springs are therefore slightly curved, so that when the blocks move apart the shape and position of each spring does not change. Thus the springs cannot communicate elastic energy to the machine and therefore exert no resultant force. This is checked before inserting a specimen. The residual restoring force and the friction are negligible.

It must be noted that the block B' does not move linearly but rotates about the pivot R. This means that there is a small strain-difference across the width of the specimen. At a mean strain of say 1%, These crystals were grown in an atmosphere of pure argon and should therefore be free from the yield phenomenon discussed by Cottrell and Gibbons (Nature **162**, 488, 1948).

the nominal strain varies from 0.99% to 1.01% across the specimen. This difference is reckoned to be negligible.

The design may be criticised in that the device measures the sum of the Bauschinger effect in the specimen and in the solder which attaches the specimen to the blocks BB'. This is inevitable, as it is not possible to attach a sensitive extensometer direct to a 1 mm diameter single crystal, 4 mm long. The layer of solder is however relatively small in thickness and large in area, and the strength of the solder decidedly larger than the strength of a single crystal, and it is reckoned that the observed effect may be entirely attributed to the specimen.

VII(c) RESULTS

After several preliminary experiments two specimens were finally tested under satisfactory conditions. Limitations of time have prevented further measurements, but it is reckoned that the results indicate that a well-defined Bauschinger effect does occur.

The specimens were both cut from the same single crystal, Cd4, grown from Johnson Matthey "Specpure"

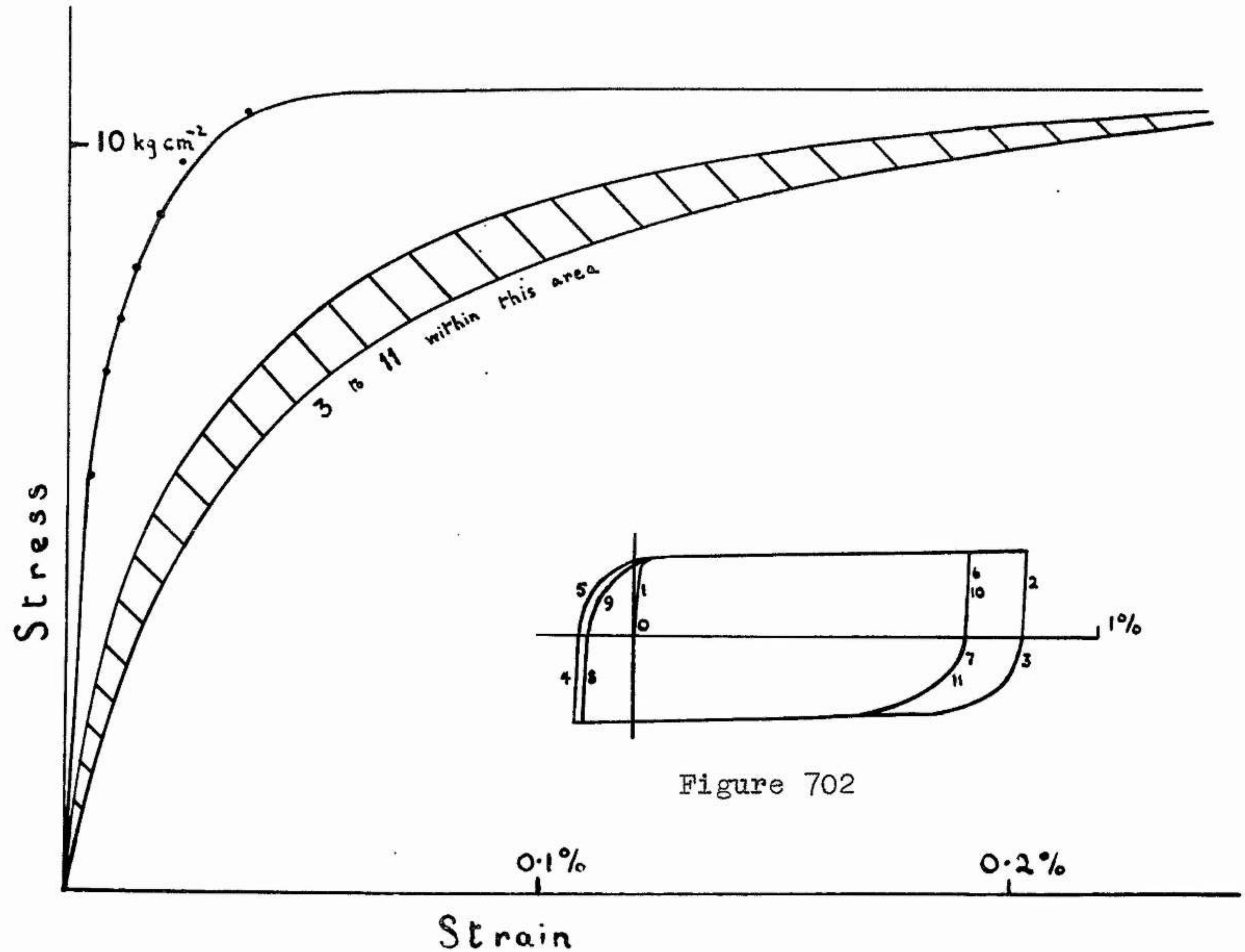

Figure 702

Figure 703   Single crystal Cd4b

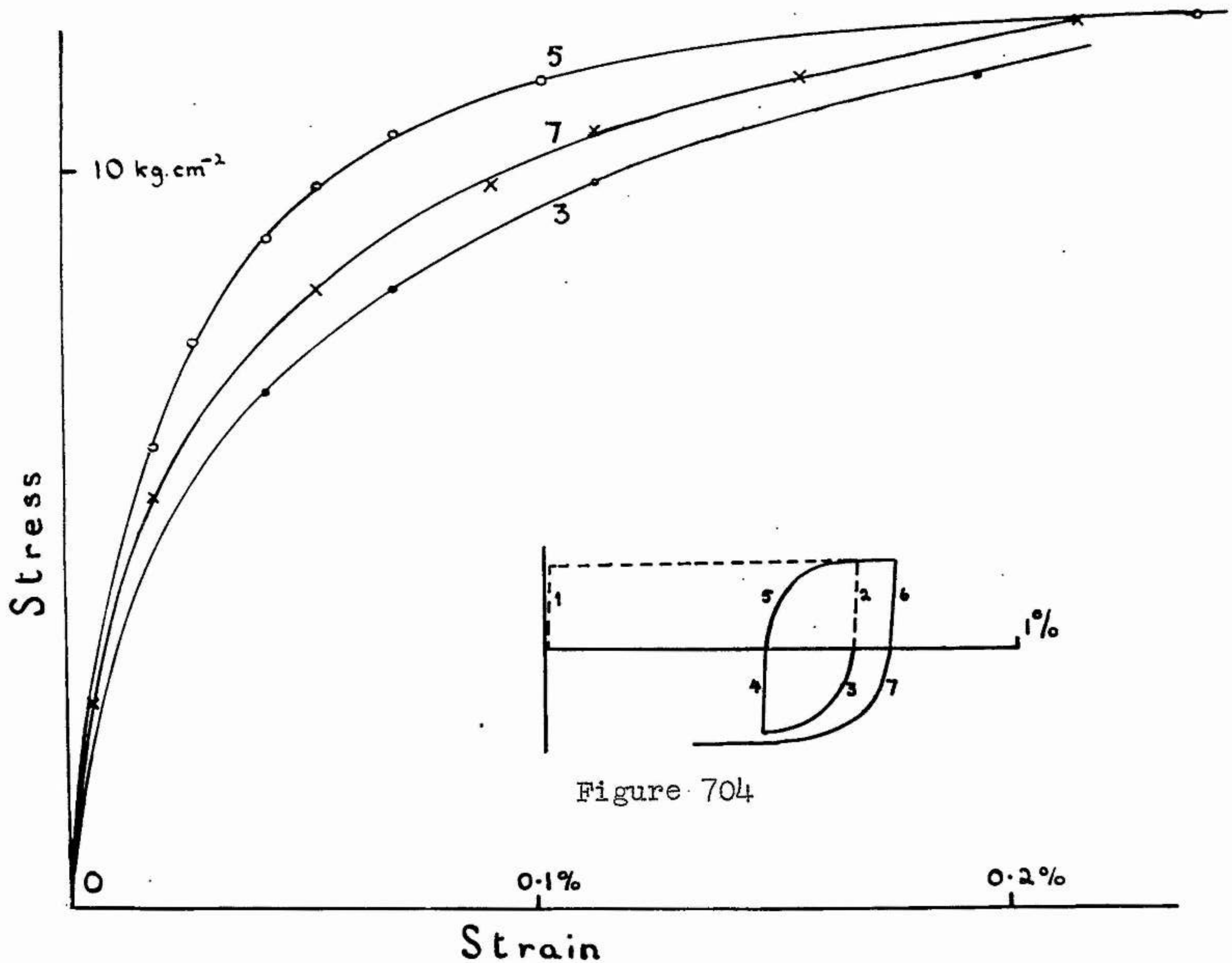

Figure 704

Figure 705 Single crystal Cd4a

cadmium. This crystal had its slip plane at 44° and its slip direction at 47° to the tension axis. Consider first specimen Cd4b. This was stressed cyclically several times between the limits as shown in figure 702. The alternate loading curves are denoted in sequence by 1, 3, 5, etc., and the unloading curves by 2, 4, 6, etc. Figure 703 shows the loading curves to larger scale. Curves 2 and 3 together correspond to the B1 curve of section II. The unloading curves, 2, 4, etc., are linear and elastic within experimental uncertainty. The loading curves 3, 5, etc., are very similar and show a large Bauschinger strain. The axes of figures 702-5 are sealed in units of resolved shear stress and resolved shear strain on the slip plane in the slip direction.

Specimen Cd4a was taken through the cycles shown in figures 704 and 705. Details of the stress-strain curve were not measured during the prior strain, curves 1 and 2. Curve 3 of figure 705 follows the finite strain of curve 1, and is the same as curves 3 to 11 of figure 703. In figure 705 curve 7 follows the rather smaller strain of curve 5, and has a Bauschinger effect a little less than normal. In the same figure curve 5 follows the even smaller strain of curve 3, and its Bauschinger strain is even less.

Thus a prior strain of order 0.5% is required to develop the full Bauschinger effect or to delete the "memory" of a previous stress reversal.

No significance is attached to the strain difference between the first loading curve 1 and the curves 3 to 11 of figure 703. It is extremely difficult to be sure that mounting the specimen introduces no plastic strain, although the process of soldering the specimen should help to anneal it. More experimental evidence would be required to establish that curve 1 is the true initial stress-strain curve of virgin material.

VIII(d) DISCUSSION

The results of the above observations show that a Bauschinger effect is observed in cadmium, and it is therefore likely that the effect is a fundamental property of single crystals of all metals.

Detailed discussion of the results is out of place here as the experiments did not cover a wide enough range of experimental conditions. It is perhaps worth observing that relative to the yield strain the strain associated with the effect is about three times larger than that observed in polycrystalline cubic metals (section II above), though having the same general character. It is thus likely that the theories put forward to account for the effect in the cubic metals (section IV, above) are also to some extent applicable in the case of cadmium single crystals.

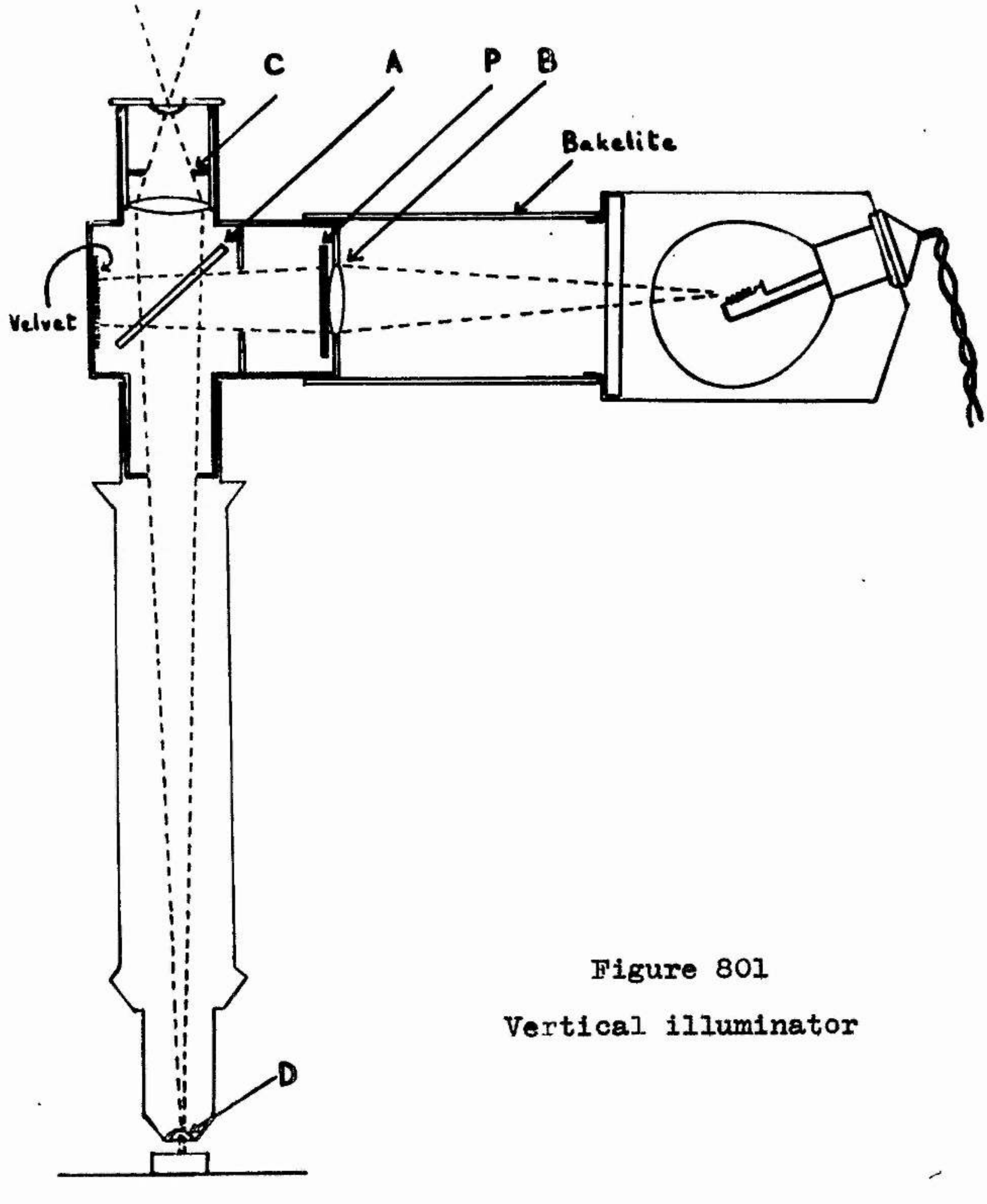

Figure 801

Vertical illuminator

VIII.

SOME APPARATUS CONSTRUCTED FOR THIS WORK

VIII(a) VERTICAL ILLUMINATOR

There being no vertical illuminator available for microphotography in the department, one was constructed as shown in figure 801. It is related to the Beck-Wrighton illuminator, but has one or two points of difference. The 45° glass slip, A, is placed near the eyepiece instead of just above the objective. Being thus near the primary image rather than near the objective, the optical quality of the glass slip is quite uncritical. This arrangement also allows the illuminator field stop, B, (whose image in the 45° glass slip is to coincide with the eyepiece field stop, C) to be brought close to the body of the microscope without the use of an auxiliary lens. The light-source is a 12 volt 24 watt car lamp inclined to the horizontal to give a source approximately 2 mm square. The condensing lens at the illuminator field stop, B, forms an image of the source on the back of the objective, just filling its entry-pupil, D. The lamp-housing is totally enclosed. It is fitted with cooling fins and is connected to the microscope by a bakelite tube which is an effective thermal insulator. The incident light is permanently plane polarised by a sheet of Polaroid at P. An analysing Polaroid can be placed above the eyepiece.

With this type of illuminator the photographic exposure is independent of the focal lengths of the objective and eyepiece and depends only on the area of the field on the photographic plate and the reflecting power of the specimen. Witha metal of high reflecting power, such as magnesium, an exposure of 2 seconds is adequate using process plates and a field 3 inches in diameter. For visual work a resistance in series with the lamp reduces the brightness.

VIII(b) SINGLE CRYSTAL FURNACE

The furnace described here was constructed to produce single crystals by the travelling furnace method (Andrade 1937). The exact adjustment of the furnace temperature in the conventional Andrade design is usually found to be somewhat critical. This is due to several factors. The chief of these is that the temperature gradient in the specimen is

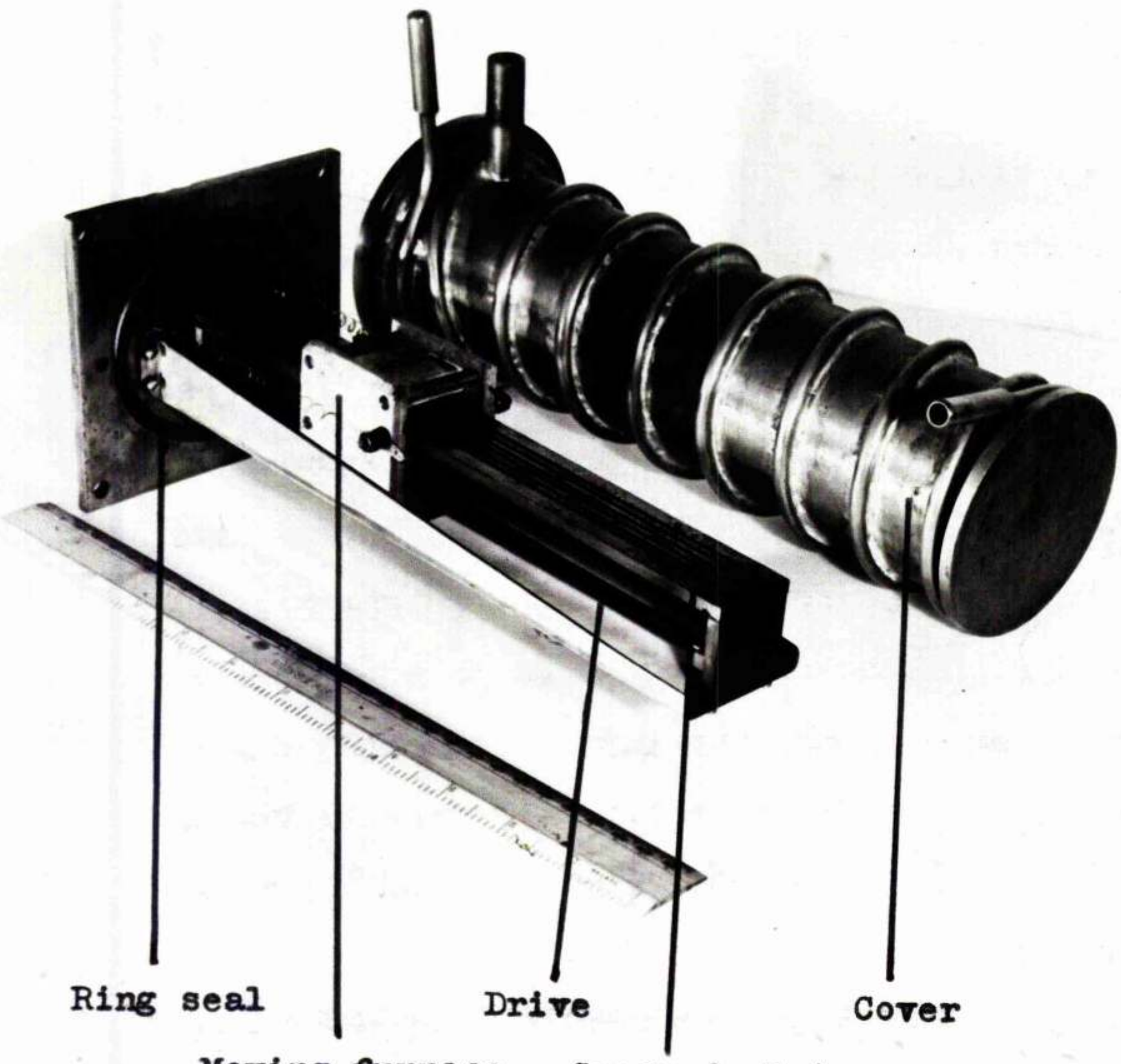

Figure 802
Single crystal furnace

considerably reduced because the specimen is of relatively high thermal conductivity and is separated from the furnace element by the silica wall of the controlled atmosphere enclosure which is of relatively low conductivity. Besides this, the heat loss from the specimen occurs principally from the sides of the specimen, and the temperature gradient behind the moving furnace, and the temperature distribution, vary with the position of the furnace along the length of the specimen. It was reckoned that these difficulties might be overcome (i) by putting the travelling furnace inside the controlled atmosphere tube rather than outside, and (ii) by growing the crystals not in silica quill tubes but in grooves on a metal plate extending well beyond the ends of the crystals, so that heat can be conducted away equally well, whatever the position of the furnace relative to the specimen.

These principles were embodied in the furnace shown in figure 802. The furnace has not been extensively tested, but it does produce ductile crystals of tin and cadmium. Figure 803 shows the temperature distribution deduced by plotting the

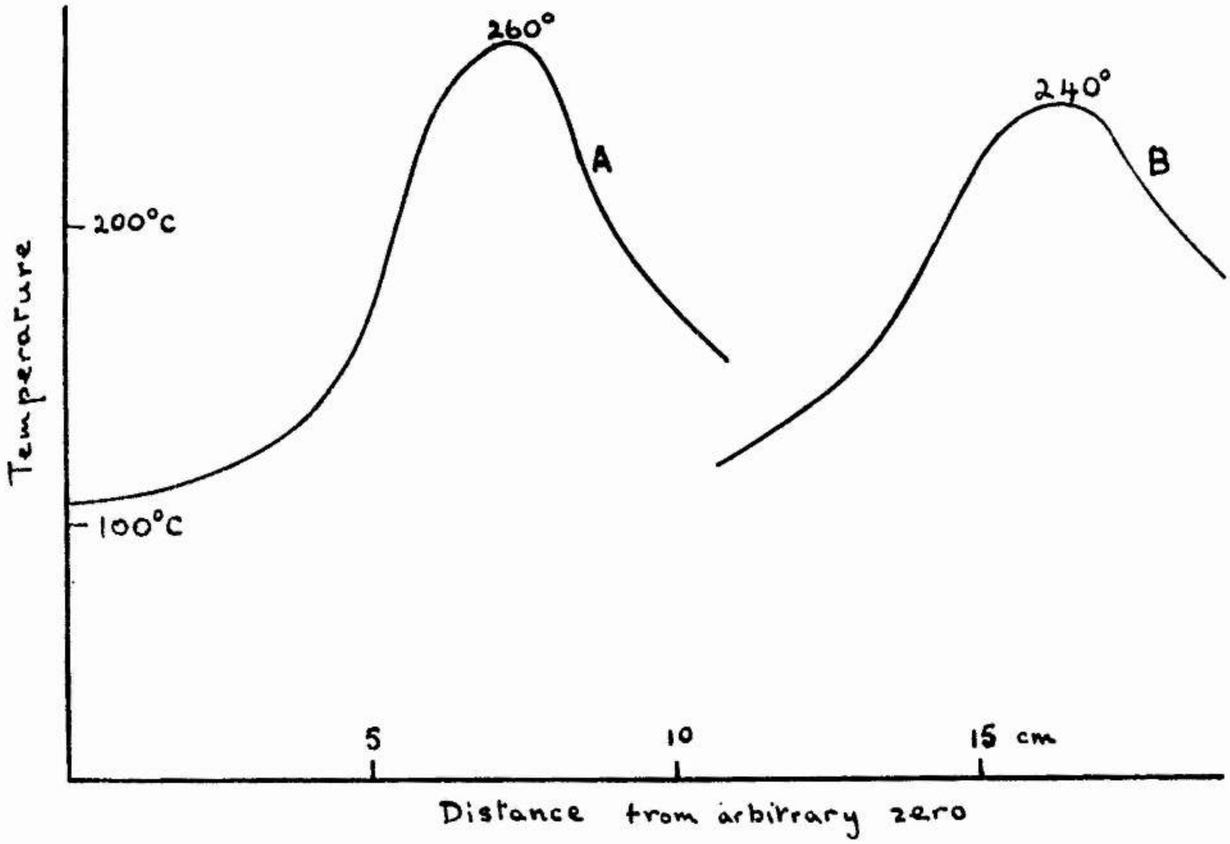

Figure 803

Temperature distribution in furnace
A - near mid-point
B - near one end

temperature of a fixed point in a specimen as the moving furnace travels past. Curve A is the distribution when the furnace is near the mid-point of a specimen 18 cm. long, and curve B when it is near one end. The temperature gradient is about 40 deg/cm for at least 2 cm on either side of the peak. The temperature distribution does not vary much with position of the furnace, and the peak temperature changes by only 8%.

REFERENCES

Andrade, E. (1937) and Roscoe, R.

Proc. Phys. Soc., 49, 153.

Barrett, C.S. and Haller, C.T. (1946)

Trans.Am.Inst.Min.Met.Eng., 171, 246.

Bauschinger, J. (1881)

Zivilingeneur, 27, 289.

Boas, W. and Schmid, E. (1929)

Zeit. Phys., 54, 16.

Brandenberger, H. (1947)

Schweiz.Arch.angew.Wiss.Techn., 13, 232, 268.

Brown, A.F. and Honeycombe, R.W.K. (1951)

Phil. Mag., 42, 1146.

Calnan, . and Tate, . (1951)

J. Inst. Met., August 1951

Cottrell, A.H. (1949)

Prog. Met. Phys. I, 77.

Cox, H.L. and Sopwith, D.G. 9(1937)

Proc. Phys. Soc., 49, 134.

Crussard, C. (1948)

Rep.Conf.Strength of Solids,Bristol; Phys.Soc.

Greenough, G.B. (1949)

Proc. Roy. Soc., 197, 556.

Honeycombe, R.W.K. (1951)

J. Inst. Met., 80, 45.

Ke, T.S. (1947)

Phys. Rev., 71, 533.

Koehler, J.S. (1941)

Phys. Rev., 60, 397.

Kunze, W. and Sachs, G., (1930)

Metallwirtschaft 9, 85.

Masing, G., (1923)

Wiss.Ver.a.d.Siemens-Konzern 3, 231.

Masing, G., (1926)

ibid. 5, 135.

Masing, G., (1926b)

ibid. 5, 175.

Masing, G. and Mauksch, W., (1926)

ibid. 5, 142. See also ibid. 4, 74, 244.

Mott, N.F., (1948)

Rep.Conf.Strength of Solids,Bristol; Phys.Soc.

Mott, N.F. (1952)

Phil. Mag., 43, 1151.

Nabarro, F.R.N. (1947)

Proc. Phys. Soc., 59, 256.

Nabarro, F.R.N. (1950)

Some recent developments in Rheology;

Brit. Rheol. Club.

Polakowski, N.H., (1951)

J. Iron & Steel Inst., 169,337.

Rahlfs, P., and Masing, G., (1950)

Zeit. Metallkunde, 41, 454.

Sachs, G., and Shoji, H., (1927)

Zeit. Phys., 45, 776.

Schmid, E. and Boas, W., (1950)

Plasticity of crystals; F.A.Hughes, Ltd.

Schmidt, W. (1933)

Zeit. Metallkunde, 25, 299.

Seitz, F. (1952)

Advances in Physics, 1, 43.

Taylor, G.I., (1934)

Proc. Roy. Soc., 145, 362.

Taylor, G.I., (1938)

J. Inst. Met., 62, 307.

Weinberg, E.H. (1952)

J. App. Phys., 23, 1277.

Wilson, D.V., (1952)

Nature, 170, 30.

Woolley, R.L. (1948)

Rep.Conf.Strength of Solids,Bristol; Phys.Soc.

Zener, C. (1941)

Phys. Rev., 60, 906.